Cooperative Behaviors in the Evolution of Antibiotic Resistance

by

Evgene Yurtsev

B.S., University of California, Santa Barbara (2008)

Submitted to the Department of Physics
in partial fulfillment of the requirements for the degree of

Doctor of Philosophy in Physics

at the

MASSACHUSETTS INSTITUTE OF TECHNOLOGY

June 2015

Signature of Author ..... Signature redacted
Department of Physics
May 14, 2015

Certified by..... Signature redacted
.....
Jeff Gore
Assistant Professor
Thesis Supervisor

Accepted by ..... Signature redacted
Nergis Mavalvala
Associate Department Head for Education

Cooperative Behaviors in the Evolution of Antibiotic Resistance

by

Evgene Yurtsev

Submitted to the Department of Physics
on May 14, 2015, in partial fulfillment of the
requirements for the degree of
Doctor of Philosophy in Physics

Abstract

Through a combination of experiments and modeling, I explored how inactivation of antibiotics by antibiotic-resistant bacteria affects the evolution of antibiotic resistance in two simple microbial communities. First, I examined the interaction between a resistant strain and a sensitive strain of the bacteria *Escherichia coli* in the presence of the β-lactam antibiotic ampicillin. Second, I investigated whether two strains of *Escherichia coli* can form a cross-protection mutualism in a multi-drug environment containing the antibiotics ampicillin and chloramphenicol. In both experimental systems, I found that inactivation of antibiotics by resistant bacteria is an important cooperative behavior which enables microbes to help each other survive in otherwise lethal antibiotic concentrations. The rich dynamical behaviors that arise even in these simple systems highlight the inherent challenge in deciphering the workings of more complex microbial communities.

Thesis Supervisor: Jeff Gore
Title: Assistant Professor

Acknowledgments

During the course of my PhD, I have had the pleasure to meet and interact with many wonderful people. In one way or another, all these people helped to make the past several years of my life very happy. Anyway, since I did not want people to start gossiping or constructing wild conspiracy theories, I tried to list all names alphabetically to make it a bit more difficult to decipher whom I liked the best! I most certainly forgot to include someone important in the acknowledgments section below. If so, please let me know; there is always the possibility of being included in the acknowledgments section of my next dissertation.

To my advisor Jeff: thank you for training me as a scientist over the past several years. You showed me time and time again that by asking the correct questions, it is possible to extract meaningful information even from a mess. One just needs to maintain a consistent (and hopefully correct) representation of how the world works, and then all else follows! You taught me that to do good science I need to take time to ask all the basic questions. And that when things get complex, then even if I fail to grasp all the details, I can still verify that the basic ideas make sense and that they work as advertised! In guiding me through the land of science, you taught me how to tackle problems and how to communicate; two skills that will benefit me for many years to come. Lastly, I wanted to thank you for your consistent enthusiasm and optimism – your support helped me power through many things that simply did not work!

I want to thank my thesis committee members, Prof. Kardar and Prof. Mirny, for both their time and patience! While I have the opportunity, I also want thank both of them for teaching one of the best classes I have taken at MIT! (Just in case you're wondering, it wasn't introduction to modern dance.) I also wanted to thank my teachers and mentors from over the years who made it possible for me to get to MIT in the first place: Mr. Birdsong, Dr. Byrum, Prof. Cannell, Prof. Forti, Prof. Hansma, Dr. May, Mr. Newton, Dr. Neri.

To the members of the Gore lab from across the years: some of you defeated me

in dodgeball, others in ping-pong or squash, but all of you consistently made the day-to-day in the lab fun! I wanted to give special thanks to Sherry and Arolyn with whom I worked very closely over the years. And if I'm already here, I'll throw an extra extended round of special thanks to Yonatan and Andrea who both served as mentors to me (usually against their wills).

To my former roommates Ben, Diego, Enrique, Jordi, Kat, Laura, Paula and Roberto: despite having lived with me, you still chose to remain friends with me long after we stopped sharing a roof. (As if deciding to live with me was not a bad enough decision to begin with?) Anyway, in this moment of emotional weakness, I want to apologize to you (the Spanish-speaking ones) for intentionally misleading you over multiple years into thinking that I was picking up Spanish from only listening to your conversations. I was secretly taking Spanish at MIT all this time.

To the friends I have made during my time at MIT: thank you for all the wonderful experiences. Of course, the end of my PhD does not mark any special turning point in our friendships – I suspect those will last for many years to come!

Peter, Patty and Rachael, thank you for being my second family in Boston and for providing me with a second home here!

Mom, dad, wonderful sibling units, grandpa and grandma, thank you keeping me in mind even though I am not always nearby!

Heather, of course, I did not forget about you! You have been by my side throughout the duration of my entire PhD, sharing many wonderful moments with me during the past few years. I wanted to thank you especially for taking care of me during the last few months when I was locked in my bat-cave night and day. In a sense this achievement is as much mine as it is yours!

I would like to dedicate this dissertation to my parents and grandparents: despite all the challenges you had to face, you always put the needs of your children ahead of your own.

Я посвящаю эту диссертацию моим родителям, бабушке и дедушке: несмотря на все выпадавшие трудности, вы всегда ставили интересы детей выше собственных.

Contents

List of Figures

List of Tables

Chapter 1

Introduction

The discovery of penicillin in 1928 marked a significant advancement in humanity's fight against disease. However, shortly after the discovery of antibiotics, researchers were already concerned about the ability of microbes to adapt and develop antibiotic resistance. It is not clear whether anyone could have anticipated just how fast this adaptation would occur. Indeed, just a few years after penicillin was made commercially available, bacterial infections resistant to treatment with penicillin were observed in patients [1, 2]. Ever since, humanity has been locked in an arms race against bacteria, striving to find new antibiotics as older antibiotics lose their potency.

The emergence of antibiotic resistance in bacteria has become a significant health concern [2, 3]. Many pathogenic bacteria that were once susceptible to antibiotic treatment have since acquired genes for antibiotic resistance. In the U.S., at least 2 million people get infected each year by bacteria that are resistant to one or more antibiotics [4]. These infections directly result in the death of at least 23,000 people [4]. Moreover, as a result of tougher drug regulations and high costs associated with developing new antibiotics, the rate at which new antibiotics have been brought into the market has been declining steadily [2, 5]. On the whole, humanity's arsenal of effective treatments against bacterial infections seems to be diminishing.

1.1 Mechanisms of Antibiotic Resistance

Significant effort has been devoted to understanding how bacteria become resistant. The efficacy of many antibiotics depends on their ability to bind either the cell wall or a target inside the cell, and disrupt the normal operations of the cell. Sensitive bacteria can become resistant by "finding" a way of preventing the drug from binding to its target.

Researchers have uncovered an abundance of mutations that enable the bacteria to achieve this goal. Some mutations can modify the permeability of the cell wall, preventing the antibiotic from ever entering the cell [6, 7]. Other mutations can modify the structure of the target site, preventing the antibiotic from binding to the target even if the antibiotic manages to get inside the cell [8, 9]. Yet another strategy involves creating more of the target – in essence, creating "back up" options for the cell [1, 10]. Some of these mutations involve no more than a few nucleotide changes in the genome, making such mutations relatively easy to acquire.

However, bacteria have been evolving in the presence of antibiotics for millions of years, and have developed a much richer arsenal of resistance mechanisms than just the "passive" mechanisms of antibiotic resistance mentioned above [11, 12]. Two examples of such mechanisms include efflux pumps and antibiotic-resistance enzymes; both mechanisms are extremely common and clinically relevant [13–15]. Bacteria can use efflux pumps to simply pump the antibiotic outside of the cell [16]. Enzymes that grant resistance to antibiotics usually work by modifying the antibiotic, rendering the antibiotic dysfunctional [13, 14]. However, antibiotic-resistance enzymes can also restructure the target of the antibiotic, preventing the antibiotic from binding to this target [12, 17].

One would rightly suspect that such elaborate mechanisms are too complicated to evolve de-novo on a short notice. Unfortunately, it turns out that there is no need to evolve them de-novo. Amongst the many important discoveries in the field of microbial genetics was the discovery of horizontal gene transfer – that genes could be transmitted between unrelated bacteria. Bacteria can pick up DNA from their

surroundings on their own or acquire DNA from viruses or extra-chromosomal pieces of DNA called plasmids that are exchanged between cells [18, 19]. Therefore, as long as the genes encoding the necessary mechanisms are present nearby, sensitive bacteria can gain access to the genes via horizontal gene transfer. An important implication of this discovery is that human pathogens can use the soil as a large reservoir of antibiotic resistance genes [20–23].

As our understanding of antibiotic resistance advances, increasingly intricate mechanisms of antibiotic resistance are being discovered. Only relatively recently did we understand that genetically identical cells can exhibit large variation in their behavior [24]. Such heterogeneous behavior has been implicated in the ability of bacterial populations sensitive to antibiotics to survive antibiotic treatment [25]. What happens is that a small fraction of the cells in a bacterial population randomly chooses to enter a dormant state. In this dormant state, the cells do not attempt to divide, which makes them less vulnerable to environmental threats. Thus, upon exposure to antibiotics, such cells are more likely to survive antibiotic treatment than the rest of the population. Eventually these dormant cells resume growth, but by that time the antibiotic may be already gone. The failure of antibiotic treatment in this scenario is particularly interesting because none of the cells is genetically resistant to antibiotics. Specifically, dormant cells that "wake up" and resume growth are as sensitive to antibiotics as they were before entering the dormant state.

1.2 The Evolution of Antibiotic Resistance

Tremendous progress was made in understanding how various processes contribute to the evolution of resistance. Loosely speaking, evolution is the set of processes that determine which new variants (mutants) can appear and the processes that determine how the frequency of different variants changes with time. Thus, one avenue of research has been concerned with understanding the availability of mutations that increase the level of resistance while a complementary avenue of research has been focused on understanding the spread of resistance variants.

In studying which mutations were available to bacteria, researchers found that the set of available mutations seemed to be context specific. For example, because mutations can interact with one another constructively and destructively, the order in which mutations are acquired can affect the likelihood of particular paths to increased resistance [26, 27]. Overall, the starting genotype, the environment and the strength of the selective pressure exerted by antibiotics can all affect the likelihood of different evolutionary paths to increased resistance [28–33].

Many clinical professionals worry that the misuse of antibiotics has increased the rate at which resistance evolves [3, 34]. For example, many patients stop taking antibiotics once the symptoms of the infections disappear. By terminating the treatment too early, the antibiotics may fail to properly eradicate the infection, requiring additional treatment later. The prolonged use of antibiotics could provide a longer window of time during which antibiotic resistance could evolve. Hence, a major line of research has been focused on understanding which antibiotics should be prescribed, for how long those antibiotics should be prescribed for, and how to get patients to better comply with treatment procedures [35].

In many studies, an implicit working assumption is that once a resistant mutant emerges, this mutant quickly increases in abundance until it dominates the entire bacterial population. This assumption is reasonable in many situations because the selective pressures exerted by antibiotics are very strong. Therefore, without any additional information, one would rightly expect that only the fittest (most resistant) bacteria would survive antibiotic treatment.

However, evidence from a multitude of microbial studies suggests that microbes live in communities [36]. The aggregation of bacteria in groups allows bacteria to help each other in unfavorable environments. One particularly important group behavior is the formation of bacterial communities called bio-films. Bio-films are spatially structured communities in which the cells "stick" to each other [37–39]. Because bio-films form on and stick to surfaces, they are a particular nuisance in bio-medical instrumentation. Antibiotics often fail to penetrate the core of bio-films, so cells at the core are exceedingly likely to survive antibiotic treatment whether they are

resistant or sensitive. As a result, bio-films are responsible for many cases of chronic infections, where treatment by antibiotics helps to alleviate the infections, but fails to remove the bio-film that causes them.

Bio-films are not the only cooperative behavior in which microbes engage. The scientific community has come to appreciate a variety of mechanisms by which bacteria collectively "resist" antibiotics [40, 41]. A simple example of another collective behavior involves the deactivation of antibiotics by resistant bacteria. Bacterial cultures that contain more cells can clear antibiotics quickly and resume growth faster. In the medical community, this effect is referred to as the inoculum effect, where infections composed of more cells can withstand higher antibiotic concentrations. The inoculum effect can be a problem when treating infections using β-lactam antibiotics [42]. Collective behaviors in bacteria range from the aforementioned biofilms to coordinated group responses mediated by the exchange of signaling molecules for communication [40, 41, 43].

The ability of bacteria to behave collectively is predicated on the presence of positive interactions between microbes. Positive interactions are interactions in which one microbe helps to increase the fitness of another microbe. Such interactions may help relatively unfit microbes to survive antibiotic treatment. Hence, these interactions may have a significant role in shaping microbial communities in the presence of antibiotics.

The study of positive interactions has long fascinated researchers. These interactions are fundamental in many complex systems, ranging from the organization of human societies to the evolution of multi-cellular life [44]. A long lasting debate in evolutionary biology has been concerned with how cooperative behaviors evolve and persist in populations. Because cooperative behaviors are amenable to exploitation by cheaters, it was not immediately clear which factors could maintain cooperative behaviors. The cumulative effort of many studies has resulted in tremendous progress in understanding these factors in general terms [45]. However, these factors must be worked out in any specific system if one needs to understand its behavior.

A common mechanism of antibiotic resistance in bacteria involves the production

of enzymes that modify and deactivate antibiotics [13, 14]. Because resistant cells clear the antibiotic from the environment, they may be able to allow sensitive cells to survive in otherwise lethal concentrations [46–48]. Although this is a common mechanism of resistance, the question of how it might affect the evolution of antibiotic resistance has received little attention.

In this thesis, we will explore how inactivation of antibiotics by resistant cells shapes the dynamics of simple microbial communities growing in the presence of antibiotics. The thesis is composed of two experimental case studies. In Chapter 2, we examine the interaction between a resistant strain and a sensitive strain of the bacteria *Escherichia coli* in the presence of the β-lactam antibiotic ampicillin. In Chapter 3, we investigate whether two strains of resistant bacteria can form a cross-protection mutualism in a multi-drug environment containing the antibiotics ampicillin and chloramphenicol. In both studies, we find that inactivation of antibiotics by resistant cells is an important interaction, enabling different bacterial strains to coexist and survive in otherwise lethal antibiotic concentrations. The rich dynamical behaviors that arise even in these simple systems highlight the inherent challenge in deciphering the workings of more complex microbial communities. We expect that our results may help provide insight into the evolution of antibiotic resistance and perhaps into how antibiotic resistance spreads during the course of antibiotic treatment.

Chapter 2

Bacterial Cheating Drives the Population Dynamics of Cooperative Antibiotic Resistance Plasmids

2.1 Overview

Inactivation of β-lactam antibiotics by resistant bacteria is a "cooperative" behavior that may allow sensitive bacteria to survive antibiotic treatment. However, the factors that determine the fraction of resistant cells in the bacterial population remain unclear, indicating a fundamental gap in our understanding of how antibiotic resistance evolves. Here, we experimentally track the spread of a plasmid that encodes a β-lactamase enzyme through the bacterial population. We find that independent of the initial fraction of resistant cells, the population settles to an equilibrium fraction proportional to the antibiotic concentration divided by the cell density. A simple model explains this behavior, successfully predicting a data collapse over two orders of magnitude in antibiotic concentration. This model also successfully predicts that adding a commonly used β-lactamase inhibitor will lead to the spread of resistance, highlighting the need to incorporate social dynamics into the study of antibiotic resistance.

2.2 Introduction

A frequent mechanism of antibiotic resistance involves the production of an enzyme that inactivates the antibiotic [13, 14]. The acquisition of such an enzyme through a plasmid often imposes a metabolic cost on the individual cell [49–51]; however, since resistant cells inactivate the antibiotic, reducing its extracellular concentration, they help protect the entire bacterial population [52, 53]. Hence, antibiotic inactivation can be viewed as a cooperative behavior, suggesting that sensitive "cheater" bacteria that do not help to break down the antibiotic may be able to survive antibiotic treatment when in the presence of resistant cells.

Previous studies have provided valuable insight into the evolutionary processes that govern the spread of antibiotic resistance [3, 26, 30, 31, 34]. However, despite the clinical importance of antibiotic resistance phenotypes, there has been a relative dearth of quantitative analysis of cooperative bacterial growth in the presence of antibiotics. Many microbiologists have observed the presence of "satellite colonies" surrounding a resistant colony on an agar plate containing the β-lactam ampicillin. The presence of satellite colonies, which are composed of cells that are in principle unable to grow in ampicillin, is evidence of the extremely cooperative nature of ampicillin resistance. Indeed, recent experiments have detected coexistence between resistant and sensitive cells using a resistance enzyme that was genetically modified to inactivate the antibiotic outside the cell [46, 54]. Furthermore, it is known in the clinic that bacteria carrying even wild-type enzymes may provide protection to pathogenic but otherwise sensitive bacteria [52, 55, 56]. The ability of sensitive bacteria to survive antibiotic treatment suggests that the spread of plasmids that encode cooperative antibiotic resistance genes should exhibit non-trivial population dynamics.

2.3 Results

2.3.1 Population dynamics of antibiotic resistance plasmids

To probe the population dynamics of such plasmids, we co-cultured a sensitive strain of *E. coli* bacteria with an isogenic strain containing an additional plasmid encoding a β-lactamase enzyme. The enzyme hydrolytically inactivates the antibiotic [57], providing high-level resistance against ampicillin. In our experiments, the bacterial culture was grown to saturation over 23 hours in the presence of ampicillin. The saturated culture was then diluted (initially by 100x) into fresh media containing the same initial antibiotic concentration, serving as the starting culture for the following day. Using flow cytometry, we were able to track how the fraction of resistant cells changed over time (Materials and Methods, Fig. B-1,B-2).

We found that in the presence of resistant bacteria, sensitive bacteria survived and even thrived at a clinically relevant [58] antibiotic concentration of 100 μg/mL, which is fifty-fold larger than their minimum inhibitory concentration (MIC) (Fig. 2-1A, Fig. B-3). A bacterial population with a high fraction of resistant cells inactivated the antibiotic quickly, allowing its sensitive cells to increase in frequency. Over time, the resistant fraction decreased until finally settling to a value of $\sim$0.25. To test whether this fraction corresponded to an equilibrium fraction, we started a culture at a fraction below the supposed equilibrium. One might have expected the resistant fraction to gradually converge to the equilibrium value. Instead, the resistant fraction initially overshot the equilibrium, jumping to $\sim$0.95, and only then proceeded to decay to the equilibrium. The resistant fraction at the end of the day therefore depends non-monotonically on the resistant fraction at the beginning of the day.

2.3.2 Using difference equation maps to study population dynamics

Since the final cell density after 23 hours of growth was approximately constant regardless of the starting conditions (Fig. B-4,B-5,B-6), the only parameter that changed

from day-to-day was the fraction of resistant cells. To examine how the final resistant fraction depended on the initial resistant fraction on a given day, we used the time course data (Fig. 2-1A) to generate a "difference equation" map (Fig. 2-1B) relating the fraction of resistant cells at the end and beginning of each day. As expected, the difference equation is non-monotonic as a result of the "overshoot" discussed previously, and the equilibrium fraction can be obtained by finding where the difference equation map crosses the 45-degree line. In principle, if the underlying difference equation is known, one can estimate the dynamics of the population over time by repeated application of the difference equation (or by the process of cobwebbing illustrated in Fig. 2-1B).

In an attempt to map the difference equation using data from a single day (instead of the eight-day time-course used in Fig. 2-1A, B), we started cultures at a range of different initial resistant fractions and measured the resulting final resistant fractions after a single day of growth (Fig. 2-1C). Such maps obtained over a single day of growth recapitulated the dynamics observed over multiple days, but with a slight overestimate of the equilibrium resistant fraction (Fig. 2-1B, Fig. B-7). As might be expected, cultures grown at higher antibiotic concentrations had a larger equilibrium fraction of resistant cells (Fig. 2-1C). However, the difference equations revealed that over a broad range of conditions, the sensitive cells could invade when present at low frequency. Starting with a resistant fraction below the equilibrium leads to an initial overshoot in the fraction of resistant cells in the population. After the overshoot, the resistant fraction proceeds to evolve to the equilibrium fraction, which is independent of the initial composition of the population. The resistant cells are not driven extinct by the sensitive "cheater" cells because β-lactamase is largely contained within the periplasmic space of the resistant cells [53, 59, 60], thereby giving them some preferential access to the benefits of their "cooperative" behavior [61]. Since both resistant and sensitive cells can invade the population when present at low frequency, we observe coexistence of the two strains even in our well-mixed liquid cultures [61–63]. This coexistence between "cooperators" and "cheaters" is similar to what is observed when individuals are playing the cooperative "snowdrift" game

[61], although it is important to note that our experimentally observed overshoot in resistant fraction over time (Fig. 2-1) indicates that the interactions between different cell types here is much richer than is assumed in the standard models in game theory.

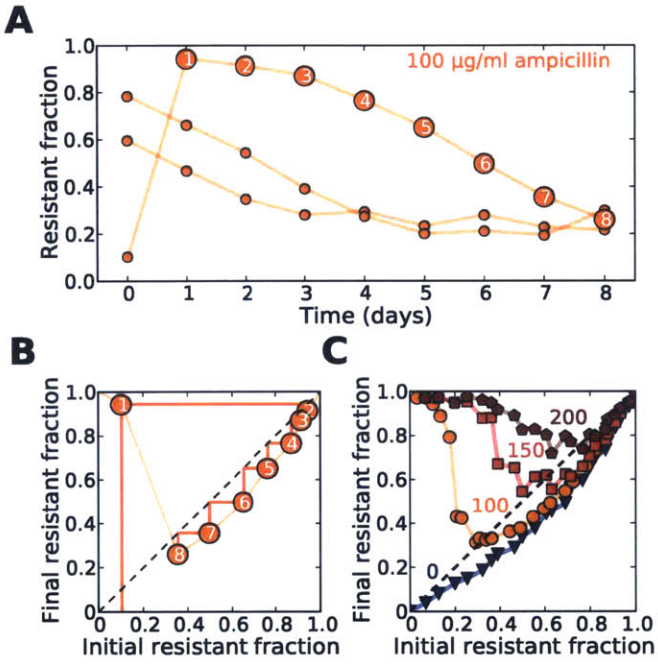

Figure 2-1: In the presence of resistant cells, sensitive cells can survive at otherwise lethal antibiotic concentrations. (A) Experimental time traces showing the evolutionary dynamics between sensitive E. coli and an isogenic strain that is resistant as the result of a plasmid containing a β-lactamase gene. A single resistant and a single sensitive colony were used to create 3 cultures with a different initial fraction of resistant cells. These 3 cultures were then grown for one day in the absence of ampicillin to make sure that resistant and sensitive cells experienced the same growth conditions (see Materials and Methods). Then, every 23 hours, the fraction of resistant cells was measured using flow cytometry, and the cultures were diluted by a factor of 100x into fresh media containing 100 μg/mL ampicillin. Each data point represents a single flow cytometry measurement. (B) The orange time trace that starts at 10that shows how the resistant fraction on day n+1 depends on the fraction on day n. The light orange line is an estimation of the difference equation. A simple trick to estimate the time dynamics with a difference equation is to use cobwebbing (dark orange lines), in which the daily dynamics are obtained by bouncing back and forth between the data line and the dashed diagonal line. (C) For each antibiotic concentration (indicated adjacent to each curve), a difference equation map was obtained experimentally by starting populations at 24 different initial fractions and measuring the final fraction after 23 hours of growth. The intersection of a given difference equation map with the diagonal line represents the equilibrium fraction for that particular condition.

2.3.3 A simple model captures the population dynamics

To better understand the population dynamics, we developed a simple model that describes the growth of the bacteria in the presence of antibiotics (Fig. 2-2A, B, Fig. B-8). For the range of antibiotic concentrations we probed, the resistant cells were essentially unaffected and grew at a constant rate of γ_R (Fig. B-8, B-9B, B-10). We assumed that sensitive cells grow at a rate $\gamma_S > \gamma_R$ for antibiotic concentrations below their MIC, but die at a rate γ_D for higher concentrations (Fig. B-3,B-8,B-9). Plating experiments showed that, in addition to cell death, we should incorporate a short lag phase that follows after inoculation of the bacteria into fresh media, during which bacteria neither divide nor die (Fig. B-9). We modeled antibiotic degradation phenomenologically using Michaelis-Menten kinetics with a maximum rate per cell V_{max} and an effective Michaelis constant K_M (A). While this model clearly neglects many aspects of bacterial growth in antibiotics, it successfully captures the key features of the dynamics (Fig. 2-1C, Fig. 2-2C) and predicts conditions that enable coexistence between resistant and sensitive cells (Fig. 2-2D).

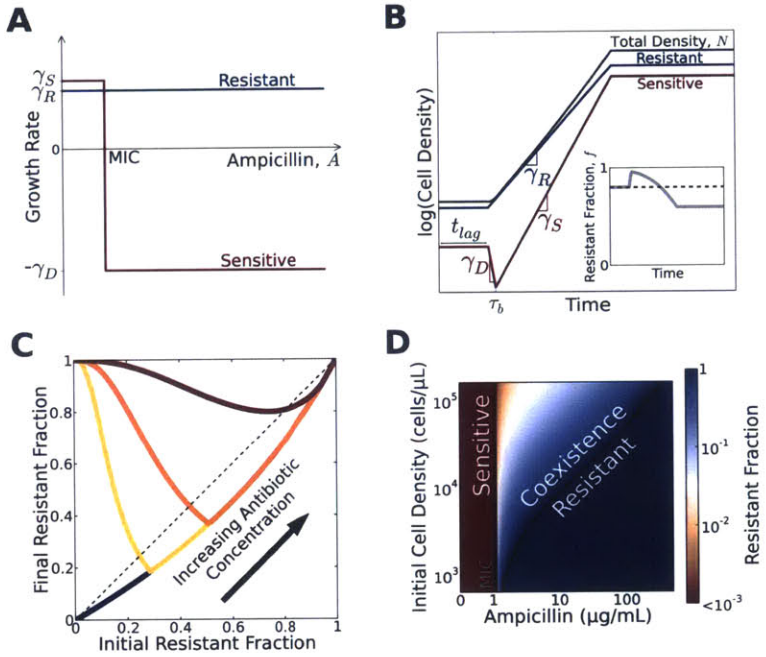

Figure 2-2: A simple model describes the population dynamics of a cooperative antibiotic resistance plasmid in the β-lactam antibiotic ampicillin. (A) Growth rates of resistant (blue) and sensitive (red) bacteria as a function of antibiotic concentration. Free of the metabolic cost associated with resistance, sensitive cells grow faster than resistant cells ($\gamma_S > \gamma_R$) at antibiotic concentrations below the MIC of the sensitive bacteria. Above the MIC, sensitive cells die at a rate of γ_D. (B) The population dynamics within a single competition cycle (one day). During the lag phase ($t < t_{lag}$), neither cell type divides nor dies, but the antibiotic is constantly hydrolyzed by resistant cells. After the lag phase, each sub-population grows at a rate that depends on the extracellular antibiotic concentration. At time τ_b, the extracellular antibiotic concentration drops below the MIC of the sensitive cells. Cell growth ceases when the total population density reaches saturation. Inset: The time trace of the resistant fraction within a single day. (C) The model gives rise to difference equations that resemble experimental data (Fig. 2-1C, Fig. 2-3A, B). (D) The equilibrium resistant fraction predicted by our model as a function of the antibiotic concentration and the initial cell density. According to the model, coexistence between resistant and sensitive cells is possible at antibiotic concentrations above the MIC of sensitive cells.

We obtained an exact analytic solution of this model that describes the dependence of the equilibrium resistant fraction, f_R, on the initial antibiotic concentration, A_i, and initial cell density, N_i. The model predicts that the equilibrium fraction scales in the following manner:

$$f_R \sim \frac{A_i + K_m \ln(A_i/\mathrm{MIC}) - \mathrm{MIC}}{V_{max} N_i} \xrightarrow{A_i \gg K_m, \mathrm{MIC}} \sim \frac{A_i}{V_{max} N_i}$$

This relationship is surprisingly insensitive to many parameters, including the length of the lag phase, rate of cell death, and cost associated with resistance (A). In particular, our analytic solution of the model predicts that the resistant fraction at equilibrium increases approximately linearly with the antibiotic concentration, a prediction borne out in experimental difference maps obtained at multiple antibiotic concentrations (Fig. 2-3A, B, C). Moreover, the model predicts that the equilibrium fraction is inversely proportional to the starting cell density. This prediction was experimentally confirmed by measuring the difference equations at four different starting cell densities. In each case, the equilibrium resistant fraction increases linearly with antibiotic concentration, but with slopes that decrease with increasing initial cell density (Fig. 2-3A, B, C). We therefore find a surprising simplicity to the population dynamics of the antibiotic resistance plasmid in the population, despite the biological complexity of the interaction between the cells and the antibiotic.

In addition to providing significant insight into the population dynamics, the model can quantitatively describe the experimental data. To acquire realistic parameters for the model, we measured the growth rate of resistant bacteria (γ_R=1.1/hr, Fig. B-9) and the relative growth rate of sensitive bacteria (γ_S/γ_R=1.15, Fig. B-11). Together these allowed us to deduce the overall metabolic cost of carrying the plasmid ($\gamma_S - \gamma_R$=~0.17/hr), which includes the cost of plasmid maintenance, of expressing the β-lactamase enzyme, and of expressing a red-fluorescent protein used for tracking the resistant fraction (Fig. B-1). Control experiments using another plasmid that did not express a fluorescent protein exhibited similar population dynamics (Fig. B-12). We proceeded to measure the death rate of sensitive bacteria in the presence of the

antibiotic (2.8/hr, Fig. B-9) and the lag time before cell growth/death (1 hr, Fig. B-9).

Using these experimentally measured parameters, we then fit our 30 measured equilibrium fractions (in Fig. 2-3C) to obtain estimates of MIC = 1.1 μg/mL, V_{max} = 10^6 molecules / (CFU·sec), and K_M = 6.7 μg/mL. This MIC is slightly lower than our measured value ($\sim$2 μg/mL, Fig. B-3) because antibiotic concentrations below the measured MIC already partially inhibit the growth of sensitive bacteria (Fig. B-3). In addition, our fitted value for the maximum rate of hydrolysis per cell V_{max} is reasonable since a single enzyme can hydrolyze as many as $\sim 10^3$ molecules per second [60]. Although the estimate of K_M agrees with literature values (from 4.9 to 26.5 μg/mL [64–66]), we note that the K_M in our model is a phenomenological parameter because antibiotic hydrolysis occurs both inside and outside the cells [59, 65]. The resistant fraction at equilibrium in our model increases linearly with the antibiotic concentration for $A > K_M$, but deviates slightly from linearity for $A < K_M$ due to the Michaelis-Menten kinetics of antibiotic degradation (Fig. 2-3C). This simple model not only captures the behavior of the equilibrium fractions, but also successfully predicts the experimental difference equations using the same parameter values (Fig. 2-3A, B, Fig. B-13).

Another way to think about the scaling predicted by the model is that, at equilibrium, the number of resistant cells is proportional to the antibiotic concentration ($N_{Ri} = f_R \cdot N_i \sim A_i$). Indeed, a plot of the equilibrium density of resistant cells against the antibiotic concentration revealed a striking collapse of the data extending over two orders of magnitude in the antibiotic concentration (Fig. 2-3D). Intuitively, more resistant cells would be required to deactivate larger amounts of the antibiotic within a fixed period of time. Non-intuitively, the model predicts that the time necessary for a bacterial population to saturate in the presence of the antibiotic is minimized at a resistant fraction that corresponds neither to the equilibrium fraction nor to a fully resistant population (Fig. B-14). Given the similarity between our experimental difference equations and the well-known "logistic equation" from theoretical ecology [67], we used our model to characterize when the equilibrium fraction is expected

to become unstable, leading to oscillations around the equilibrium. We found that the equilibrium fractions should become unstable as the antibiotic concentration decreases; however, the size of the oscillations does not become large enough to observe experimentally (Fig. B-15).

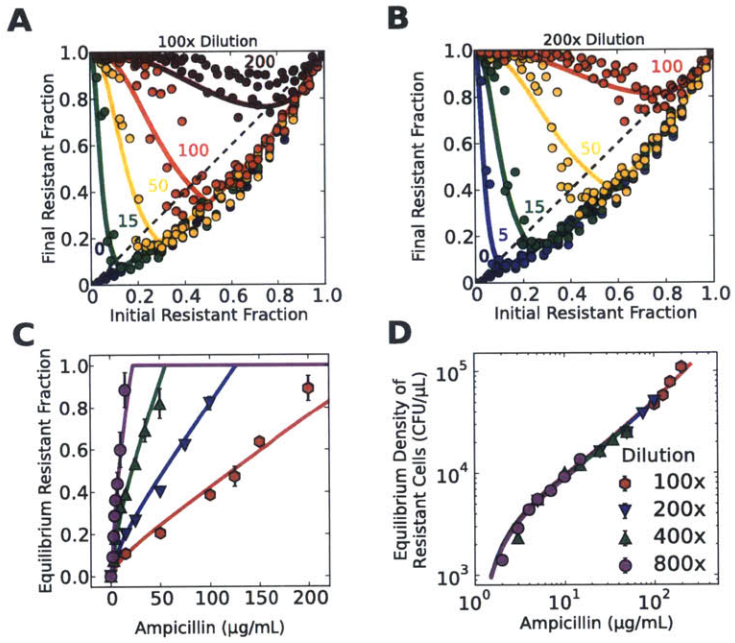

Figure 2-3: Experimental difference equations confirm model predictions regarding the equilibria and dynamics of resistant and sensitive bacteria. (A-B) Experimental difference equations obtained at two dilution factors (100x and 200x) and different antibiotic concentrations. At a given antibiotic concentration, an increase in the dilution ratio leads to stronger selection for resistance. Each difference equation plotted in a, b includes data obtained on 3 different days. Measurement error from flow cytometry was typically smaller than symbol size. (C) The equilibrium fractions as a function of ampicillin concentration at four different dilution factors (see Fig. B-13 for difference equations). The relationship is approximately linear for antibiotic concentrations higher than K_m. The equilibrium fractions were extracted from the difference equation plots by determining the intersection between the difference equations and the diagonal line (dashed line in (A)). Error bars represent standard error of the mean (n=3). (D) Plotting the initial density of resistant cells at equilibrium as a function of antibiotic concentration reveals a data collapse that extends over two orders of magnitude in the concentration. (A-D) Solid curves show a single fit of the model to all the experimental data.

2.3.4 Addition of a β-lactamase inhibitor selects for resistance

Given the predictive power of the model, we explored the expected consequences of adding a β-lactamase inhibitor such as tazobactam, which is used clinically together with many β-lactam antibiotics [57, 59, 68]. Tazobactam competitively binds β-lactamase enzymes [68, 69] and prevents them from hydrolyzing the antibiotic, leading to an increase in the effective Michaelis constant K_M. A sufficiently large increase in the Michaelis constant (K_M) can significantly compromise the ability of resistant cells to degrade the antibiotic, leading to complete inhibition of bacterial growth (Fig. B-16). However, if the increase in K_M is not sufficiently large, the resistant cells may survive the treatment, but the larger K_M would hinder their ability to protect sensitive cells against the antibiotic. Specifically, since the equilibrium fraction of resistant cells is proportional to K_M, the model predicts that adding a β-lactamase inhibitor will lead to an increase in the resistant fraction. We have tested this prediction and found that the addition of tazobactam can indeed result in a completely resistant population (Fig. 2-4A, Fig. B-17).

Not only does the model provide qualitative insight, it also makes surprisingly accurate quantitative predictions about the population dynamics that take place in the presence of the inhibitor. Although the actual mechanism of inhibition is more complicated [57], we modeled tazobactam as a competitive inhibitor, which increases the Michaelis constant K_M to $K_{eff} = K_M \cdot (1 + [I]/K_I)$, where $[I]$ and K_I are the inhibitor concentration and dissociation constant, respectively. Since the equilibrium fraction increases linearly with K_M, the model predicts that it should also increase linearly with the inhibitor concentration $[I]$. To probe this predicted dependence of the equilibrium fraction on the inhibitor concentration, we measured the equilibrium fractions from maps of difference equations obtained at varying tazobactam concentrations (Fig. 2-4B, C). We successfully fit the new 31 equilibrium fractions (Fig. 2-4C) using one additional free parameter K_I, confirming the predicted linear dependence on the inhibitor concentration. The K_I from the fit (4.6 ng/mL) was well within literature values (3 to 11.4 ng/mL [69–71]). Remarkably, using the value of

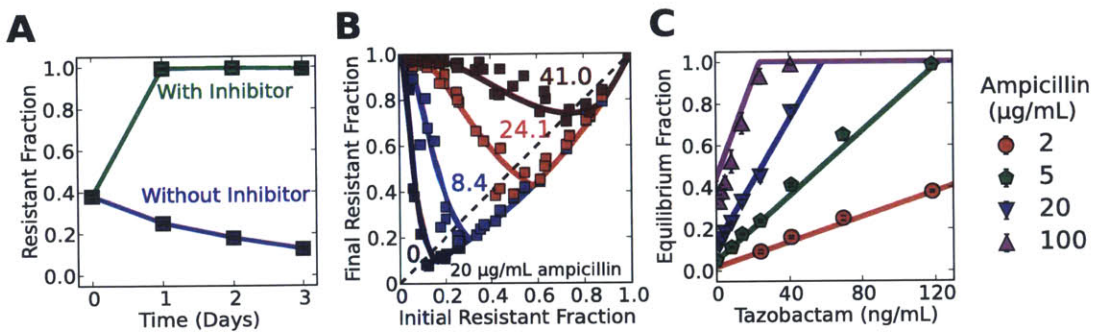

Figure 2-4: As predicted by the model, addition of the β-lactamase inhibitor tazobactam increases the fraction of resistant cells in the population. (A) Sensitive *E. coli* cells increase in frequency when grown in 20 μg/mL ampicillin in the absence of tazobactam; however, the addition of the inhibitor at a concentration of 1000 ng/mL results in a completely resistant bacterial population. Cultures were diluted daily by a factor of 100x into fresh media containing 20 μg/mL ampicillin. Error bars represent standard error of the mean of 4 different bacterial cultures. (B) Experimental difference equation maps for 4 different concentrations of the inhibitor tazobactam (in ng/mL) at a background of 20 μg/mL ampicillin and dilution factor of 100x (see Fig. B-17 for more difference equations). Each difference equation map contains data obtained on 3 different days. (C) As predicted by the model, the equilibrium fractions depend linearly on the concentration of the inhibitor tazobactam with a slope that depends on the ampicillin concentration. The equilibrium fractions were extracted from the difference equation plots by determining the intersection between the difference equations and the diagonal line (dashed line in (A)). Error bars represent standard error of the mean (n=3). (B-C) Solid curves show a fit of the model to all the experimental data with a single free parameter of $K_I = 4.6$ ng/mL (other parameters held fixed).

K_I obtained from the fits to the equilibrium fractions successfully recapitulated the dynamics across the entire range of the difference equations (Fig. 2-4B, Fig. B-17).

To verify that our conclusions were not limited to tazobactam, we tried the β-lactamase inhibitor sulbactam, which is often administered together with ampicillin clinically [58, 68, 69]. We found that at least for our experimental conditions (*E. coli* bacteria inoculated at an initial cell density $\sim 10^5$ cells/μL), the addition of sulbactam can lead to the accelerated spread of resistant bacterial cells in a range of clinically relevant antibiotic concentrations (Fig. B-18).

2.4 Discussion

We have presented a quantitative analysis of the population dynamics that stem from the cooperative nature of antibiotic inactivation, and which can lead to coexistence between sensitive cells and resistant cells. Our analysis was based on two key features: (1) the presence of a metabolic cost associated with being resistant, and (2) the inactivation of the antibiotic by resistant cells. When both features apply, our model suggests that resistant and sensitive cells may coexist at high concentrations of the antibiotic, with the fraction of resistant cells approximately proportional to the antibiotic concentration divided by the cell density. We found that this simple dependence on antibiotic concentration and cell density successfully predicts the equilibrium fraction of resistant cells over two orders of magnitude in antibiotic concentration (Fig. 2-3D).

This model not only agrees quantitatively with experimental data, but it also provides insight into the conditions that enable coexistence between resistant and sensitive cells. For example, a recent study observed coexistence with a mutated β-lactamase enzyme that inactivated the antibiotic outside of the cell [54], allowing resistant cells to efficiently "share" their resistance with the bacterial population to support coexistence. However, in our study, we were able to observe coexistence even with a wild-type β-lactamase enzyme, which is primarily periplasmic [59]. To properly interpret these results, it is important to recognize that the site of antibiotic inactivation determines the degree of preferential protection offered to resistant cells. Furthermore, as long as resistant cells are sufficiently protected to be unaffected by

the antibiotic, only the overall rate of antibiotic inactivation is important in determining the dynamics between resistant and sensitive cells. Hence, even if antibiotic inactivation occurs inside the cell, it is still a cooperative behavior that may allow sensitive cells to survive.

The interplay between initial cell density and antibiotic concentration is often important in determining growth dynamics in antibiotics [42, 72]. Likewise, our model suggested that the key parameter in governing the population dynamics was not the antibiotic concentration, but the ratio between the antibiotic concentration and the initial cell density. Specifically, we found that at high cell densities, resistant cells could protect sensitive cells against antibiotic concentration as high as 200 μg/mL (Fig. 2-3A), which is a hundred-fold higher than the minimum inhibitory concentration of sensitive cells. Given the cooperative nature of antibiotic inactivation, it is likely that other ecological factors will be important to consider when attempting to understand the evolution of antibiotic resistance [73–75].

One might worry that our conclusions may be limited to laboratory strains since natural strains would be better adapted to plasmids found in the wild. However, our model and experiments argue that the equilibrium fraction depends only weakly on the fitness cost of carrying the resistance plasmid (Fig. B-19). Compensatory mutations that alleviate the cost of resistance [49–51] will increase the time it takes the population to settle into its equilibrium fraction, but will not significantly change that fraction. Since our model only uses a few key phenotypic traits to characterize the outcome of bacterial growth in the antibiotic, it should be broadly applicable in describing both intra-species [54] and inter-species [46] dynamics.

Within the framework of our model an important qualitative difference between using a bactericidal versus a bacteriostatic antibiotic is that the overshoot of the resistant fraction above the equilibrium fraction should only appear when using a bactericidal antibiotic (Fig. 2-1A, Fig. B-20). The lower the initial resistant fraction is, the longer it takes for the antibiotic to be inactivated, and the more opportunity there is for a bactericidal antibiotic to kill the sensitive strain and promote the growth of the resistant strain.

Throughout our experiments, we limited ourselves to antibiotic concentrations which do not affect the growth of resistant cells. However, at high enough concentrations, a bactericidal antibiotic may lead to lysis of resistant cells and the subsequent release of their beta-lactamase enzymes into the extra-cellular space [76]. Since these enzymes inactivate the antibiotic even faster extracellularly, the death of resistant cells may further increase the cooperative nature of bacterial growth in the antibiotic [77]. Such a scenario may explain the observed non-monotonic selection for resistance and difference equation maps that deviate from our model at high concentrations of the β-lactam antibiotic piperacillin (Fig. B-21).

Understanding how the fraction of resistant bacteria changes with time is a central goal in studying antibiotic resistance. This already difficult task is further complicated by cooperative behaviors that allow resistant microbes to "share" their resistance with the rest of the bacterial population. The cooperative nature of antibiotic inactivation causes the fitness of resistant cells to decrease as their fraction in the bacterial population increases (i.e., it leads to negative frequency dependent selection [54], Fig. 2-3A, B). Overall, this enables coexistence between resistant and sensitive cells, even in the absence of the spatial structure present in biofilms [78–80], interactions between bacteria and antibiotic degradation products [81], bacterial persistence [82], and indole production [83]. Since antibiotic inactivation is a frequent mechanism of antibiotic resistance [14], similar population dynamics may appear with other classes of antibiotics (e.g., macrolides, aminoglycosides) and with chromosomally encoded enzymes. However, despite the potential ubiquity of cooperative antibiotic resistance, the social aspect of antibiotic resistance remains under-appreciated, highlighting the importance of quantitatively characterizing social interactions to gain a thorough understanding of the maintenance of phenotypic and genotypic diversity within populations.

2.5 Materials and Methods

2.5.1 Strains

All strains are derived from *Escherichia coli* DH5α. The resistant strain contained the pFPV-mCherry plasmid [84] (also see Addgene plasmid 20956), expressing a TEM-1 β-lactamase enzyme and an mCherry fluorescent protein. In addition, the resistant and sensitive strains expressed cerulean and yellow fluorescent protein genes, respectively, under the promoter P_{lac}UV5, and a kanamycin resistant gene, both carried on the plasmid pZS25O1+11 [85, 86] (origin of replication: pSC101). Control experiments in which the cerulean and yellow fluorescent markers were swapped gave nearly identical difference equation maps (Fig. B-22).

2.5.2 Competition Experiments

All cultures were grown in a shaker at 500 rpm and 37 °C. Before the competition experiments, single colonies of resistant and sensitive strains were grown separately in 5 mL lysogeny broth (LB) together with antibiotics for selection for 23 hours. The saturated cultures (corresponding to a density of $\sim 10^7$ cells/μL) were diluted by a factor of 100x and co-cultured at different fractions in 96 well-plates containing LB and 5 μg/mL of kanamycin for another 23 hours to synchronize the growth state of both strains (see Fig. B-11). All competition experiments were carried out using synchronized mixed cultures. The cultures were diluted into 96 well-plates containing 5 μg/mL of kanamycin, LB, and appropriate concentrations of ampicillin, tazobactam and sulbactam, and grown for another 23 hours. In multi-day experiments, cultures were serially diluted into 96-well plates containing freshly prepared media with appropriate concentrations of antibiotics. Control experiments showed that the population dynamics were similar regardless of whether kanamycin was absent or present at 5 μg/mL (Fig. B-23). In addition, control experiments showed that similar growth dynamics apply in other β-lactam antibiotics (Fig. B-24). Fractions were determined using flow cytometry on a BD-LSR II and confirmed by plating (Fig. B-1,B-2).

Chapter 3

Seasonality Gives Rise to Oscillatory Dynamics in a Bacterial Cross-Protection Mutualism

3.1 Overview

Understanding how bacteria survive and respond to antibiotic exposure is important both clinically and ecologically. A common mechanism of antibiotic resistance involves the inactivation of antibiotics by resistant bacteria. Inactivation of antibiotics is a cooperative behavior, which can allow resistant bacteria to protect sensitive bacteria against antibiotics, altering the dynamics of how antibiotic resistance spreads. However, despite the prevalence of antibiotic inactivation as a mechanism of antibiotic resistance, how it affects the population and evolutionary dynamics of microbial populations remains poorly understood, particularly in the presence of more than one antibiotic. Here, we investigate whether two *Escherichia coli* strains can protect each other in the presence of chloramphenicol and ampicillin. Our experiments reveal that the two strains can form an effective cross-protection mutualism, helping each other survive in antibiotic concentrations that inhibit growth of either strain alone. Moreover, we find that "seasonality" (introduced by periodic dilution into fresh media sup-

plemented with antibiotics) gives rise to large oscillations in the relative abundances of the two strains, with an oscillation period longer than the period between successive antibiotic exposures. While the mutualism remains stable in modest antibiotic concentrations, the mutualism collapses at high antibiotic concentrations due to the oscillations which destabilize the mutualism. The ability of the two strains to form a successful cross-protection mutualism without requiring a period of co-evolution indicates that similar mutualisms may frequently arise in course of the antibiotic treatment and in natural environments such as the soil.

3.2 Introduction

Mutualisms are reciprocal positive interactions between two species. Because mutualisms are thought to be fundamentally important in many ecosystems, ecologists have devoted significant time studying their evolution, stability, and ecological function [87–94]. One of the best studied mutualisms is the one formed between flowering plants and their pollinators. In this mutualism, the pollinator mediates the reproduction of the plant and in return receives nutrition [94]. More broadly, positive interactions are abundant in nature and can take on many forms: one species can increase the fitness of another by providing nutrition, protection, or transportation [94, 95], and the benefits from a positive interaction may arise immediately or at a later time.

The desire to understand the basic forces that shape microbial communities has created a recent surge of interest in microbial mutualisms [96–102]. So far the majority of studies of microbial mutualisms have focused on cross-feeding [97–99, 103] due to the apparent abundance of this type of interaction. However, another potentially frequent microbial interaction involves the protection of one microbe by another [40, 41, 83], which could lead to the formation of cross-protection mutualisms. Protective interactions are especially interesting in the context of antibiotic resistance, where they may influence the spread of antibiotic resistance genes [47, 104].

A common mechanism of antibiotic resistance in bacteria involves the production

of enzymes that modify and deactivate the target antibiotic [13, 14]. Resistant cells can protect sensitive cells by reducing the concentration of active antibiotics in the environment, allowing their sensitive neighbors to survive in otherwise lethal concentrations [46–48]. Hence it is conceivable that cooperative antibiotic deactivation could allow a bacterial community composed of multiple resistant bacterial strains to survive in a multi-drug environment, even if some strains were not individually resistant to each drug present. In this work, we investigate whether two bacterial populations can form a cross-protection mutualism in a two-drug environment and explore the dynamical properties of this mutualism.

3.3 Results

3.3.1 A cross-protection mutualism

To explore the possibility of a microbial cross-protection mutualism, we developed a model system that consists of two strains of *E. coli*, each of which is resistant to a different antibiotic. Each strain produces an enzyme that deactivates one of the two antibiotics in the environment, thereby potentially allowing the other strain to survive the presence of the antibiotic. The first strain is ampicillin-resistant as a result of a plasmid carrying a gene encoding a β-lactamase enzyme, which deactivates ampicillin (Fig. 3-1A). This enzymatic deactivation can take place in the extracellular medium, thus leading to immediate benefits to the sensitive partner. The second strain is chloramphenicol-resistant as a result of a plasmid carrying a gene encoding the chloramphenicol acetyltransferase Type I enzyme, which deactivates the antibiotic chloramphenicol [105]. Although this enzymatic deactivation occurs inside the cell, diffusion of chloramphenicol between the media and the interior of resistant cells may cause the extra-cellular concentration of the antibiotic to decrease enough to allow the growth of sensitive cells. Given that each strain has the potential to provide at least partial protection to the other strain, it may be possible that the two strains could help each other survive in environments containing both antibiotics (Fig. 3-1A).

To probe the extent to which the partnership between the two strains enables survival, we propagated the strains together with daily dilutions into fresh media (Fig. 3-1B, see also Materials and Methods). We found that the co-culture was able to survive for at least ten days with daily a 100-fold dilutions into fresh media containing 10 μg/ml ampicillin and 11 μg/ml chloramphenicol (Fig. 3-1E, C-1). These antibiotic concentrations are fourfold larger than the minimum inhibitory concentration (MIC) of the sensitive strain to each antibiotic, suggesting that survival of the co-culture relies on each partner of the mutualism protecting the other. Indeed, we found that neither of the two strains could survive this environment alone (Fig. 3-1C-D). Our two antibiotic resistant strains therefore form an effective obligatory mutualism that allows for survival in antibiotic concentrations that are many times higher than those at which the strains can survive on their own.

An important aspect of the mutualism between these two strains is that the co-culture survives many days of growth and dilution (Fig. 3-1E, C-1). It would have been possible for the mutualism to allow the co-culture to grow (and even saturate) over the first day but for the co-culture not to survive subsequent dilution-growth cycles. Indeed, we found that our co-culture saturated during the first day of growth up to even higher antibiotic concentrations but that the population collapsed soon thereafter (Fig. C-2, C-1). Initial growth of the co-culture therefore does not guarantee that the mutualism is stable: in addition to maintaining a high total population density, a mutualism requires that the underlying subpopulation dynamics are sustainable.

3.3.2 Seasonality gives rise to strong oscillatory dynamics

To explore the population dynamics of the mutualism, we co-cultured our two strains in a variety of antibiotic concentrations and measured the population sizes of each partner strain using a combination of spectrophotometry and flow cytometry. Spectrophotometry enabled us to measure the total population size of the co-culture. Flow cytometry allowed us to measure the relative abundances of each strain because the antibiotic resistant plasmids also encoded different colored fluorescent proteins (see

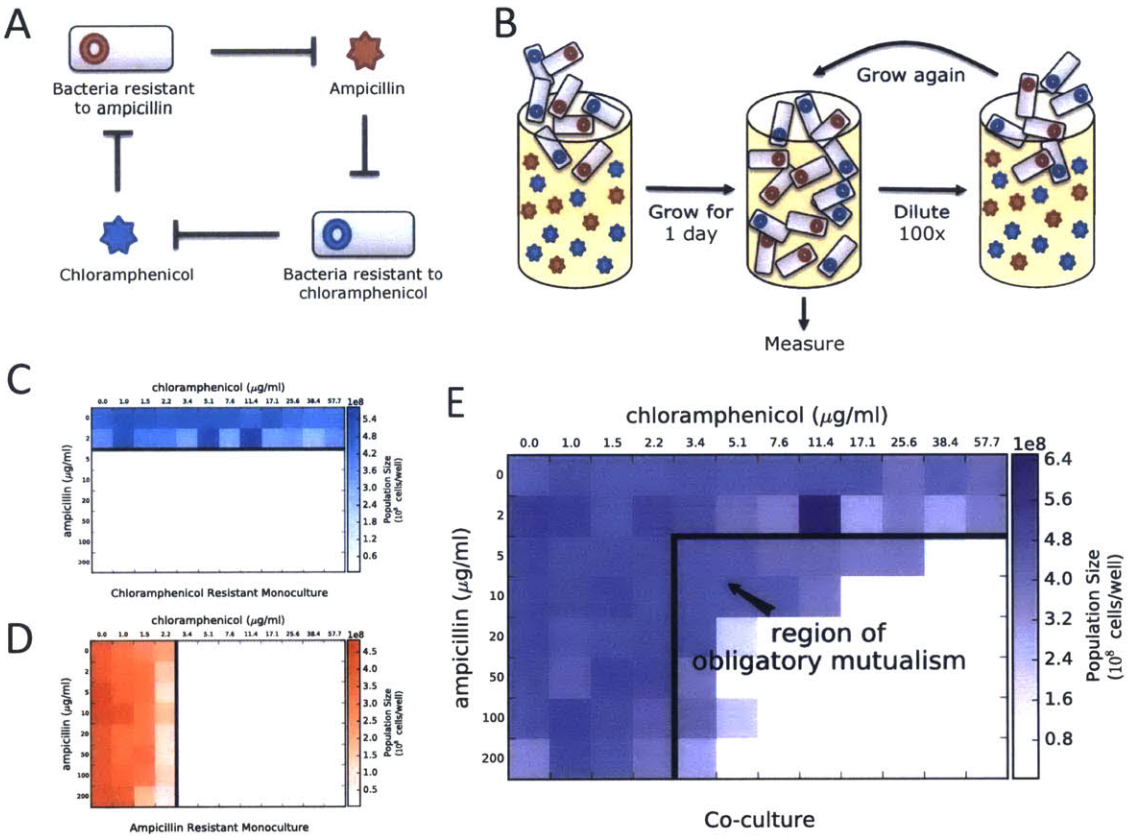

Figure 3-1: Two strains of resistant bacteria can form a mutualism in a multi-drug environment by protecting each other from antibiotics. (A) In an environment containing the antibiotics ampicillin and chloramphenicol, a mutualism might form between bacteria producing a beta-lactamase enzyme (which protects against ampicillin) and bacteria producing a chloramphenicol acetyltransferase enzyme (which protects against chloramphenicol). Both resistant genes are carried on plasmids (see Materials and Methods). (B) In our serial dilution experiments, we periodically diluted microbial cultures into fresh growth medium, replenishing the supply of nutrients and antibiotics. To track population dynamics, we determined the size of each subpopulation by combining spectrophotometry measurements of the total culture density together with flow cytometry measurements of the relative abundances of each subpopulation. (C) A chloramphenicol resistant mono-culture can survive in high concentrations of chloramphenicol but cannot survive alone in ampicillin concentrations above 2 μg/ml. (D) Similarly, an ampicillin resistant mono-culture can survive in high concentrations of ampicillin but cannot survive alone in chloramphenicol concentrations above 2.2 μg/ml. (E) A co-culture of the two strains can survive above the concentrations at which the individual strains survive alone, indicating that the two populations form an obligatory mutualism. The populations shown in (C,D,E) were subject to five daily dilution cycles at 100X.

Materials and Methods, Fig. C-3). Combining the results of these two measurements, we calculated the subpopulation sizes.

The population dynamics of the co-culture in the region of obligatory mutualism revealed remarkable oscillations in the abundances of the two partner strains (Fig. 3-2). These oscillations typically had a period of three days, and the ratio of the fractions spanned four orders of magnitude (Fig. 3-3A). Importantly, these oscillations occurred with a period (three days) longer than the period of the daily dilution (one day), meaning that the oscillations are not a trivial consequence of the daily growth-dilution cycle. We therefore conclude that, in addition to the positive-negative feedback loops often found in predator-prey systems, cross-protection mutualisms can exhibit oscillations in population abundances as well.

To see why this cross-protection mutualism might exhibit oscillations, we should consider the dynamics of the two bacterial populations and the two antibiotics. Suppose that initially one of the strains is significantly more abundant than the other. This strain rapidly deactivates its "target" antibiotic, allowing its mutualistic partner to start growing. A key ingredient driving the oscillations is the inability of the first strain to start growing until its partner becomes abundant. After reaching a large population size, the partner strain can deactivate the antibiotic that inhibited the growth of the first strain, allowing the first strain to finally start growing. However, at this point, it is too late for the first strain to catch up with its partner which is far more abundant. Because in each cycle the strain that starts out being more abundant ends up being less abundant, the mutualism might exhibit period 2 oscillations. Asymmetries in how the two bacterial populations respond to antibiotics and deactivate antibiotics can give rise to oscillations with more interesting periods.

A simple mechanistic model incorporating the basic time dynamics of the two strains and the two antibiotics can indeed yield an obligatory mutualism with period three oscillations (Fig. C-4). Moreover, this model and the reasoning provided in the previous paragraph suggest that the oscillations that we observe experimentally are due to the "seasonality" imposed as a result of our daily dilution (Fig. C-6, C-7, C-5). In particular, our model predicts that in a continuous culture experiment in

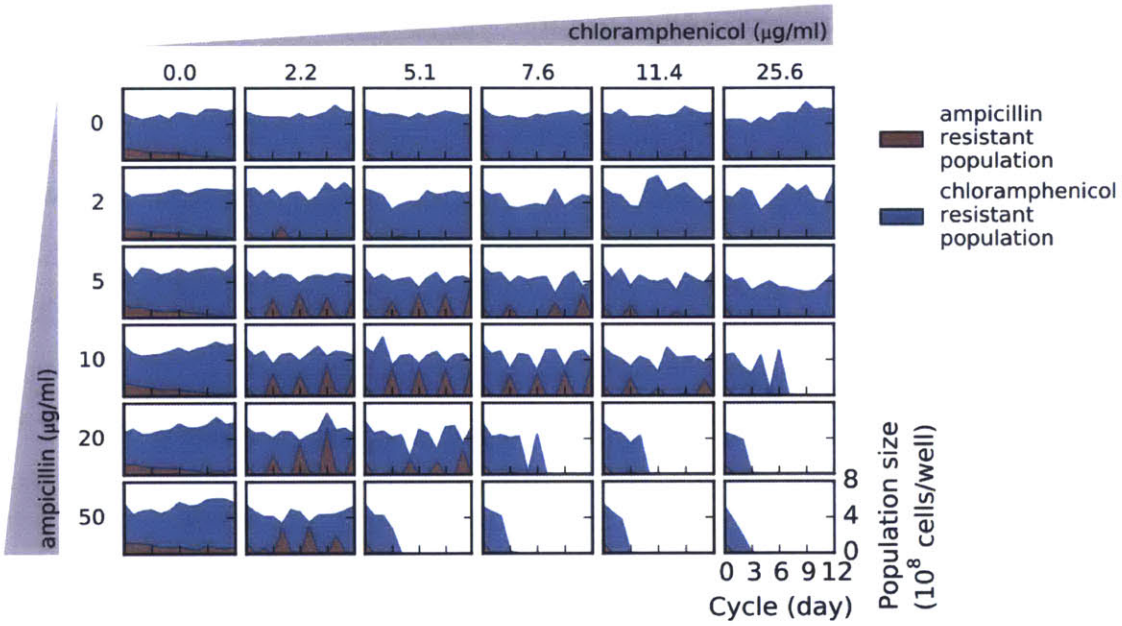

Figure 3-2: The subpopulation sizes of the two mutualists oscillate over a broad range of antibiotic concentrations, both in and out of the region where the mutualism is obligatory. Many of the mutualisms settled into a period-3-like oscillation, which had a period longer (period 3) than the period between successive exposures to antibiotics (period 1). These oscillations were substantial in magnitude with the relative abundances of the two mutualists changing by as much as 10^4-fold. The red region of each subplot represents the size of the ampicillin resistant subpopulation and the blue region represents the size of the chloramphenicol resistant subpopulation. In this experiment, the co-cultures were diluted by a 100-fold every 24 hours into fresh media supplemented with antibiotics. When subject to a smaller dilution strength (10-fold), the mutualism survived in even larger antibiotic concentrations and the oscillations shifted to higher antibiotic concentrations (Fig. C-10).

which the antibiotics are constantly added (and cells constantly removed) there will be no oscillations in the population abundances (Fig. C-5).

To test this prediction we performed a (pseudo) continuous experiment by diluting the co-cultures every hour by a small amount (1.2-fold) into fresh medium supplemented with ampicillin (10 μg/ml) and chloramphenicol (5.1 μg/ml), mimicking a chemostat operating at a fixed dilution rate (Fig. 3-3B). We found that with frequent dilution the co-culture was able to form a stable mutualism, with the strain fractions reaching a stable equilibrium without oscillations. The dilution time and amount in these experiments was chosen so that the effective "dilution rate" would be equivalent to that in our batch culture experiments, but a stable equilibrium was observed even for higher dilution rates (Fig. C-8). Moreover, within the daily dilution experiments we could also remove the oscillations by reducing the amount by which we diluted each day (Fig. C-9, C-10). These experiments confirm that it is the seasonality of periodic dilutions that is driving the oscillations that we observe in daily batch culture.

A major question for any oscillations observed in populations is whether the oscillations are due to a true limit cycle that has a well-defined amplitude and period. This is important because the classic Lotka-Volterra model of predator-prey populations displays oscillations that are neutrally stable and therefore have an amplitude and period that is determined by the initial conditions [106]. To probe the nature of the oscillations that we observe in our experiments, we initiated co-cultures at a wide range of starting fractions in the same antibiotic concentrations (10 μg/ml ampicillin and 5.1 μg/ml chloramphenicol). Because these populations grew to the carrying capacity by the end of each cycle, the fraction of the ampicillin resistant subpopulation was sufficient to specify the trajectories. Consistent with our oscillations being a true limit cycle, we found that a wide range of starting conditions all led to the same period-3-like oscillation pattern (Fig. 3-4A). Although this oscillation pattern is suggestive of a period 3 limit cycle, the combination of experimental noise and time required to converge to the limit cycle make it difficult to distinguish period 3 from longer periods (e.g., period 6). We note that while in this example all the trajectories

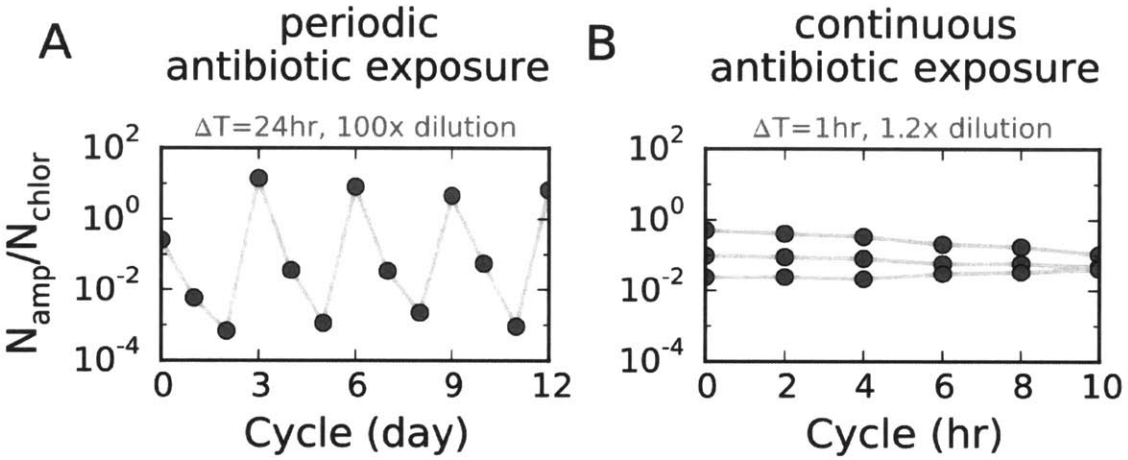

Figure 3-3: "Seasonality" (imposed by periodic dilution of the co-culture into fresh media containing antibiotics) gives rise to oscillations in the relative abundances of the two mutualists. (A) Under periodic exposure to antibiotics, the relative abundances of the two mutualists in the co-culture oscillate by as much as 10^4-fold. (B) Under (pseudo)-continuous exposure to antibiotics, the relative abundances of the two mutualists converge to an equilibrium ratio. To transition from the periodic / seasonal regime (subplot A) to the (pseudo)-continuous regime (subplot B), we decreased the time between consecutive dilutions from $\Delta T = 24$ hrs to $\Delta T = 1$ hr and the dilution strength from 100-fold to 1.2-fold. The dilution amount in the (pseudo)-continuous regime was chosen so that the death rate due to dilution, $\ln(\text{dilution strength})/\Delta T$, would be equivalent between the two regimes. In these experiments, the amount of antibiotic added in each cycle was sufficient to raise the concentration of ampicillin and chloramphenicol to 10 μg/ml and 5.1 μg/ml, assuming that all the antibiotic from the previous cycle was fully inactivated.

ended up oscillating in phase with one another, in general the phase of the oscillations depends on the starting condition. We observed stable, limit cycle oscillations in a range of antibiotic concentrations, both in and out of the region where the mutualism was obligatory (Fig. C-11, C-12).

3.3.3 Oscillations can destabilize the mutualism

At the antibiotic concentrations in which we observe an obligatory mutualism it is perhaps expected that survival of the co-culture requires starting with sufficiently large concentrations of each partner in the mutualism. To test this expectation, we measured trajectories of co-cultures starting at a broad range of initial conditions, including extreme relative subpopulation fractions and very low cell densities. We found that the ability of the mutualism to survive and converge to the limit cycles depends on its initial subpopulation composition: specifically, when the initial population size of either mutualist was too small, the mutualism collapsed (Fig. 3-4B).

Based on our measurements of the population dynamics over a broad range of conditions, we propose a simple time-discrete framework to provide a qualitative explanation of the population dynamics of the mutualism in the presence of periodic antibiotic exposure (Fig. 3-4C). In this framework, depending on the initial population composition, the mutualism either converges to a limit cycle or collapses. The boundary that separates the set of trajectories that map to each fate is referred to as the separatrix (we note that since this system displays discrete dynamics the separatrix does not have to be well-defined in this way, but we believe that this approach adequately describes our experimental data).

This framework suggests a simple explanation for why the mutualism might collapse as the environment deteriorates (either via increased antibiotic concentrations or via increased dilution rates): deteriorating the environment could push the limit cycle oscillation closer to the separatrix, increasing the likelihood that the oscillations would push the population composition of the mutualism too far to oscillation one side (Fig. 3-5A).

To test the intuition provided by this model, we proceeded to map the separatrix

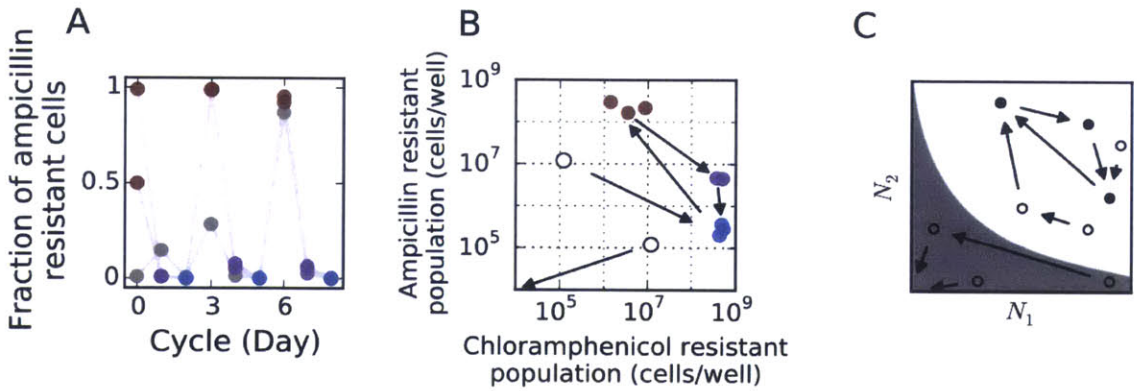

Figure 3-4: In the presence of seasonality, the mutualism has a limit cycle in which the two mutualists stably coexist while oscillating. (A) Examining the mutualisms where the total population size remained close to the carrying capacity, we found that the fraction of the ampicillin resistant subpopulation settled to a period-3-like oscillation. (Color coding indicates the phase of the oscillation.) (B) The ability of the mutualism to survive and converge to the limit cycle depends on its subpopulation composition. When the population of either mutualist is too small, the mutualism collapses. (C) A discrete-time framework of an obligatory mutualism featuring a "healthy state" characterized by a limit cycle and a "collapsed state", with a boundary (called a separatrix) separating the sets of subpopulation compositions converging to the two states. (A-B) Experiments were carried out in an environment inside the region of obligatory mutualism (100x dilution strength, 24 hr dilution cycle, 10 μg/ml ampicillin, 5.1 μg/ml chloramphenicol). (B-C) Open circles indicate population compositions that have not converged yet to the limit cycle.

in relatively modest antibiotic concentrations (Fig. 3-5B, 3-4B, 10 μg/ml ampicillin, 5.1 μg/ml chloramphenicol). We assumed that the current population composition probabilistically determines its future composition independent of history (i.e., that the dynamics follow a Markov process). We approximated the separatrix as the set of population compositions that lead to a 50% probability of reaching a healthy population size in the next cycle (cutoff at $2 \cdot 10^8$ cells/well). Indeed, failure to reach a healthy population size frequently led the mutualism to collapse shortly afterwards (Table C.1). We confirmed that, in this environment, the limit cycle was far away from the separatrix, consistent with our observation that any mutualism that successfully converged to the limit cycle was stable for a long time (Fig. 3-4B).

To study how the mutualism collapses, we mapped the separatrix in progressively harsher environments containing more chloramphenicol. As expected, increasing the amount of chloramphenicol pushed the limit cycle and separatrix toward each other (Fig. 3-5B, C-13). Importantly, only one extreme of the limit cycle got close to the separatrix. Specifically, the collapse was caused by losing too much of the ampicillin resistant subpopulation, which prevented the mutualism from attaining a high density in the following cycle (Fig. 3-5B). As might be expected from trajectories venturing close to the separatrix, as the antibiotic concentration increased the trajectories became more erratic, gradually losing their characteristic period 3 oscillation (Fig. 3-5B, C-14, C-15).

3.3.4 Evolutionary stability of the mutualism

Up to now we have focused on the ecological stability of the mutualism allowing survival of the co-culture in a multi-drug environment. It is also important to consider the evolutionary stability of the mutualism; i.e., the ability of the mutualism to survive invasion. For example, the base DH5α *E. coli* strain lacking both plasmids that encode resistance is sensitive to both antibiotics, and would therefore rely on the mutualistic strains for survival (Fig. C-16). On the other hand, this strain does not pay the metabolic cost associated with maintaining the plasmid, giving it a growth advantage relative to either resistant strain in the absence of antibiotics. As such, it

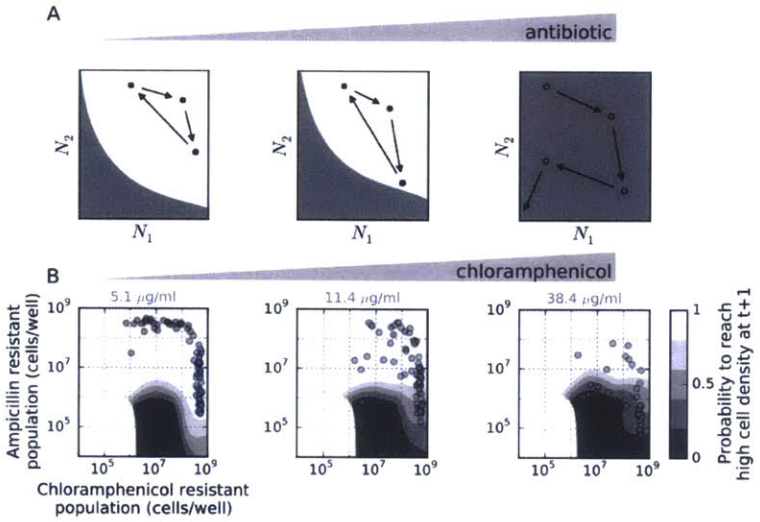

Figure 3-5: The mutualism collapses in harsher environments because the oscillations skew the ratio between the two mutualists, destabilizing the mutualism. (A) In the time-discrete framework of the obligatory mutualism, increasing the antibiotic concentration brings the limit cycle and the separatrix closer to one another. Upon hitting the separatrix, the limit cycle disappears, leading to the subsequent collapse of the mutualism. (B) In the relatively benign environment (100x dilution strength, 24 hr dilution cycle, 10 μg/ml ampicillin, 5.1 μg/ml chloramphenicol), the limit cycle was far away from the separatrix, indicating that in this environment the mutualism should persist indefinitely. However, in environments with higher chloramphenicol concentrations, the limit cycle and the separatrix were significantly closer, destabilizing the mutualism and causing it to collapse. To determine the location of the separatrix, we estimated the probability that a particular initial population composition reached a healthy population size in the next cycle (cutoff at approximately half the carrying capacity or $2 \cdot 10^8$ cells/well). The separatrix was approximated as the set of population compositions that led to a 50% probability of reaching a healthy population size in the next cycle. Because stochasticity "blurs" the separatrix, the limit cycle does not hit the separatrix suddenly; rather, the probability of the population to survive worsens as it crosses the separatrix. In these experiments, the co-cultures were diluted by a 100-fold every 24 hours into a medium containing 10 μg/ml of ampicillin and the indicated amount of chloramphenicol. Points correspond to snapshots of the different co-cultures measured over the course of the experiment, showing data after the first two cycles of growth. Color-coding indicates the inferred phase of the oscillation whenever a robust oscillation pattern was detected. No experimental measurements were taken for the white region in the bottom-left of the subplots.

can be considered a cheater strain, because it benefits from the mutualists but does not contribute to the common good.

This reasoning led us to ask whether or not a sensitive strain could exploit the mutualists for protection against antibiotics, proliferate in the population, and destabilize the mutualism or alter the limit cycle oscillations. Interestingly, we found that the sensitive strain, when seeded at a low subpopulation fraction on the first day along with the mutualistic resistant strains, did not affect the survival of the mutualism (Fig. C-17). Upon further inspection, we found that sensitive cells arise naturally due to plasmid loss, and comprise a few percent of the total population in our original experiments probing the mutualism (Fig. C-18). This multi-drug environment therefore leads to coexistence of all three bacterial strains: the two resistant strains together with the sensitive strain.

In contrast to a sensitive strain, a double resistant strain is self-sufficient and does not require protection from the mutualistic strains to survive (Fig. 3-6A). The double resistant strain carries both plasmids conferring antibiotic resistance. While a double resistant cell can grow in the presence of both antibiotics (up to higher antibiotic concentrations than allowed by the mutualism and before deactivation allows the single resistant cells to grow), its growth rate in the absence of antibiotics is lower because of the fitness cost associated with having two plasmids. We note that over the time course of our experiments we did not observe any double resistant cells arising naturally (unsurprising since the plasmids we used are not conjugative).

To explore whether the double resistant strain could invade and/or displace the mutualism, we added a small fraction of double resistant cells to mutualism cultures six days into a coexistence experiment (Fig. 3-6BC). Strikingly, upon introducing the double resistant strain, the oscillations disappeared. In addition, we found that the double resistant population was able to take root in the culture, eventually displacing the ampicillin resistant strain. Presumably this happens because the fitness cost due to the inhibition of growth by chloramphenicol is larger than the fitness cost associated with acquiring the chloramphenicol resistance plasmid. Once the ampicillin resistant cells are gone, the double resistant cells protect the chloramphenicol

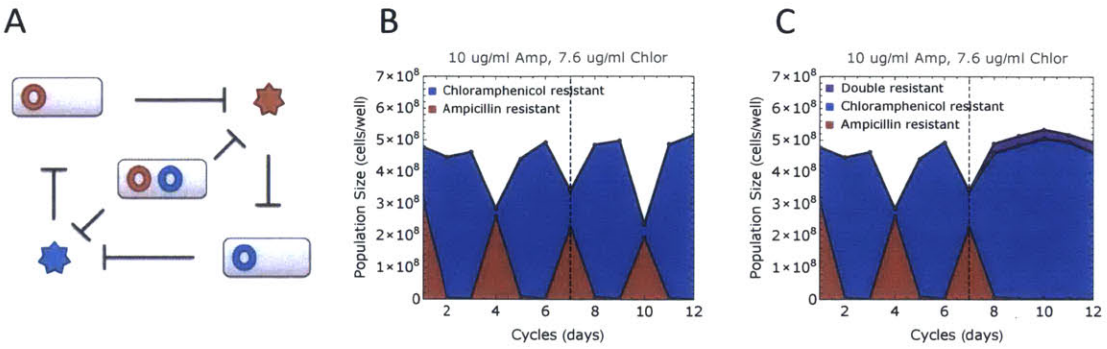

Figure 3-6: Upon successful invasion of the mutualism by a double resistant strain, the oscillations vanish, suggesting that the existence oscillations depends on how resistance is allocated in the microbial population. (A) A double resistant strain is self-sufficient and does not require protection from the mutualistic strains to survive. (B) In the absence of the invader, the ampicillin and chloramphenicol resistant subpopulation oscillate. (C) After introduction of the double resistant strain on the seventh day to a replicate culture of (B), the double resistant invader established in the microbial population, squeezing out the ampicillin resistant subpopulation and removing the oscillations.

resistant cells from ampicillin, resulting in one-sided cooperation where the double resistant cells are cooperators and the chloramphenicol resistant cells are cheaters. This situation parallels a previously studied system where ampicillin resistant cells protected sensitive cells and where the two populations settled to an equilibrium fraction [47].

3.4 Discussion

In this work, we have shown that a pair of antibiotic deactivating *E. coli* strains can successfully and readily form an obligatory mutualism in a multi-drug environment. Because the capacity to form the mutualism only depends on the production of resistance enzymes, the mutualism does not require a period of co-evolution as long as the enzymes are readily expressed. Although we implemented this mutualism in two otherwise isogenic strains of *E. coli*, such cross-protection interactions could occur between different species. Given the generality of this cooperative resistance mechanism, we speculate that such interactions could lead to similar obligatory mutualisms

in natural bacterial populations, such as in soil bacteria [11, 20].

The persistent survival over many dilution cycles that we observed suggests that this obligatory mutualism can survive indefinitely over a broad range of antibiotic concentrations. However, we note that while studying the stability of the mutualism over time, we found that some co-cultures survive transiently in the presence of the antibiotics only to collapse later (Fig. 3-2, C-2). This finding is reminiscent of a previously published report exploring the possibility of a bacterial mutualism between an ampicillin-resistant strain and a kanamycin-resistant strain, where the authors found that the co-culture was viable only the first day of growth [107], presumably because kanamycin deactivation was not sufficiently cooperative. This observation highlights the need to explore conditions in which the mutualism is stable over the long-term.

While exploring the dynamical behavior of the cross-protection mutualism, we found that periodic exposure to antibiotics gave rise to oscillations in the subpopulations sizes of the two mutualists, with an oscillation period longer than the time between consecutive antibiotic exposures. Ecologists have been long fascinated by the mechanisms that can give rise to cyclical dynamics in natural populations [67, 108–113]. Well-studied mechanisms typically involve consumer-resource interactions (e.g., predator-prey, host-parasite), which can cause population oscillations either on their own or in combination with exogenous forcing either random or periodic [109]. In comparison, mutualistic interactions are generally considered to be stabilizing. While the possibility of limit cycle oscillations in mutualisms has been explored in a few recent theoretical studies [92, 93, 114–116], there is scant experimental evidence supporting their existence in natural populations. A noteworthy experimental study by Shou *et al.* of a synthetic cross-feeding mutualism in yeast did find oscillatory dynamics in the population sizes of the mutualists within the course of a single growth cycle [98]; however, evidence that the subpopulation ratio was converging toward a fixed point by the end of the cycle suggests that periodic forcing would not give rise to oscillations in this system. Hence, while periodic forcing seems to be able to generate limit cycles in our microbial mutualism, such oscillations may be more

characteristic of cross-protection interactions rather than cross-feeding interactions (see supplementary materials).

The abundance of antibiotic inactivation enzymes found in microbial soil communities [20–22] and in clinically relevant pathogens [52] suggests that cross-protection mutualisms may frequently arise naturally and may have interesting implications for the evolution of antibiotic resistance. Since many plasmids carrying genes conferring resistance are readily spread via horizontal gene transfer [1, 13, 18], the type of cooperative interactions explored here may be able to evolve rapidly. Furthermore, the ability of the two strains to protect each other and survive in a multi-drug environment may provide a possible path for a multi-drug resistant strain to evolve. Although our experimental system used plasmids that do not conjugate (and we did not observe horizontal gene transfer during the timescale of our experiments), the results of our double-resistant invasion experiment suggest that even if a double-resistant strain were to arise, the tradeoff between producing a resistance enzyme and overall fitness can prevent the double-resistant strain from fixing. We expect that our results may provide insight into the evolution of antibiotic resistance in the soil (which serves as a large reservoir of resistance genes), and perhaps into how antibiotic resistance spreads during the course of multi-drug treatment in the clinic.

Materials and Methods

Strains

All strains are derived from *Escherichia coli* DH5α, which was sensitive to both ampicillin and chloramphenicol (Fig. C-16). The chloramphenicol resistant strain is an *E. coli* DH5α strain transformed with the pBbS5c-RFP plasmid [117]. The plasmid encodes a gene for monomeric red fluorescent protein and a gene for chloramphenicol acetyltransferase (type I) enzyme. It has a pSC101 origin of replication. The plasmid was obtained from Jay Keasling (Addgene plasmid #35284). The ampicillin resistant strain is an *E. coli* DH5α strain transformed with a plasmid encoding a gene for the β-

lactamase enzyme (TEM-1) and an enhanced yellow fluorescent protein (EYFP). The plasmid was assembled using the 2011 BioBrick distribution kit [118]. We combined a constitutive promoter (J23116) with a sequence encoding a ribosome binding site, EYFP and 2 stop codons (E0430). This construct was cloned into a vector containing the BioBrick pSB6A1 backbone. The double resistant strain was transformed with both plasmids.

Experiments

Initial single cultures of our strains were grown for 24 hours in culture tubes (3 or 5 ml) in LB supplemented with antibiotic for selection (50 μg/ml ampicillin, 25 μg/ml chloramphenicol for the ampicillin-resistant strain and the chloramphenicol-resistant strain respectively) at 37 °C and shaken at 300 rpm. The following day, co-cultures of the two strains were grown at varying initial population fractions in LB without antibiotics. Subsequently, serial dilution experiments were done in well-mixed batch culture. Every cycle, the culture was diluted by a fixed amount into fresh LB medium supplemented with the antibiotics ampicillin and chloramphenicol. Except for where noted otherwise, each cycle lasted about $\sim$ 23.5 hrs and cultures were diluted by a hundred fold. Cultures were shaken at 500 rpm at a temperature of 37 °C. Growth medium was prepared using BD's DifcoTM LB Broth (Miller) (Cat# 244620). Ampicillin stock was prepared by dissolving ampicillin sodium salt (Sigma-Aldrich Cat# A9518) in LB at a concentration of 50 mg/ml. The solution was filter sterilized and stored frozen at -80 °C and thawed before use. Chloramphenicol stock was prepared by dissolving chloramphenicol powder (Sigma Cat# C0378) in 200 proof pure ethanol (KOPTEC) at a concentration of 25 mg/ml. This solution was filter sterilized and stored at -20 °C.

Measurement and Data Analysis

At the end of each growth cycle, we took spectrophotometry (Thermo Scientific Varioskan Flash at 600nm) and flow cytometry (Miltenyi Biotec MACS Quant VYB)

measurements of the culture to determine subpopulation sizes. Relative abundances were confirmed by plating (Fig. C-3). Data analysis were performed using a combination of Mathematica, matplotlib [119], and IPython [120].

Appendix A

Modeling antibiotic resistance

A.1 Overview

Here, we present a model of bacterial growth in the antibiotic. We show that the way the equilibrium fraction scales with the initial antibiotic concentration, A_i, and cell density, N_i, is independent of many aspects of bacterial growth in the antibiotic. As long as the antibiotic is inactivated according to Michaelis-Menten kinetics, the equilibrium fraction scales approximately as $f_{eq} \propto (A_i + K_M \ln(A_i))/N_i$.

Section (A.2) defines the parameters used in the models. Section (A.3) provides a summary of the analytical expressions of the equilibrium fractions for different model variations. Section (A.4) shows how various aspects of bacterial growth in the antibiotic are incorporated into the models. Two of the models are solved in section (A.5). Finally, in section (A.6), we discuss the model used in the main text.

A.2 Definition of Parameters

Parameter	Definition
γ_R	growth rate of resistant cells
γ_S	growth rate of sensitive cells
γ_D	death rate of sensitive cells

Parameter	Definition
$\Delta\gamma$	$\gamma_S - \gamma_R > 0$
V_{max}	hydrolysis rate
K_M	Michaelis-Menten constant
A_i	initial antibiotic concentration
MIC	antibiotic concentration above which sensitive cells die
ΔA	$A_i - MIC \geq 0$
f_i	initial resistant fraction
f_f	final resistant fraction
f_{eq}	$f_{eq} = f_i = f_f$ is the equilibrium fraction
$N_{Ri} \equiv N_R(0)$	initial number of resistant cells
$N_{Rf} \equiv N_R(\tau_{sat})$	final number of resistant cells
$N_{Si} \equiv N_S(0)$	initial number of sensitive cells
$N_{Sf} \equiv N_S(\tau_{sat})$	final number of sensitive cells
$N_i = N_{Ri} + N_{Si}$	the initial number of both resistant and sensitive cells
$N_{sat} = N_{Rf} + N_{Sf}$	saturation number of both resistant and sensitive cells
τ_{lag}^R	for $t < \tau_{lag}$ resistant cells neither divide nor die
τ_{lag}^S	for $t < \tau_{lag}$ sensitive cells neither divide nor die
τ_{sat}	time at which saturation is reached
τ_b	time at which the antibiotic is broken down

A.3 Analytic Solutions for the Equilibrium Fraction

#	Lag Phase		Cell Death	Antibiotic Inactivation	f_{eq}
1	✗	$\tau_{lag}^R = \tau_{lag}^S = 0$	✗	$\frac{dA}{dt} = -V_{max} N_{Ri}$	$\frac{\Delta A}{V_{max} N_i \frac{1}{\gamma_R} \ln(\frac{N_{sat}}{N_i}) \frac{\Delta\gamma}{\gamma_S}}$
2	✗	$\tau_{lag}^R = \tau_{lag}^S = 0$	✗	$\frac{dA}{dt} = -V_{max} N_R(t)$	$\frac{\Delta A}{V_{max} N_i \{\frac{1}{\gamma_R}[(\frac{N_{sat}}{N_i})^{\frac{\Delta\gamma}{\gamma_S}} - 1]\}}$
3	✗	$\tau_{lag}^R = \tau_{lag}^S = 0$	✗	$\frac{dA}{dt} = -V_{max} N_R(t) \frac{A}{A+K_M}$	$\frac{\Delta A + K_M \ln(\frac{A_i}{MIC})}{V_{max} N_i \{\frac{1}{\gamma_R}[(\frac{N_{sat}}{N_i})^{\frac{\Delta\gamma}{\gamma_S}} - 1]\}}$
4	✗	$\tau_{lag}^R = \tau_{lag}^S = 0$	✓	$\frac{dA}{dt} = -V_{max} N_R(t)$	$\frac{\Delta A}{V_{max} N_i \{\frac{1}{\gamma_R}[(\frac{N_{sat}}{N_i})^{\frac{\Delta\gamma}{\gamma_S+\gamma_D}} - 1]\}}$
5	✓	$\tau_{lag}^R = \tau_{lag}^S \neq 0$	✗	$\frac{dA}{dt} = -V_{max} N_R(t)$	$\frac{\Delta A}{V_{max} N_i \{\tau_{lag}^R + \frac{1}{\gamma_R}[(\frac{N_{sat}}{N_i})^{\frac{\Delta\gamma}{\gamma_S}} - 1]\}}$
6	✓	$\tau_{lag}^R = \tau_{lag}^S \neq 0$	✓	$\frac{dA}{dt} = -V_{max} N_R(t)$	$\frac{\Delta A}{V_{max} N_i \{\tau_{lag} + \frac{1}{\gamma_R}[(\frac{N_{sat}}{N_i})^{\frac{\Delta\gamma}{\gamma_S+\gamma_D}} - 1]\}}$
7	✓	$\tau_{lag}^R = \tau_{lag}^S \neq 0$	✓	$\frac{dA}{dt} = -V_{max} N_R(t) \frac{A}{A+K_M}$	$\frac{\Delta A + K_M \ln(\frac{A_i}{MIC})}{V_{max} N_i \{\tau_{lag} + \frac{1}{\gamma_R}[(\frac{N_{sat}}{N_i})^{\frac{\Delta\gamma}{\gamma_S+\gamma_D}} - 1]\}}$
8	✓	$\tau_{lag}^R \neq \tau_{lag}^S$	✓	$\frac{dA}{dt} = -V_{max} N_R(t) \frac{A}{A+K_M}$	$\frac{\Delta A + K_M \ln(\frac{A_i}{MIC})}{V_{max} N_i \{\tau_{lag}^R + \frac{1}{\gamma_R}[e^{\frac{\gamma_R\gamma_D(\tau_{lag}^S - \tau_{lag}^R)}{\gamma_S+\gamma_D}} (\frac{N_{sat}}{N_i})^{\frac{\Delta\gamma}{\gamma_S+\gamma_D}} - 1]\}}$
9	✓	$\tau_{lag}^R \neq \tau_{lag}^S$	✓	$\frac{dA}{dt} = -V_{max} N_{Ri} \frac{A}{A+K_M}$	$\frac{\Delta A + K_M \ln(\frac{A_i}{MIC})}{V_{max} N_i \{\frac{\gamma_S \tau_{lag}^R + \gamma_D \tau_{lag}^S}{\gamma_S+\gamma_D} + \frac{\Delta\gamma}{\gamma_R(\gamma_S+\gamma_D)} \ln(\frac{N_{sat}}{N_i})\}}$

A.4 Summary of Models

Here, we explain models 1, 4, and 8 in more detail, writing down the system of differential equations that corresponds to each model. In all the models, we assume that cell growth ceases when the total cell density reaches the saturation density (N_{sat}). Hence, if τ_{sat} corresponds to the time when $N_R + N_S = N_{sat}$, then for $t \geq \tau_{sat}$:

$$\begin{aligned} \frac{dN_R}{dt} &= 0 \\ \frac{dN_S}{dt} &= 0 \end{aligned}$$

A.4.1 Model 1

Here, resistant cells divide at a characteristic rate of γ_R. Sensitive cells divide at a rate of γ_S when the antibiotic concentration, A, is below their MIC value. When the antibiotic concentration is above their MIC, sensitive cells do not divide. Antibiotic is broken down at constant rate proportional to the initial number of resistant cells ($N_{Ri} = f_R N_i$).

$$\begin{aligned} \frac{dN_R}{dt} &= \gamma_R N_R \\ \frac{dN_S}{dt} &= \begin{cases} \gamma_S N_S & A < MIC \\ 0 & A > MIC \end{cases} \\ \frac{dA}{dt} &= -V_{max} N_{Ri} \end{aligned}$$

A.4.2 Model 4

Next, we incorporate cell death into the model, saying that for antibiotic concentration above the MIC of sensitive cells, sensitive cells die at a rate $-\gamma_D$. This gives the set of equations:

$$\begin{aligned}
\frac{dN_R}{dt} &= \gamma_R N_R \\
\frac{dN_S}{dt} &= \begin{cases} \gamma_S N_S & A < MIC \\ -\gamma_D N_S & A > MIC \end{cases} \\
\frac{dA}{dt} &= -V_{max} N_R
\end{aligned}$$

Note that in this example, antibiotic breakdown at time t is proportional to the number of resistant cells at time t (rather than the initial number of resistant cells).

A.4.3 Model 7

To more realistically model bacterial growth in the antibiotic, we can use Michaelis-Menten Kinetics for antibiotic inactivation; i.e., $\frac{dA}{dt} = -V_{max} N_{Ri} \frac{A}{A+K_M}$. In addition, we can introduce a lag phase during which cells neither grow nor die, giving:

For $t < \tau_{lag}$:

$$\begin{aligned}
\frac{dN_R}{dt} &= 0 \\
\frac{dN_S}{dt} &= 0 \\
\frac{dA}{dt} &= -V_{max} N_{Ri} \frac{A}{A+K_M}
\end{aligned}$$

For $t \geq \tau_{lag}$:

$$\begin{aligned}
\frac{dN_R}{dt} &= \gamma_R N_R \\
\frac{dN_S}{dt} &= \begin{cases} \gamma_S N_S & A < MIC \\ -\gamma_D N_S & A \geq MIC \end{cases} \\
\frac{dA}{dt} &= -V_{max} N_R \frac{A}{A + K_M}
\end{aligned}$$

Whether it is necessary to incorporate Michaelis-Menten Kinetics or not depends on the values of K_M and MIC. If $K_M \ll MIC$, then antibiotic breakdown proceeds essentially at saturation for antibiotic concentrations above the MIC.

A.5 Sample Derivation of Equilibrium Fractions

The models presented thus far describe how bacteria grow in the antibiotic during the course of a single day. These models provide a way to investigate the evolutionary dynamics between resistant and sensitive cells by allowing one to determine how the final resistant fraction, f_f, after 23 hours of growth depends on the initial resistant fraction, f_i, antibiotic concentration, A_i, and cell density, N_i. It is straightforward to integrate these models numerically to find the required dependence; however, it is challenging to gain intuition from numerical solutions. Fortunately, we can obtain an exact analytical expression for the dependence of equilibrium resistant fraction ($f_i = f_f = f_{eq}$) on the initial antibiotic concentration and cell density.

We will first derive two useful relations between the initial and final cell densities that hold at the equilibrium fraction, and then proceed to use these relations to derive an analytical expression for the equilibrium fraction.

A.5.1 Equilibrium Relations

At equilibrium, $f_f = f_i$. This is equivalent to saying that:

$$\frac{N_{Rf}}{N_{sat}} = \frac{N_{Ri}}{N_i}$$

Therefore,

$$\boxed{\frac{N_{Rf}}{N_{Ri}} = \frac{N_{sat}}{N_i}} \tag{A.1}$$

If we use the same logic as above but start from the expression $1 - f_f = 1 - f_i$, we get:

$$\boxed{\frac{N_{Sf}}{N_{Si}} = \frac{N_{sat}}{N_i}} \tag{A.2}$$

A.5.2 Solving Model 1

Model 1 (see A.4.1) ignores lag and cell death, and it assumes that antibiotic hydrolysis proceeds at a constant rate proportional to the initial cell density of resistant cells. Due to its simplicity, we can solve this model without doing much algebra.

Step 1: Solve for the time when the antibiotic concentration drops below the MIC

$$\frac{dA}{dt} = -V_{max} N_{Ri}$$

$$\frac{\Delta A}{\tau_b} = V_{max} N_{Ri}$$

$$\boxed{\tau_b = \frac{\Delta A}{V_{max} N_{Ri}}}$$

Step 2: Solve for the saturation time

Let's start with the equation (A.1):

$$\frac{N_{Rf}}{N_{Ri}} = \frac{N_{sat}}{N_i}$$

For this simple model, the number of resistant cells increases with time according

to the equation: $N_{Rf} = N_{Ri}e^{\gamma_R \tau_{sat}}$; therefore, $\frac{N_{Rf}}{N_{Ri}} = e^{\gamma_R \tau_{sat}}$, so:

$$e^{\gamma_R \tau_{sat}} = \frac{N_{sat}}{N_i},$$

giving:

$$\boxed{\tau_{sat} = \frac{1}{\gamma_R} ln(\frac{N_{sat}}{N_i})}$$

Step 3: Solve for the equilibrium fraction

$$\frac{N_{Sf}}{N_{Si}} = \frac{N_{sat}}{N_i} \quad (A.2)$$

Since the sensitive cells do not start growing until the antibiotic is broken down, the number of sensitive cells increases with time according to the equation: $N_{Sf} = N_{Si}e^{\gamma_S(\tau_{sat}-\tau_b)}$; therefore, $\frac{N_{Sf}}{N_{Si}} = e^{\gamma_S(\tau_{sat}-\tau_b)}$. Combining this with the previous expression, we get:

$$e^{\gamma_S(\tau_{sat}-\tau_b)} = \frac{N_{sat}}{N_i}$$

$$\tau_{sat} - \tau_b = \frac{1}{\gamma_S} \ln(\frac{N_{sat}}{N_i})$$

Next, we substitute in the expressions we got for τ_{sat} and τ_b:

$$\frac{1}{\gamma_R} ln(\frac{N_{sat}}{N_0}) - \frac{\Delta A}{V_{max} N_{Ri}} = \frac{1}{\gamma_S} \ln(\frac{N_{sat}}{N_i})$$

$$\frac{\Delta A}{V_{max} N_{Ri}} = (\frac{1}{\gamma_R} - \frac{1}{\gamma_S}) ln(\frac{N_{sat}}{N_i})$$

$$\frac{\Delta A}{V_{max} N_i f_{eq}} = \frac{1}{\gamma_R} ln(\frac{N_{sat}}{N_i})^{\frac{\Delta\gamma}{\gamma_S}}$$

$$\boxed{f_{eq} = \frac{\Delta A}{V_{max} N_i \frac{1}{\gamma_R} ln(\frac{N_{sat}}{N_i})^{\frac{\Delta\gamma}{\gamma_S}}}}$$

A.5.3 Solving Model 7

Model 7 (see A.4.3) incorporates a few more features, so the algebra is a bit messier, but the same general procedure applies.

Step 1: Solve for the time when the antibiotic concentration drops below the MIC

The antibiotic is inactivated according to Michaelis-Menten kinetics:

$$\frac{dA}{dt} = -V_{max} N_R \frac{A}{A + K_M},$$

where $N_R(t < \tau_{lag}) = N_{Ri}$ and $N_R(\tau_{lag} < t < \tau_{sat}) = N_{Ri} e^{\gamma_R (t - \tau_{sat})}$. We need to solve this differential equation to find the time, τ_b, at which the antibiotic concentration drops below the MIC of sensitive cells.

$$\frac{A + K_M}{A} dA = -V_{max} N_R dt$$

$$\int (1 + \frac{K_M}{A}) dA = -\int V_{max} N_R dt$$

$$(A + K_M \ln(A))|_{A_i}^{MIC} = -\int_0^{\tau_b} V_{max} N_R dt$$

$$-\Delta A + K_M \ln(\frac{MIC}{A_i}) = -V_{max} N_{Ri} (\tau_{lag} + \frac{1}{\gamma_R} e^{\gamma_R (t - \tau_{lag})}|_{\tau_{lag}}^{\tau_b})$$

$$\Delta A + K_M \ln(\frac{A_i}{MIC}) = V_{max} N_{Ri} (\tau_{lag} + \frac{1}{\gamma_R} (e^{\gamma_R (\tau_b - \tau_{lag})} - 1))$$

$$\frac{\Delta A + K_M \ln(\frac{A_i}{MIC})}{V_{max} N_{Ri}} = \tau_{lag} + \frac{1}{\gamma_R} (e^{\gamma_R (\tau_b - \tau_{lag})} - 1)$$

Let's introduce $\tau_b^* = \tau_b^0 + \tau_b^1$, where $\tau_b^0 = \frac{\Delta A}{V_{max} N_{Ri}}$ and $\tau_b^1 = \frac{K_M \ln(\frac{A_i}{MIC})}{V_{max} N_{Ri}}$. Then,

$$\tau_b^* = \tau_{lag} + \frac{1}{\gamma_R} (e^{\gamma_R (\tau_b - \tau_{lag})} - 1)$$

$$\frac{1}{\gamma_R} (e^{\gamma_R (\tau_b - \tau_{lag})} - 1) = \tau_b^* - \tau_{lag}$$

$$e^{\gamma_R(\tau_b-\tau_{lag})} - 1 = \gamma_R(\tau_b^* - \tau_{lag})$$

$$\gamma_R(\tau_b - \tau_{lag}) = \ln(1 + \gamma_R(\tau_b^* - \tau_{lag}))$$

$$\boxed{\tau_b = \tau_{lag} + \frac{1}{\gamma_R}\ln(1 + \gamma_R(\tau_b^* - \tau_{lag}))}$$

Step 2: Solve for the saturation time

$$\frac{N_{Rf}}{N_{Ri}} = \frac{N_{sat}}{N_i} \quad (A.1)$$

$$e^{\gamma_R(\tau_{sat}-\tau_{lag})} = \frac{N_{sat}}{N_i}$$

$$\gamma_R(\tau_{sat} - \tau_{lag}) = \ln(\frac{N_{sat}}{N_i})$$

$$\boxed{\tau_{sat} = \tau_{lag} + \frac{1}{\gamma_R}\ln(\frac{N_{sat}}{N_i})}$$

Step 3: Solve for the equilibrium fraction

$$\frac{N_{Sf}}{N_{Si}} = \frac{N_{sat}}{N_i} \quad (A.2)$$

$$e^{\gamma_S(\tau_{sat}-\tau_b)-\gamma_D(\tau_b-\tau_{lag})} = \frac{N_{sat}}{N_i}$$

$$\gamma_S(\tau_{sat} - \tau_b) - \gamma_D(\tau_b - \tau_{lag}) = \ln(\frac{N_{sat}}{N_i})$$

$$\gamma_S\tau_{sat} + \gamma_D\tau_{lag} - (\gamma_S + \gamma_D)\tau_b = \ln(\frac{N_{sat}}{N_i})$$

$$\gamma_S\tau_{lag} + \frac{\gamma_S}{\gamma_R}\ln(\frac{N_{sat}}{N_i}) + \gamma_D\tau_{lag} - (\gamma_S + \gamma_D)\tau_b = \ln(\frac{N_{sat}}{N_i})$$

$$(\gamma_S + \gamma_D)\tau_{lag} - (\gamma_S + \gamma_D)\tau_b = (1 - \frac{\gamma_S}{\gamma_R})\ln(\frac{N_{sat}}{N_i})$$

$$(\gamma_S + \gamma_D)\tau_{lag} - (\gamma_S + \gamma_D)(\tau_{lag} + \frac{1}{\gamma_R}\ln(1 + \gamma_R(\tau_b^* - \tau_{lag}))) = (1 - \frac{\gamma_S}{\gamma_R})\ln(\frac{N_{sat}}{N_i})$$

$$-\ln(1 + \gamma_R(\tau_b^* - \tau_{lag})) = \frac{\gamma_R - \gamma_S}{\gamma_S + \gamma_D}\ln(\frac{N_{sat}}{N_i})$$

$$1 + \gamma_R(\tau_b^* - \tau_{lag}) = (\frac{N_{sat}}{N_i})^{-\frac{\gamma_R-\gamma_S}{\gamma_S+\gamma_D}}$$

$$\gamma_R \tau_b^* = \gamma_R \tau_{lag} + (\frac{N_{sat}}{N_i})^{\frac{\gamma_S - \gamma_R}{\gamma_S + \gamma_D}} - 1$$

$$\gamma_R \frac{\Delta A + K_M \ln(\frac{A_i}{MIC})}{V_{max} N_{Ri}} = \gamma_R \tau_{lag} + (\frac{N_{sat}}{N_i})^{\frac{\gamma_S - \gamma_R}{\gamma_S + \gamma_D}} - 1$$

$$\boxed{f_{eq} = \frac{\Delta A + K_M \ln(\frac{A_i}{MIC})}{V_{max} N_i \{\tau_{lag} + \frac{1}{\gamma_R}[(\frac{N_{sat}}{N_i})^{\frac{\gamma_S - \gamma_R}{\gamma_S + \gamma_D}} - 1]\}}} \tag{A.3}$$

A.6 Fitting Experimental Data

To fit the experimental data, we used model #7 which incorporates cell death, Michaelis-Menten hydrolysis and lag time (see section A.4.3). We fit the equilibrium fractions (Figure 3C) to the full analytical solution of this model (Eq. A.3), acquiring estimates for the parameters MIC, V_{max}, K_M.

We then plugged the values of MIC, V_{max}, K_M into the differential equations describing model #7 (see section A.4.3) and integrated the differential equations numerically to recapitulate the difference equation maps (Figure 3A, B).

To fit the data with the tazobactam inhibitor (Figure 4C), we used equation A.3, modifying $K_M \rightarrow K_{eff} = K_M \cdot (1 + [I]/K_I)$. We fit the data using a single free parameter (K_i). (Other parameter values were held fixed. The values of MIC, V_{max} and K_m were set to those acquired in the fit of Figure 3C.)

A.6.1 Qualitative Behavior of the Equilibrium Fraction

The analytical expression of the equilibrium fraction is (Eq. A.3):

$$f_{eq} = \frac{\Delta A + K_M \ln(\frac{A_i}{MIC})}{V_{max} N_i \{\tau_{lag} + \frac{1}{\gamma_R}[(\frac{N_{sat}}{N_i})^{\frac{\Delta\gamma}{\gamma_S + \gamma_D}} - 1]\}}$$

Because in our experiments N_i varies by less than an order of magnitude and $\frac{\Delta\gamma}{\gamma_S + \gamma_D} \ll 1$, the equilibrium fraction can be approximated by the expression:

$$f_{eq} \approx C \frac{\Delta A + K_M \ln(\frac{A_i}{MIC})}{V_{max} N_i}, \tag{A.4}$$

where $C = \frac{1}{\tau_{lag} + \frac{1}{\gamma_R}[(\frac{N_{sat}}{N_i})^{\frac{\Delta\gamma}{\gamma_S+\gamma_D}} - 1]}$.

Using the numbers in section (A.6.2), C works out to be $\approx 0.84\ \text{hr}^{-1}$ for a dilution factor of 100x, and $\approx 0.78\ \text{hr}^{-1}$ for a dilution factor of 800x. This amounts to less than a 10% change in C, which means that C can be treated essentially as a constant. With C a constant, equation A.4 implies that the equilibrium fraction (f_{eq}) scales approximately inversely with the initial cell density (N_i).

Furthermore, for initial antibiotic concentrations higher than the dissociation constant ($A_i \gg K_M$), the contribution of the logarithmic term becomes small and the expression simplifies to:

$$f_{eq} \approx C\frac{\Delta A}{V_{max}N_i}$$

This relationship indicates that plotting the number of resistant cells at equilibrium (f_{Ri}) vs. the initial antibiotic concentration (A_i) should yield a line with a slope of $(\frac{C}{V_{max}})$:

$$\boxed{f_{Ri} = f_{eq} \times N_i \approx \frac{C}{V_{max}}\Delta A = \frac{C}{V_{max}}A_i - \frac{C}{V_{max}}MIC}$$

A.6.2 Parameter Values for Simulations

The following table lists the parameters used for simulations (see supplementary figures for details):

Parameter	Meaning	Value	Source
γ_R	growth rate of resistant cells	$1.1\,\text{hr}^{-1}$	measured experimentally
$\frac{\gamma_S}{\gamma_R}$	relative fitness of sensitive cells	1.15	measured experimentally
γ_D	death rate of sensitive cells	$2.8\,\text{hr}^{-1}$	measured experimentally

Parameter	Meaning	Value	Source
τ_{lag}	lag time	$\sim 1\,\mathrm{hr}$	measured experimentally[1]
N_{sat}	cell density at saturation (after 23 hours of growth)	$1.2 \times 10^7 \frac{cells}{\mu L}$	measured experimentally
V_{max}	hydrolysis rate	$\sim 10^6 \frac{molecules}{cell \times second}$	determined from fit
K_M	Michaelis-Menten constant for ampicillin inactivation	$6.7 \frac{\mu g}{mL}$	determined from fit
K_I	dissociation constant for tazobactam-enzyme complex	$4.56 \frac{ng}{mL}$	determined from fit
MIC	minimum inhibitory concentration of sensitive cells	$\sim 1.1 \frac{\mu g}{mL}$	determined from fit

[1]The lag time shows some variability. For simplicity, we took it to be 1 hour. Changing the value of the lag time mainly changes the fit value for V_{max}, but it hardly affects the dynamics.

Appendix B

Supporting Figures for Chapter 2

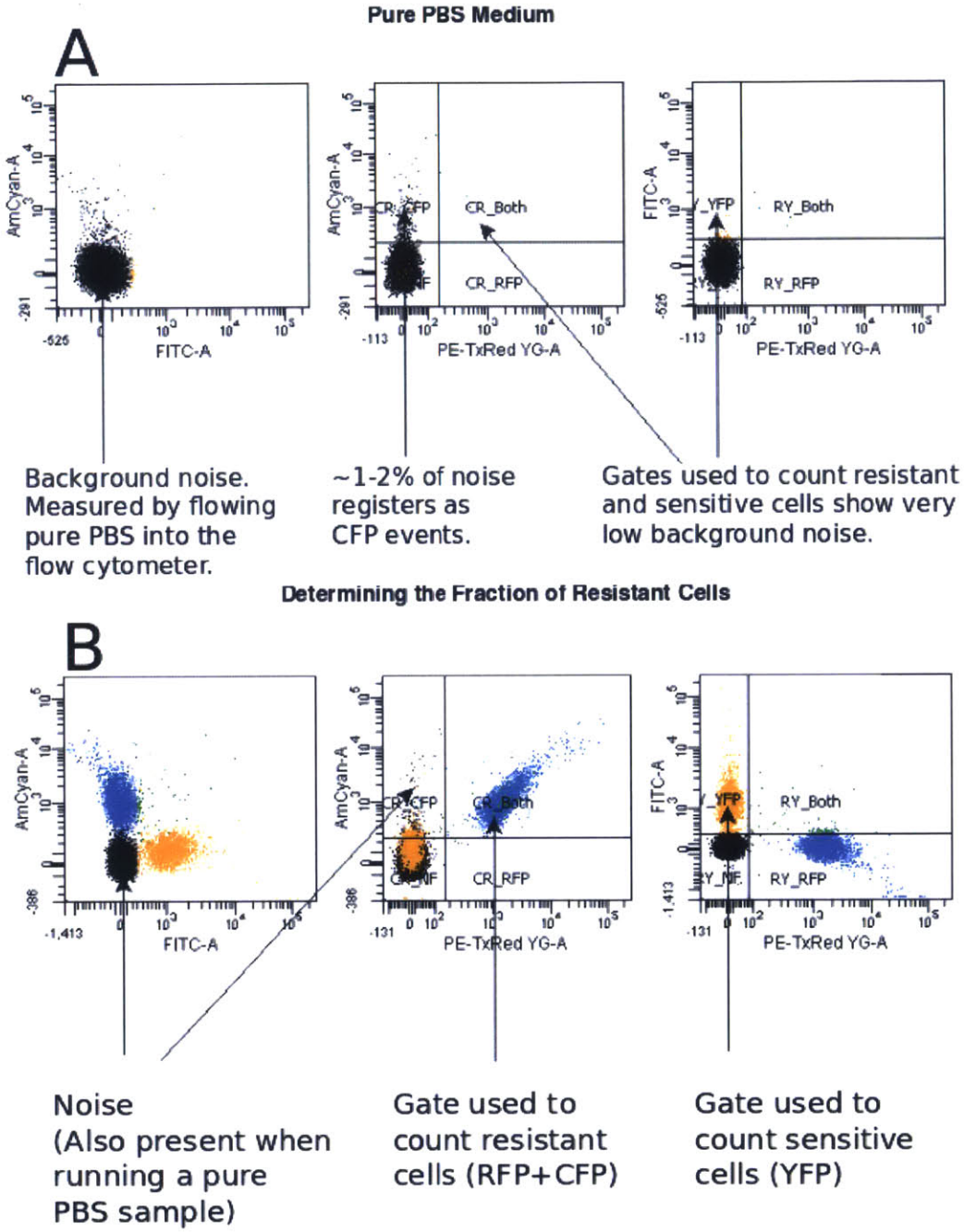

Figure B-1: Measurement of resistant fraction using flow cytometry. Shown is raw data from the flow cytometer: (A) PBS medium with no cells, and (B) a mixture of resistant and sensitive cells in PBS. To calculate the fraction of resistant bacteria, the number of fluorescent events registered in the gates corresponding to resistant and sensitive cells is counted (B). In addition, we measure the rate of false positives due to noise (A), and use it to correct the fraction of resistant bacteria. Because the noise level is low, the difference between corrected and uncorrected fractions is only ~0.01-0.03. The error in the fraction due to binomial counting statistics is small (~0.01) since there are thousands of events.

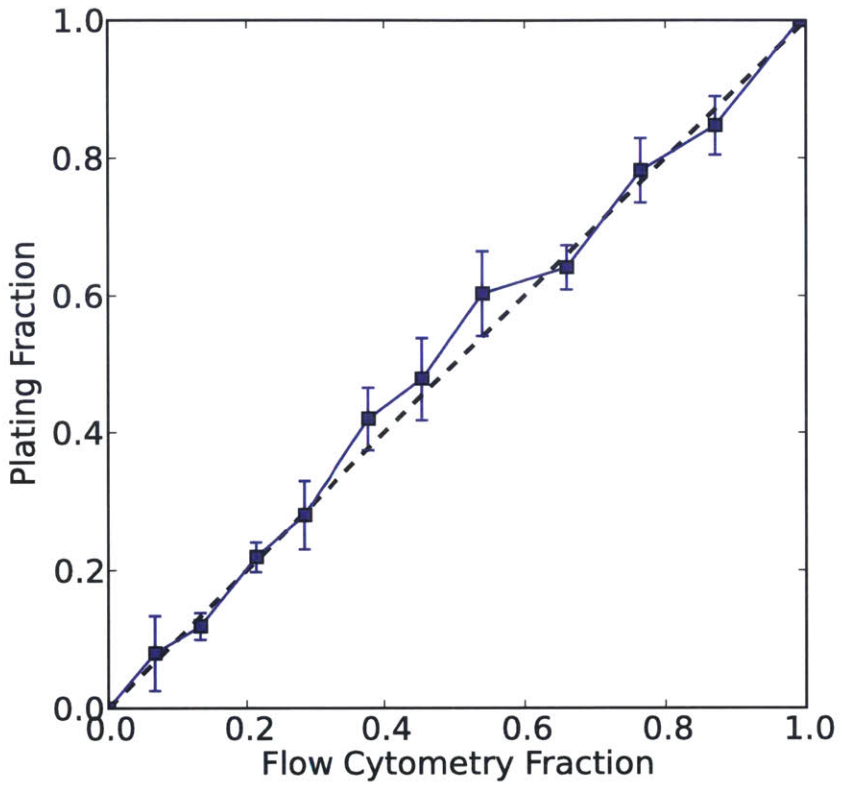

Figure B-2: Calibration of resistant fraction. The fraction of resistant cells measured by plating is equivalent to that measured on the flow cytometer. Sensitive and resistant cultures were grown from single colonies in 5 mL of LB with antibiotics at 37 °C for 23 hours. The saturated sensitive and resistant cultures were mixed at different ratios yielding 12 mixed cultures. For each mixed culture, the fraction of resistant cells was determined using flow cytometry (Fig. B-1). In addition, each mixed culture was plated on an LB-agar Petri dish, and the fraction of resistant cells was determined by counting the number of resistant and sensitive colony forming units (CFUs). Resistant and sensitive cells had different fluorescent markers, and were easy to tell apart using a fluorescent microscope. Error bars represent binomial counting error. The error associated with the fraction determined using flow cytometry is smaller than the size of the symbol.

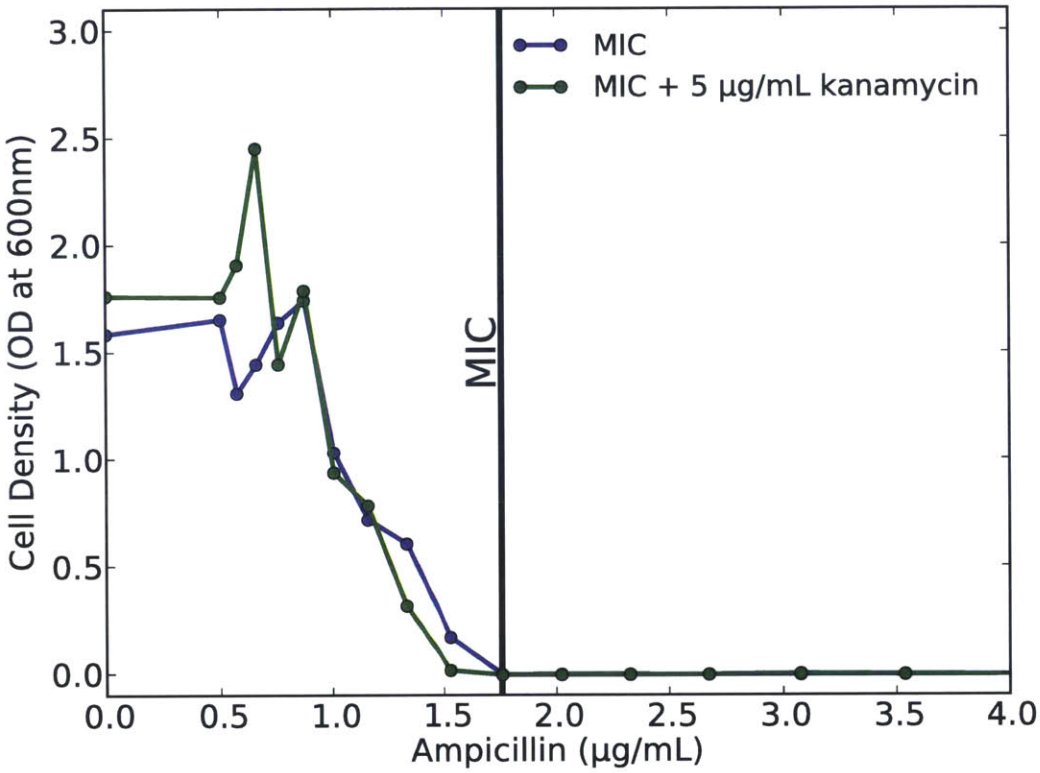

Figure B-3: Growth of sensitive cells in the antibiotic. The minimum inhibitory concentration (MIC) was determined by the lowest ampicillin concentration that inhibited bacterial growth (i.e., yielding no visible cell growth). In the experiment shown above, this concentration corresponds to $\sim$1.8 μg/mL, and was not affected by the addition of 5 μg/mL of kanamycin. Notably, ampicillin starts to affect the growth of sensitive cells even at concentrations below the MIC. This fact is ignored by our model, which implies that the model's MIC may be slightly different from the measured MIC. To measure the MIC, sensitive cells were grown in 5 mL of LB and 5 μg/mL of kanamycin for 23 hours. The saturated culture was then diluted into media containing different ampicillin concentrations and grown for 23 hours starting at an initial cell density of $\sim 4 \cdot 10^3$ CFU/mL. The 23 hour growth cycle was used to closely mimic the competition experiments. Our MIC was measured at a low cell density to more accurately characterize the effect of antibiotic on killing single cells. Alternatively, measuring the MIC using the standard cell density of $\sim 5 \cdot 10^5$ CFU/mL and 20 hours of growth, yielded an MIC of $\sim$2 μg/mL. Regardless of the method used to measure the MIC, ampicillin starts to affect the growth of sensitive cells even at concentrations below the MIC.

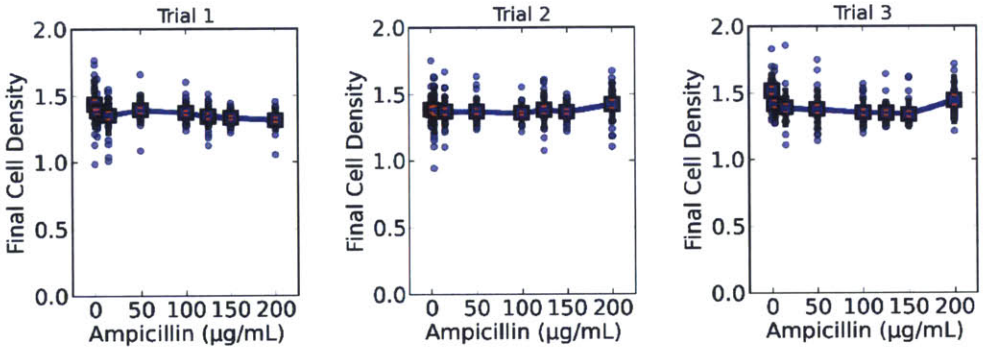

Figure B-4: Final cell density is independent of ampicillin concentration. Shown is the cell density after 23 hours of growth in LB with 5 μg/mL of kanamycin and varying concentrations of ampicillin. Experiments were carried out at a dilution factor of 100x. Circles correspond to individual data points, squares to the means, the black error bars to the standard deviations, and the red error bars to the standard errors of the mean. Cell density corresponds to the optical density measured at 600 nm. Experiments were repeated on 3 different days (trials 1-3). These are the three experiments from which Fig. 2-3 was generated.

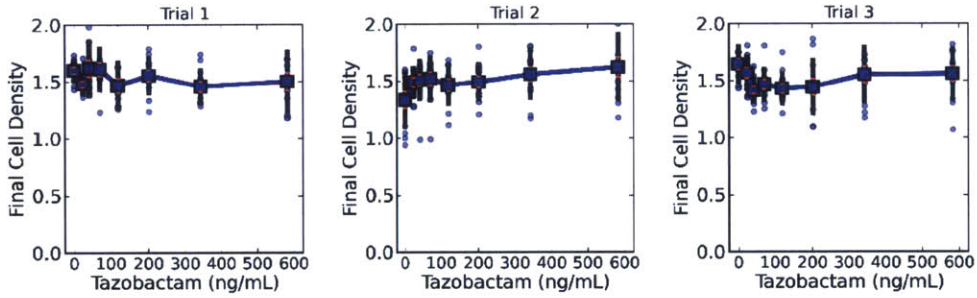

Figure B-5: Final cell density is independent of tazobactam concentration. Shown is the cell density after 23 hours of growth in LB with 5 μg/mL of kanamycin, 2 μg/mL of ampicillin and varying concentrations of tazobactam. Experiments were carried out at a dilution factor of 100x. Circles correspond to individual data points, squares to the means, the black error bars to the standard deviations, and the red error bars to the standard errors of the mean. Cell density corresponds to the optical density measured at 600 nm. Experiments were repeated on 3 different days (trials 1-3). These correspond to the three experiments from which Fig. 2-4B, C were generated.

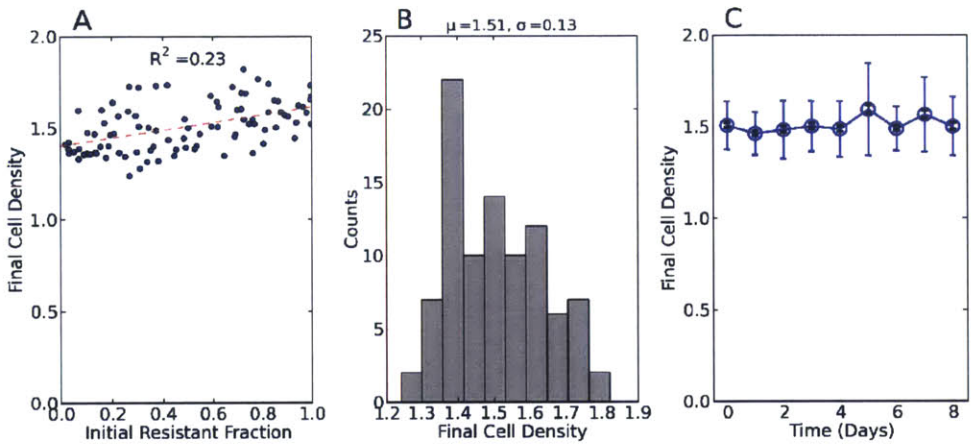

Figure B-6: Final cell density vs initial fraction and time. Cells were grown for 23 hours in LB with 5 μg/mL of kanamycin, and 100 μg/mL of ampicillin. (A) Shows the dependence of the final cell density (OD600) on the initial resistant fraction at the end of the first day. The final cell density depends weakly on the initial resistant fraction. (B) A histogram of the final cell density at the end of the first day. (C) The saturated cultures were propagated at a dilution factor of 100x over multiple days. The final cell density does not change significantly with time. The blue error bars represent the standard deviation while the black error bars represent the standard error of the mean. Final cell density corresponds to the optical density measured at 600 nm. Data comes from the same experiment as used to generate Fig. 2-1A in the main text.

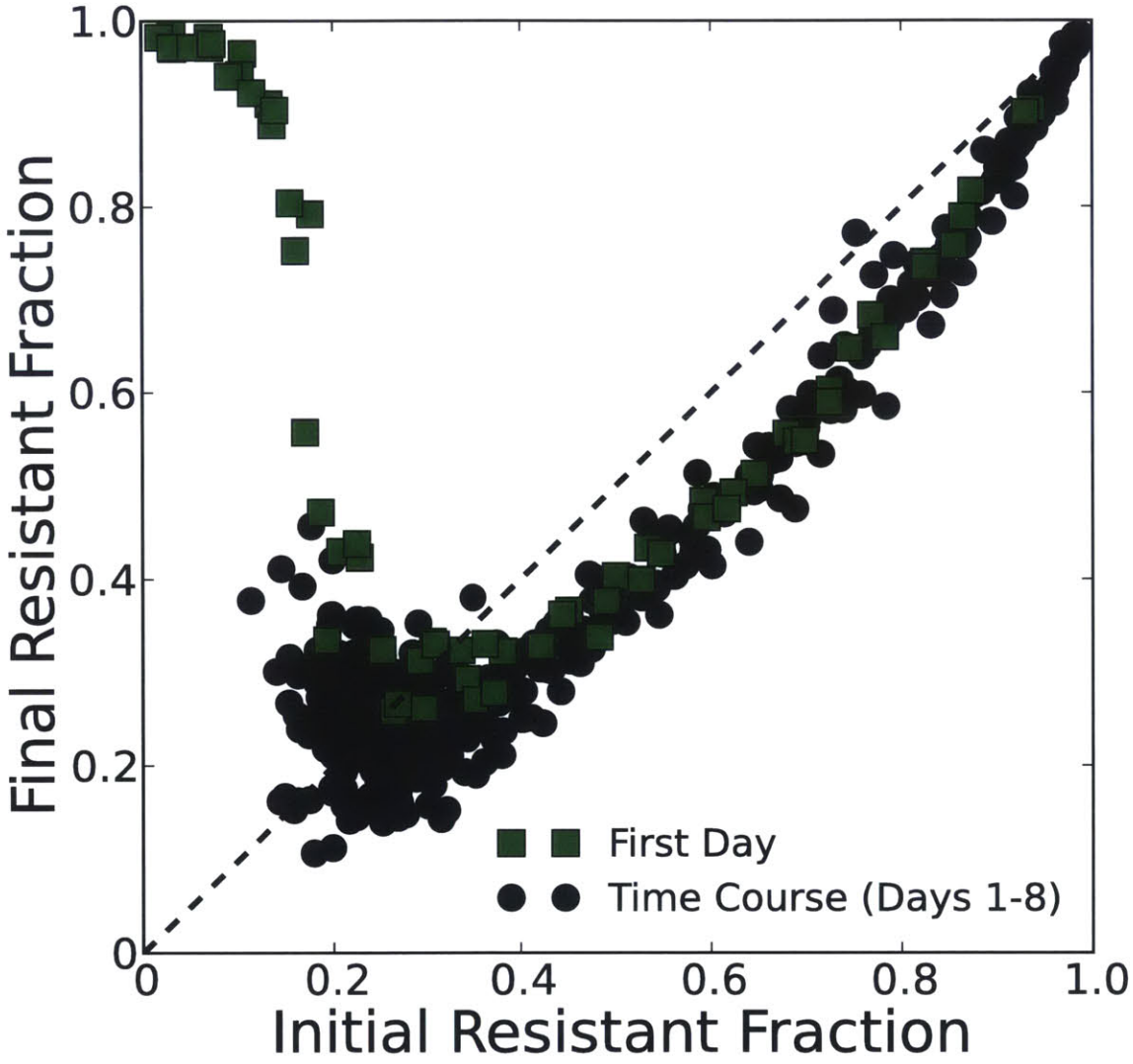

Figure B-7: Difference equations obtained on consecutive days. The difference equation obtained on the first day (green squares) slightly overestimates the resistant fraction seen on consecutive days (black circles). Cultures were grown in LB with 5 μg/mL kanamycin, 100 μg/mL ampicillin at a dilution factor of 100x.

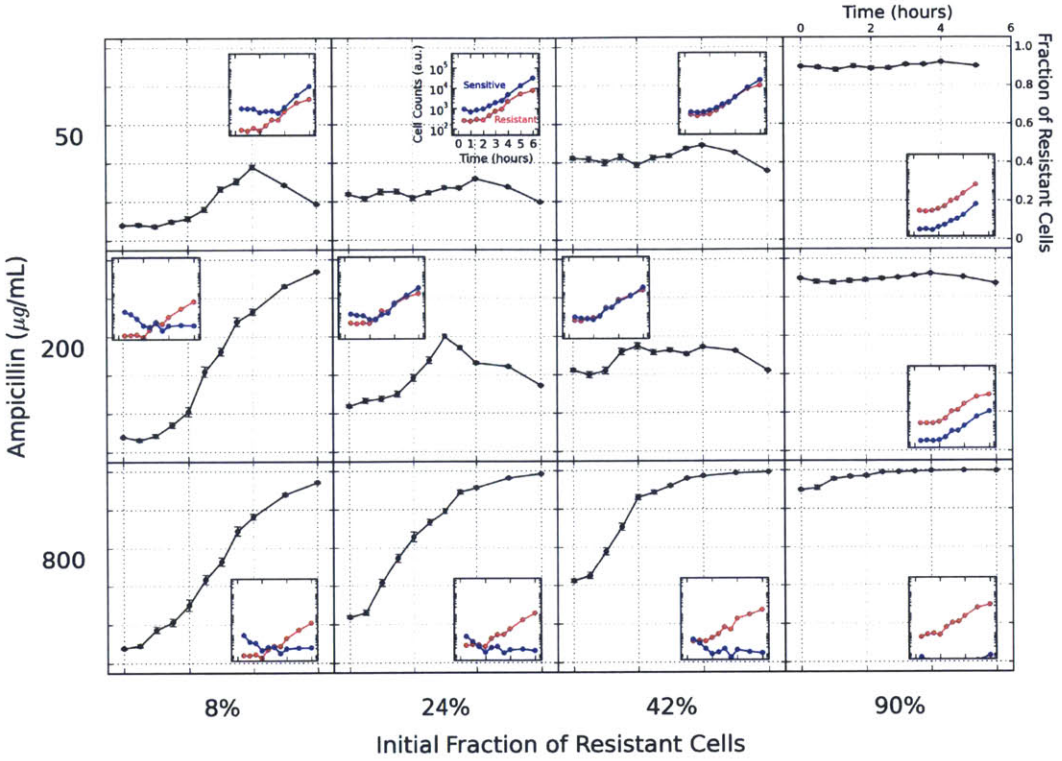
Time (hours)
Fraction of Resistant Cells
Ampicillin (μg/mL)
50
200
800
Cell Counts (a.u.)
Sensitive
Resistant
Time (hours)
8%
24%
42%
90%
Initial Fraction of Resistant Cells

Figure B-8: Intra-day growth dynamics in ampicillin of bacterial populations containing both resistant and sensitive cells. Bacterial populations containing resistant and sensitive cells were grown in 200 μL of LB with specified concentrations of ampicillin. Every 30 to 60 minutes, 1 μL of each bacterial culture was transferred into 199 μL of PBS, and the sample was measured on the flow cytometer. Each measurement yielded the number of resistant and sensitive cells (red and blue lines in the insets), as well as the fraction of resistant cells (black lines) during one time point in the course of bacterial growth in the antibiotic.

The data shows that at lower initial antibiotic concentrations and higher initial fractions of resistant cells, sensitive cells grow virtually unhindered by the antibiotic. In contrast, at higher antibiotic concentrations and lower initial fractions of resistant cells, the antibiotic can kill a significant fraction of the sensitive cells before it is inactivated. In addition, consistent with our modeling assumptions, sensitive cells can recover and resume growth after experiencing cell death.

The measurement at time $t = 0$ was carried at a higher cell density on the flow cytometer (different dilution into PBS), yielding cell counts that were artificially higher than the cell counts for t > 0. Consequently, we omitted the cell counts for $t = 0$, but we did include the fraction of resistant cells since it is unaffected by the different cell density.

The error bars on the fraction of resistant cells show the error associated with small cell numbers (approximated as $\sqrt{f(1-f)/N}$, where f is the fraction of resistant cells and N is the total number of cells). This error is less than 5% for most measurements (since N > 100 cells).

When measuring the fraction of resistant cells continuously over the course of bacterial growth, rather than just at the initial and final times as is done elsewhere in this study, one must worry about additional sources of noise. One issue is that the fluorescence of sensitive cells decreases during the first few hours of growth, leading to overestimation of the fraction of resistant cells. In addition, it is possible that sensitive cells can still lyse in PBS if they were on the verge of lysing before being diluted into PBS. This means that the measured fraction of resistant cells may exhibit some dependence on the time elapsed between dilution into PBS and the subsequent measurement on the flow cytometer. Re-measurements of the same samples in PBS gave mostly the same fractions of resistant cells (i.e., within the shown error bars); however, a few of the fractions were off by ~10-15%. Nonetheless, most of the dynamics are dominated by significantly larger changes in fraction than can be caused by noise.

Cultures were grown at 37 °C in a shaking incubator in the absence of kanamycin. Also, please see the discussion in Fig. B-24 regarding the change in the equilibrium fractions.

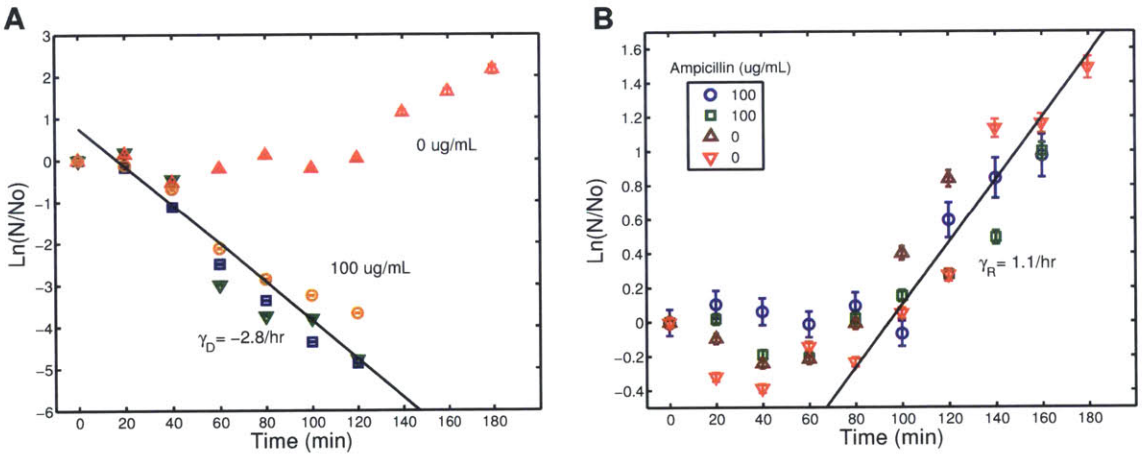

Figure B-9: Growth dynamics in ampicillin of sensitive cells and resistant cells grown separately. Resistant and sensitive cells were grown at 37 °C in 5 mL of LB and 5 μg/mL of kanamycin with either 0 μg/mL or 100 μg/mL of ampicillin. Every 20 minutes, the number of Colony Forming Units (CFUs), N, was obtained by plating cultures on LB-agar Petri dishes. (A) Sensitive cells exhibit a lag phase ~30-120 minutes, and die at a rate of ~2.8/hr when ampicillin is present. (B) Resistant cells exhibit a lag phase of ~80-100 minutes, and grow at a rate of ~ 1.1/hr, regardless if grown either in the absence or presence of ampicillin. In modeling growth in the antibiotic, we took the lag time of both resistant and sensitive cells to be 1 hour long. The different markers correspond to different trials. No represents the number of CFUs at time 0 in each trial.

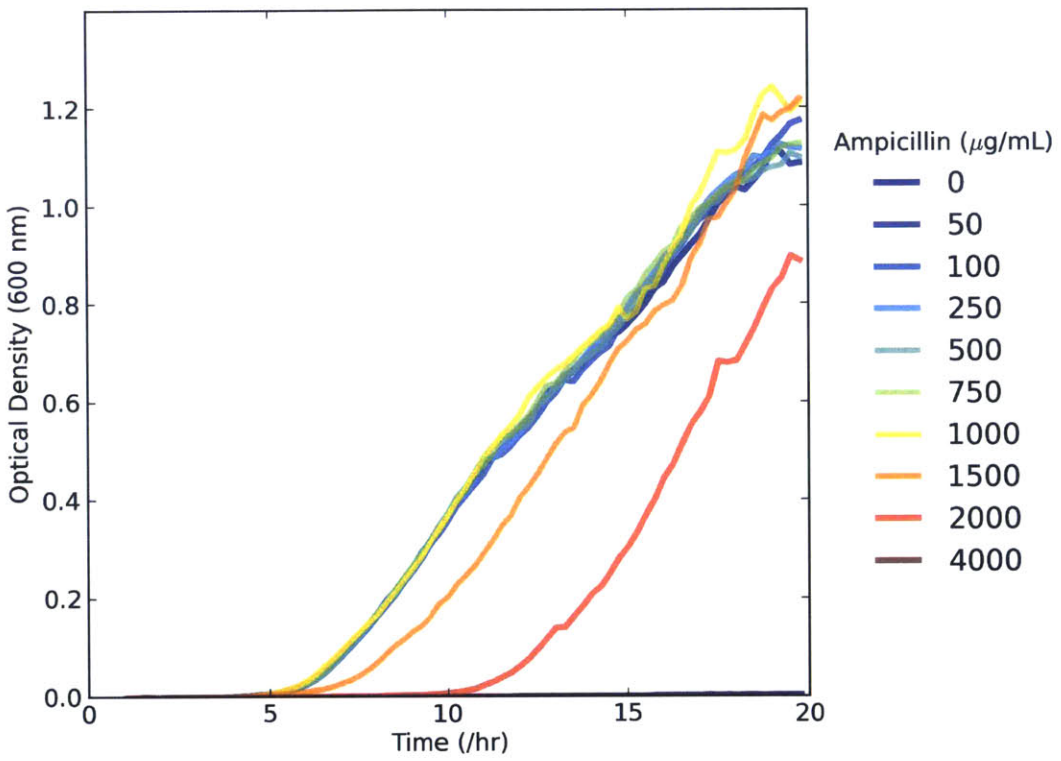

Figure B-10: Resistant cells in ampicillin. The growth of resistant cells is unaffected at the range of antibiotic concentrations probed in our experiments (up to $\sim$200 μg/mL). Resistant cells were inoculated at an initial cell density corresponding to a dilution of $\sim 10^5$ from saturation into a 96-well plate with 200 μL of LB supplemented with ampicillin. The plate was placed into a shaking incubator at 37 °C, with optical density measurements taken every $\sim$15 minutes. This strain is equivalent to the one used in the main text except for its kanamycin resistance plasmid which encodes a yellow fluorescent protein instead of a cyan fluorescent protein.

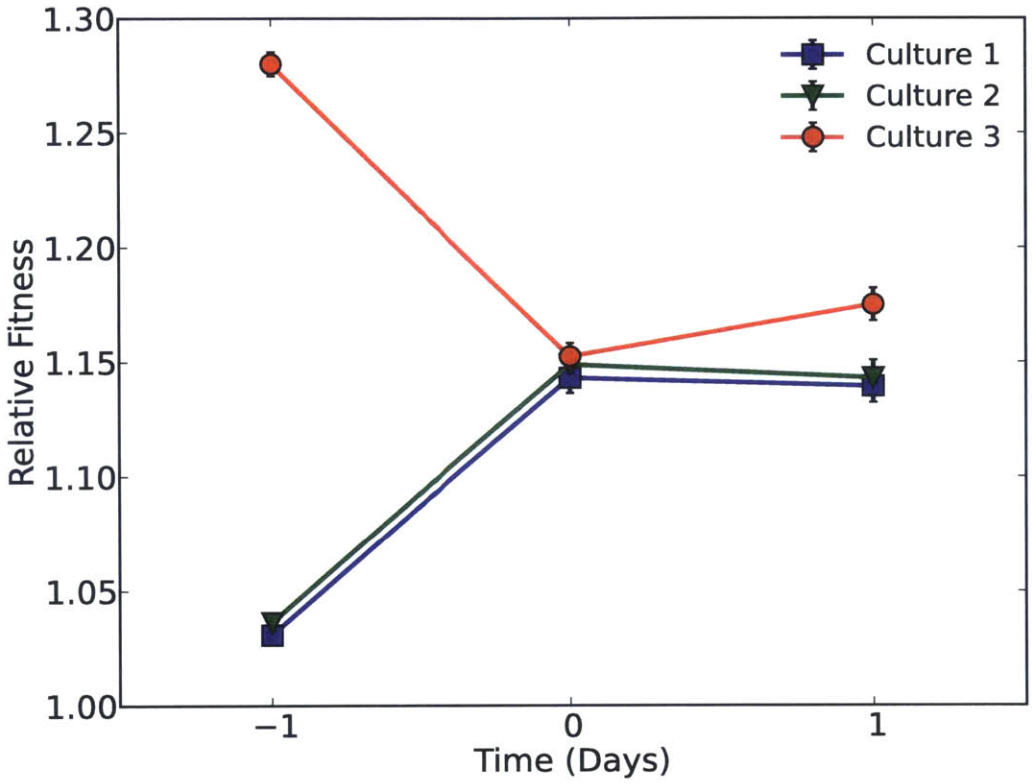
1.30
1.25
1.20
1.15
1.10
1.05
1.00
Relative Fitness
−1
0
1
Time (Days)
Culture 1
Culture 2
Culture 3

Figure B-11: Sensitive cells grow faster than resistant cells in the absence of the antibiotic ampicillin.

3 sensitive and 3 resistant cultures were grown from single colonies in 5 mL of LB with antibiotics at 37 °C for 23 hours. Each of the three saturated sensitive culture was mixed with one of the three saturated resistant cultures. The fraction of resistant cells in the mixed cultures was measured using flow cytometry (Day -1). The mixed cultures were then diluted by a factor of 100x into a 96-well plate in which they were grown in 200 μL of LB with 5 μg/mL kanamycin for a day. The fraction of resistant cells in the saturated cultures grown in the 96-well plates was measured using flow cytometry (Day 0). Cultures were propagated for another day (Day 1) under the same growth conditions as in Day 0 (diluted by factor of 100x into 96-well plate with 200 μL of LB at 5 μg/mL kanamycin), and the fractions of resistant cells were measured again using flow cytometry.

The relative fitness between the sensitive and resistant cells was calculated for each day of growth using the equation $r = ln(N_{Sf}/N_{Si})/ln(N_{Rf}/N_{Ri})$, where N_{Si}, N_{Sf}, N_{Ri}, N_{Rf} are the initial sensitive cell density, final sensitive cell density, initial resistant cell density, and final resistant cell density, respectively. The densities of the subpopulations were determined by combining flow cytometry measurements (yielding fractions of each subpopulation) together with optical density measurements at 600 nm (yielding total density of bacterial population). The initial densities correspond to those of the freshly inoculated culture, whereas the final densities correspond to those of the saturated culture (after a day of growth). For each culture, error bars in the relative fitness represent the standard error of the mean over multiple replicates.

Importantly, we found that the relative fitness on Day -1 is an unreliable measure of the relative fitness between the two strains. Prior to being co-cultured together on Day -1, the two strains were grown separately in 5 mL of LB. We suspect that random differences between the growth histories of the two strains when grown separately lead to fluctuations in the relative fitness measured on Day -1.

For the following days (Days 0 and 1), the two strains experienced the same growth histories, and the measurements of the relative fitness across different cultures yielded consistent results. Consequently, all experiments were carried out after co-culturing the two strains together for a day in the absence of ampicillin before using them to measure difference equation maps.

The value of the relative fitness, r, used for modeling was the average of the relative fitness values across the three cultures obtained on Day 1 (r=1.15).

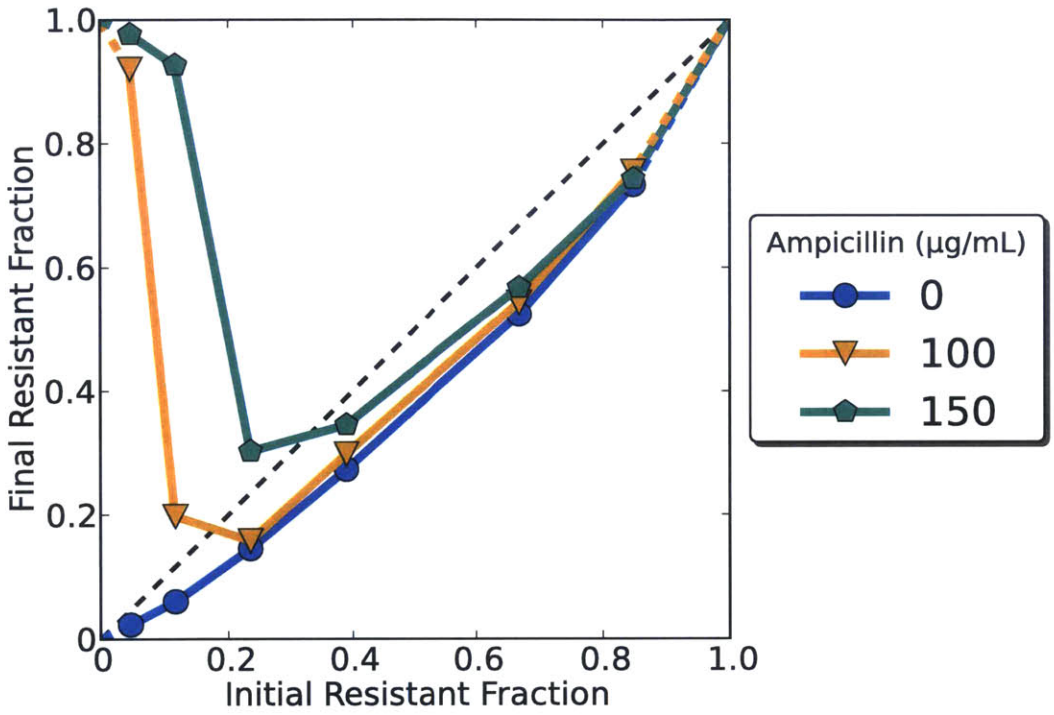

Figure B-12: Difference equation with a different plasmid. The evolutionary dynamics are not specific to the type of plasmid that encodes the β-lactamase gene. Shown are difference equations that were mapped for a resistant strain in which the resistance was carried by the pBR322 plasmid (New England Biolabs, Beverly, MA, identical to TEMwt). Unlike the resistance plasmid used in the main text, this plasmid does not encode a fluorescent protein. Quantitative differences are expected as hydrolysis rates, growth rates, lag times may vary between different plasmids; however, the qualitative features of the evolutionary dynamics remain robust; i.e., phenotypes have high fitness when rare, and for every ampicillin concentration, there is a characteristic fraction of resistant cells at equilibrium. Data was acquired in LB with 5 μg/mL of kanamycin at 100x dilution.

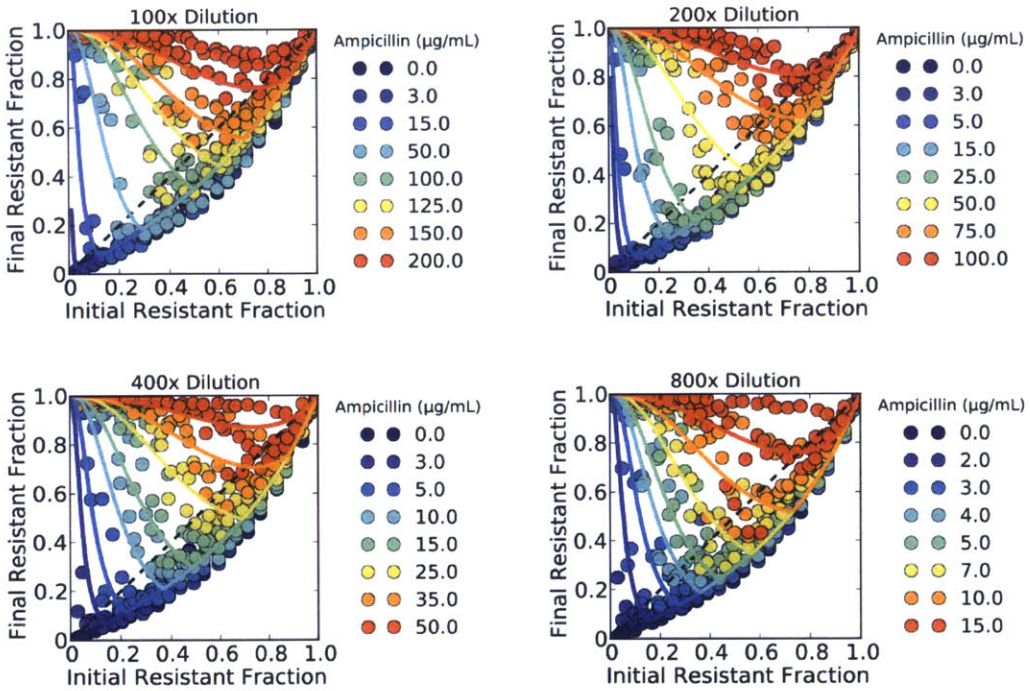

Figure B-13: Difference equation maps at different dilution factors. Each difference equation was measured on 3 different days. The 100x and 200x difference equations shown in the main text (Fig. 2-3A, B) only include a subset of the data. Solid curves represent a single fit of the model to all experimental data.

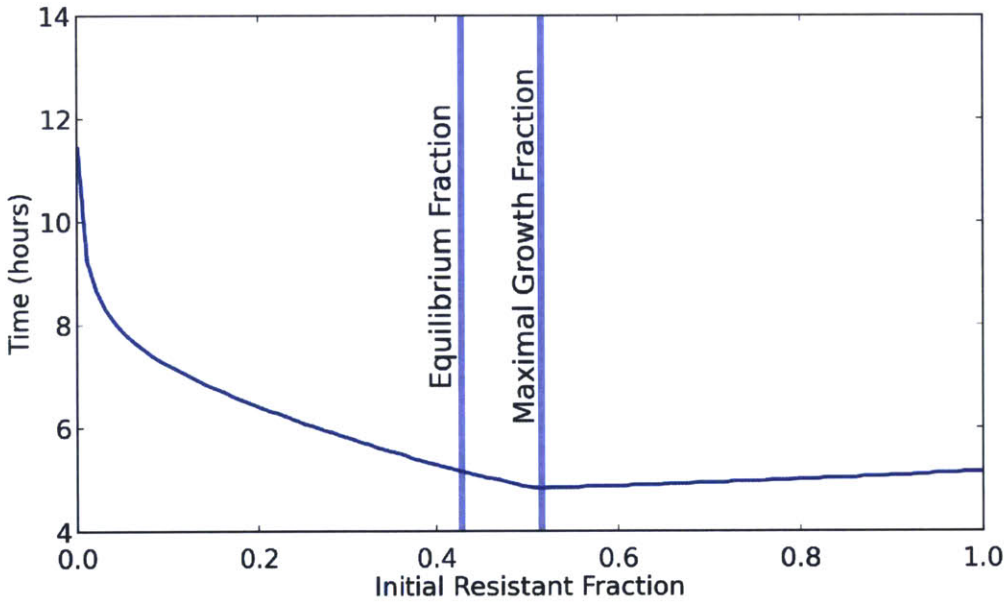

Figure B-14: A fraction of resistant and sensitive cells maximizes population growth rate. Simulations indicate that the fraction that maximizes the population growth rate (the time to reach saturating cell density) corresponds neither to the equilibrium fraction nor to an entirely resistant population. Notably, at the equilibrium fraction, the population growth rate is not substantially lower than that of a purely resistant population. This simulation was carried for the 100 μg/mL ampicillin and 100x dilution factor condition.

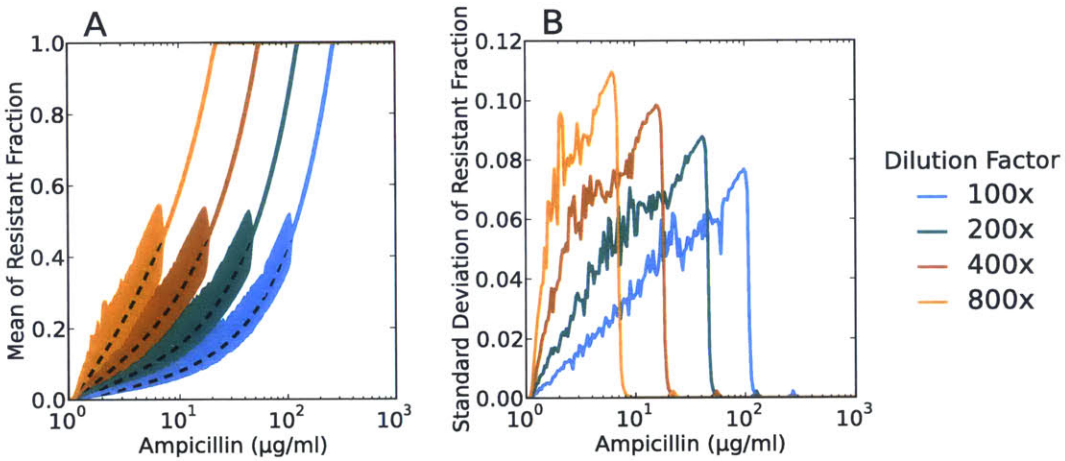

Figure B-15: Oscillatory dynamics. Equilibrium points can be stable or unstable. As the antibiotic concentration decreases, the slope of the difference equation at the fixed point increases in magnitude, and the equilibrium points become unstable. For an unstable equilibrium point, the resistant fraction starts to oscillate about that fixed point. Shown are the results of simulations of the evolutionary dynamics over the course of 50 days. For each antibiotic concentration and dilution factor, the population was started at an initial resistant fraction slightly offset from the equilibrium fraction, and the first 10 days of simulation were disregarded. (A) Shown are the mean resistant fraction (dark thick line, color), the standard deviation of the resistant fraction (lighter color) and the location of the fixed point (black dashed line). Note that for unstable fixed points, the mean fraction is slightly higher than the equilibrium fraction due to the asymmetric nature of the oscillations. (B) Shown is the standard deviation as a function of the ampicillin concentration. The size of the fluctuations is generally small (standard deviation lower than 0.1), making it difficult to tell apart the oscillations from experimental noise in this system. The parameters used in the simulations were acquired from fits to the experimental data (described in the main text). Parameter values are provided in section A.6.2.

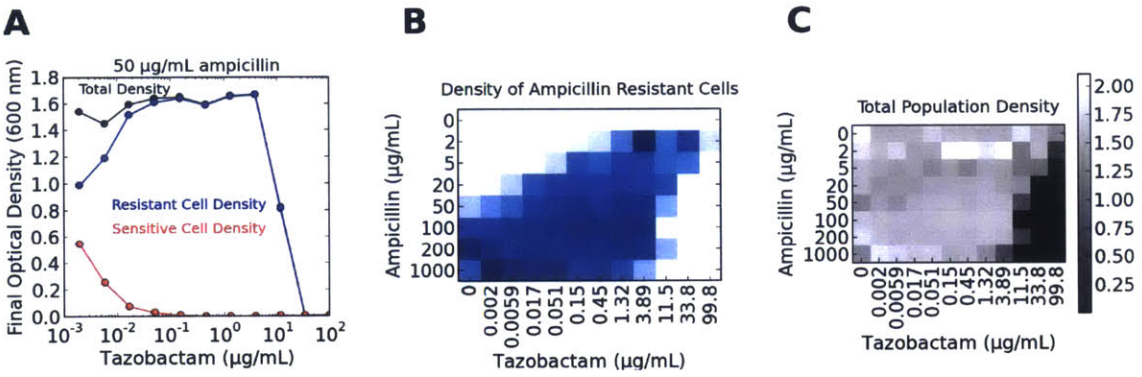

Figure B-16: Selection for resistance in ampicillin and tazobactam. (A) While high concentrations of the inhibitor successfully kill the bacterial population, low and intermediate concentrations of the inhibitor accelerate the spread of resistant cells. Heat maps showing (B) the final density of resistant subpopulation (blue is high density) and (C) the final density of entire bacterial population (white is high density) as a function of the antibiotic and inhibitor concentrations. Subplot (A) corresponds to a slice of subplots (B) and (C) subplots at a fixed ampicillin concentration of 50 μg/mL. In these experiments, a saturated culture with $\sim$10% resistant cells was diluted by a factor 100x into a medium of LB supplemented with ampicillin and tazobactam. After 23 hours of growth, the density of resistant and sensitive cells was measured by combining flow cytometry measurements with an optical density measurement at 600 nm. No kanamycin was present in these experiments.

Also, please see the discussion in Fig. B-24 regarding the change in the equilibrium fractions.

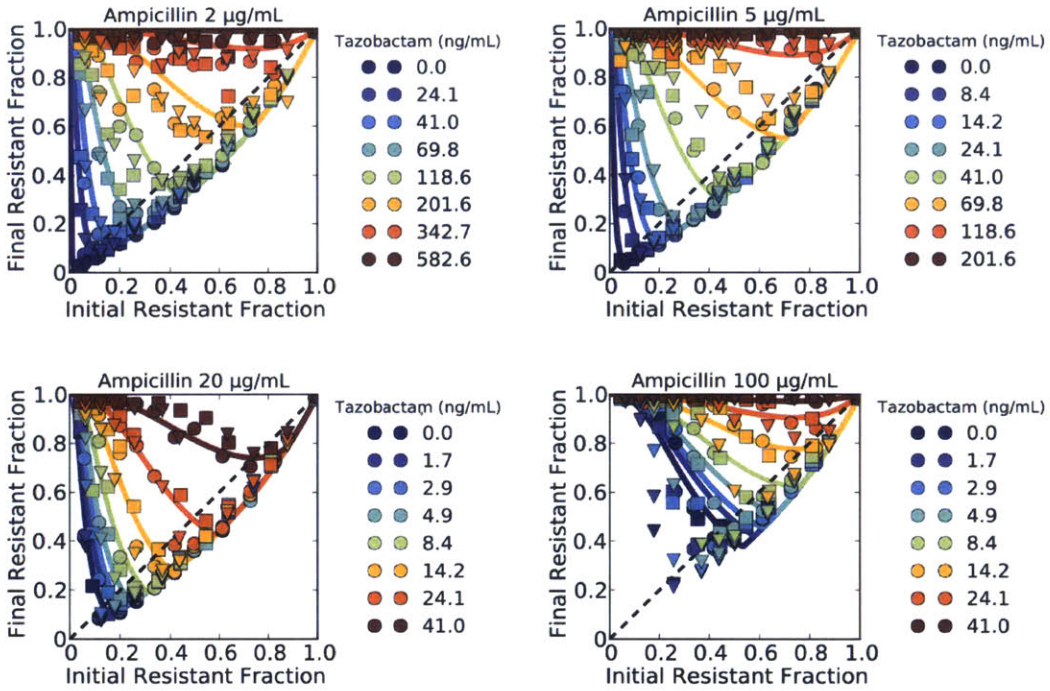

Figure B-17: Difference equation maps in the presence of the inhibitor tazobactam. Each difference equation was measured on 3 different days. The data and analysis presented in Fig. 2-4B, C use these difference equation maps. Data was collected at a dilution factor of 100x. Solid curves represent a single fit of the model to all experimental data.

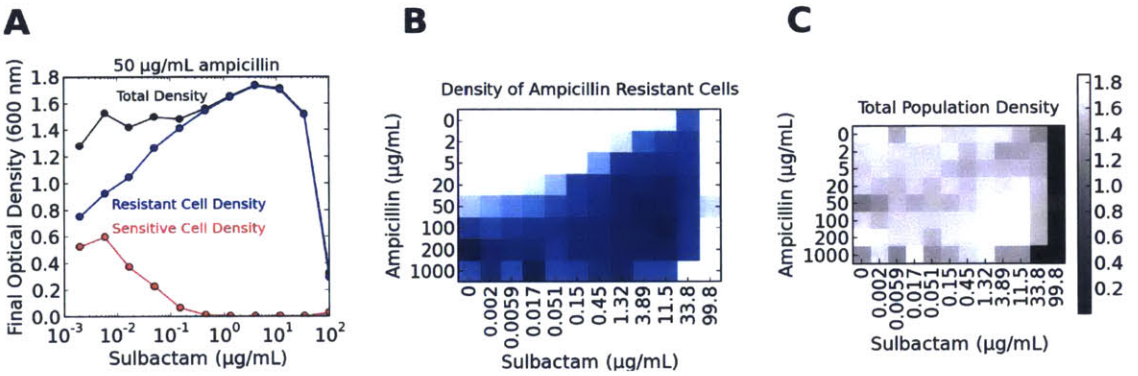

Figure B-18: Selection for resistance may be possible at clinically relevant concentrations. Clinically, ampicillin is combined often with the β-lactamase inhibitor sulbactam. Depending on how the drugs are administered, the peak serum concentration of ampicillin may be between 40 μg/mL - 150 μg/mL while that of sulbactam may be between 10 μg/mL - 120 μg/mL [58, 68, 121]. (A-C) Resistant cells spread at an accelerated rate in the lower concentration ranges of ampicillin/sulbactam while at the higher concentration ranges the growth of the bacterial population is inhibited.

Although resistant cells proliferate across a range of clinically relevant concentrations in our experiments, we want to stress that the minimum inhibitory concentrations of ampicillin/sulbactam is expected to change with the microorganism, and with the initial cell density of the bacterial population. Moreover, the use of ampicillin together with sulbactam is clinically known to be effective against many bacterial infections.

Subplot (B) shows a heat map of the final density of resistant subpopulation (blue is high density). Subplot (C) shows a heat map of the final density of entire bacterial population (white is high density) as a function of the antibiotic and inhibitor concentrations. Subplot (A) corresponds to a slice of subplots (B) and (C) at an ampicillin concentration of 50 μg/mL.

In these experiments, a saturated culture with $\sim$10% resistant cells was diluted by a factor 100x into a medium of LB supplemented with ampicillin and sulbactam. After 23 hours of growth, the density of resistant and sensitive cells was measured by combining flow cytometry measurements with an optical density measurement at 600 nm. No kanamycin was present in these experiments.

Also, please see the discussion in Fig. B-24 regarding the change in the equilibrium fractions.

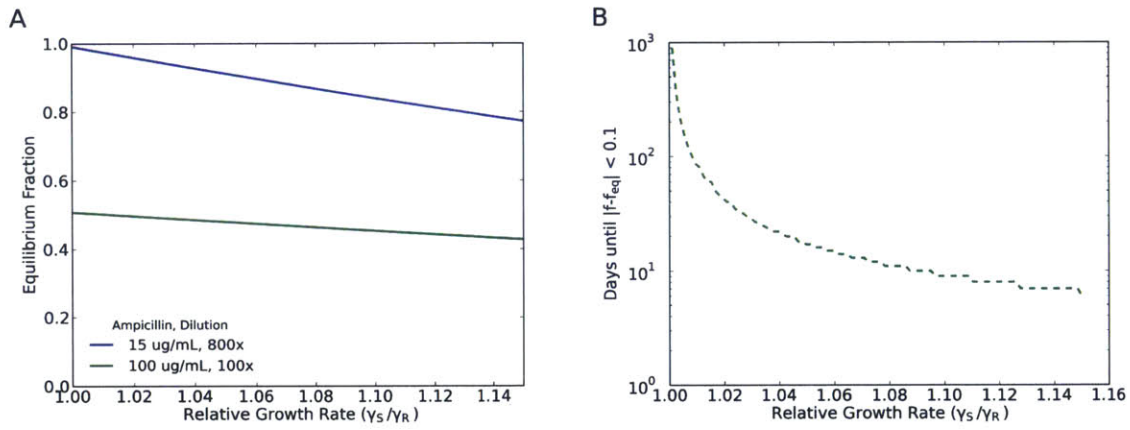

Figure B-19: Effects of the cost of resistance on the equilibrium fraction and the time to reach equilibrium. (A) The equilibrium fraction depends only weakly on the cost of resistance. For example, if the cost of resistance ($\Delta\gamma = \gamma_S - \gamma_R$) decreases by 50% - which corresponds the relative growth rate ($r = \gamma_S/\gamma_R$) decreasing from 1.15 to 1.07 - the equilibrium fraction increases by ~8% ($f_{eq} \sim 0.43 \rightarrow f_{eq} \sim 0.47$) for the 100 μg/mL ampicillin and 100x dilution factor condition. (B) The time to reach equilibrium can change significantly with the cost of resistance. In this simulation, for each relative growth rate, the population was started at a resistant fraction of 0.99, and the time to reach a fraction within 0.1 of the equilibrium was determined. The simulation was carried out for the 100 μg/mL ampicillin and 100x dilution factor condition. As the cost of resistance approaches 0 ($r = 1$), the time to reach equilibrium increases. Note that when the cost of resistance is precisely 0 ($r = 1$), the equilibrium fraction becomes degenerate. In this case, as long as the antibiotic is cleared within the lag time, the fraction of resistant cells does not change since with $r = 1$, the growth rates of resistant and sensitive cells are identical. Parameter values values are provided in section A.6.2.

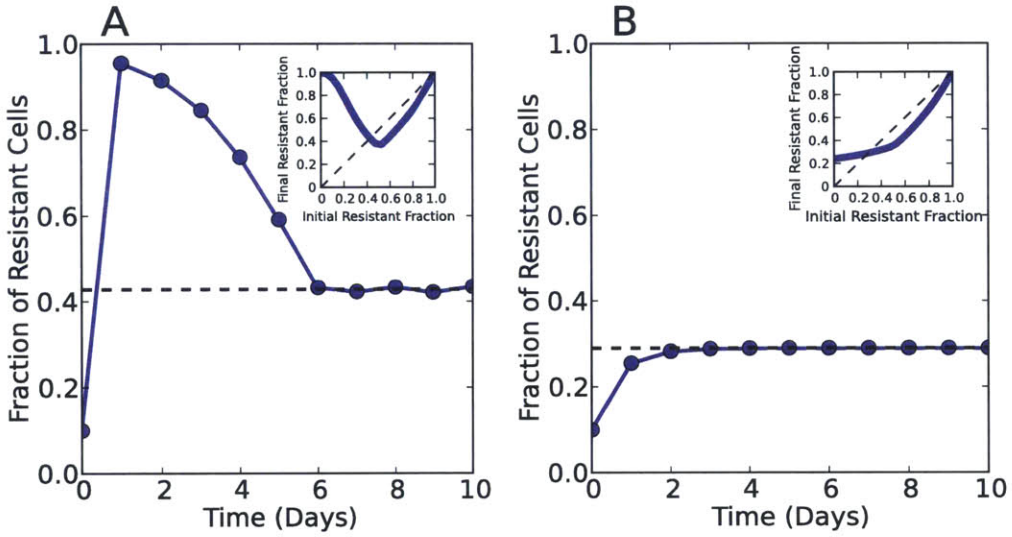

Figure B-20: Difference between bactericidal and bacteriostatic antibiotics. Time course and difference equation map for the death rate of sensitive cells set to (A) 2.8/hr vs. (B) 0/hr. The plots show that the killing of sensitive cells by the antibiotic is responsible for the overshoot of the fraction above the equilibrium fraction when starting at a low initial fraction of resistant cells and for the "V" shape of the difference equation maps. This occurs because below the equilibrium fraction, there are not enough resistant cells to inactivate the antibiotic before it starts to affect the growth of sensitive cells. By killing sensitive cells, a bactericidal antibiotic exerts stronger selection for resistant cells than a bacteriostatic antibiotic that just inhibits the growth of sensitive cells. Simulations were run for an antibiotic concentration of 100 μg/mL and a dilution factor of 100x. Other parameter values can be found in the modeling section of the Supplementary Materials.

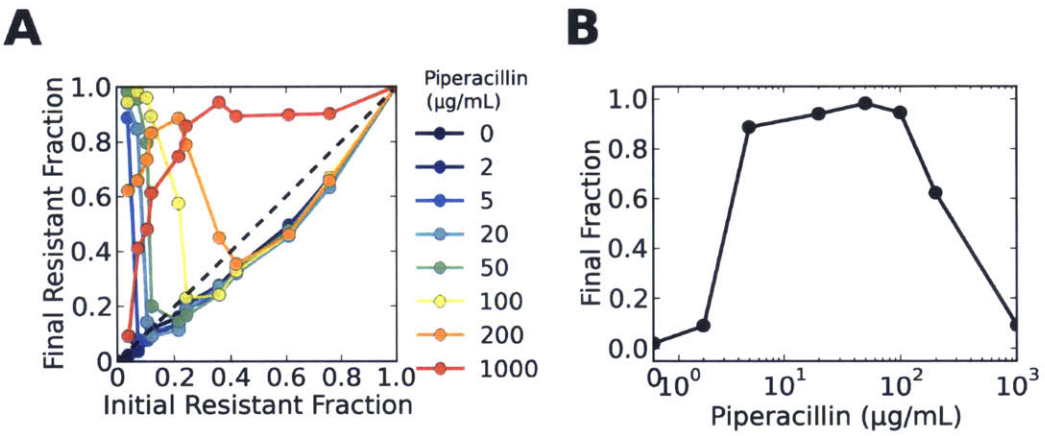

Figure B-21: Non-monotonic behavior in piperacillin. (A) Difference equation map collected in the antibiotic piperacillin. This difference equation maps behaves in accordance with model expectations at low antibiotic concentrations. However, it deviates from predicted behavior at high concentrations of the antibiotic, in which the difference equation maps start to curve down at low initial fractions of resistant cells. (B) Final fraction of resistant cells as a function of the antibiotic concentration revealing non-monotonic selection for resistance with increasing antibiotic concentrations. The non-monotonic behavior is significant: the final resistant fraction reduces from nearly 1 at intermediate piperacillin concentrations to $\sim$0.1 at high piperacillin concentrations, revealing nearly complete cancellation of selection for resistance at high antibiotic concentrations. For all shown data points, the cultures grew to the same saturation density. Subplot (B) is a cross section through subplot (A) corresponding to an initial fraction of resistant cells at $\sim$4%. Data was acquired at a 100x dilution in an LB medium in the absence of kanamycin.

One possible explanation for the deviation from our model and the non-monotonic behavior is that, at the higher antibiotic concentrations, resistant cells begin to lyse releasing β-lactamase enzymes into the extra-cellular space [76]. Extracellularly these enzymes hydrolyze their antibiotic more quickly (higher substrate concentration), leading to the survival of more sensitive cells.

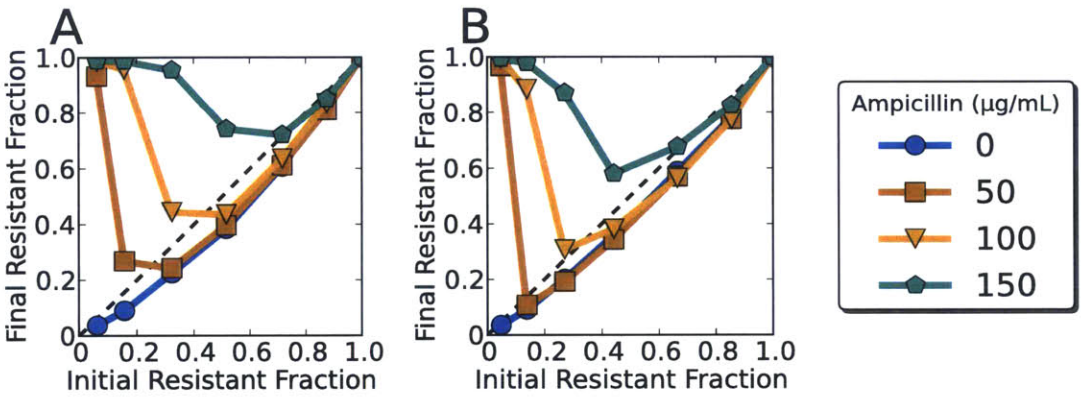

Figure B-22: Controls showing difference equations obtained with fluorescent markers swapped. The resistant and sensitive strains used in the main text expressed CFP and YFP, respectively. To show that the evolutionary dynamics were independent of any differential cost involved in expressing CFP vs. YFP, we created control strains in which we swapped the fluorescent markers in places. (A) Difference equation obtained with resistant and sensitive strains from the main text. (B) Difference equation obtained with CFP and YFP swapped. Data was acquired in LB with 5 μg/mL of kanamycin at 100x dilution.

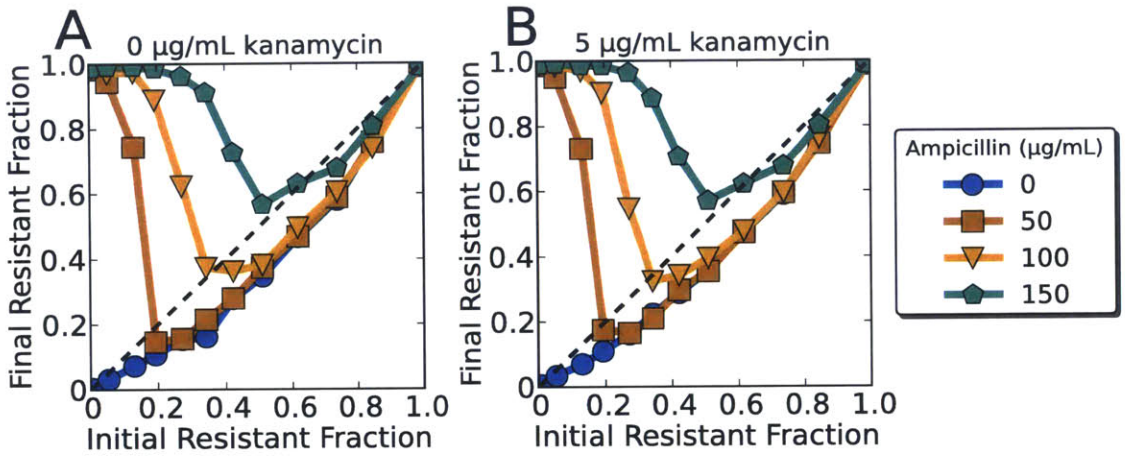

Figure B-23: Addition of 5 μg/mL kanamycin does not significantly affect the evolutionary dynamics. Both resistant and sensitive cells carry a plasmid that encodes for fluorescence and kanamycin resistance. To make sure that this plasmid was not lost during multi-day experiments, a background concentration of 5 μg/mL of kanamycin was added. Kanamycin was used only as a precaution, and its absence or presence (at 5 μg/mL) did not affect the evolutionary dynamics. Difference equations were mapped for 4 different antibiotic concentrations in (A) no kanamycin or in (B) 5 μg/mL kanamycin. Data was acquired at 100x dilution.

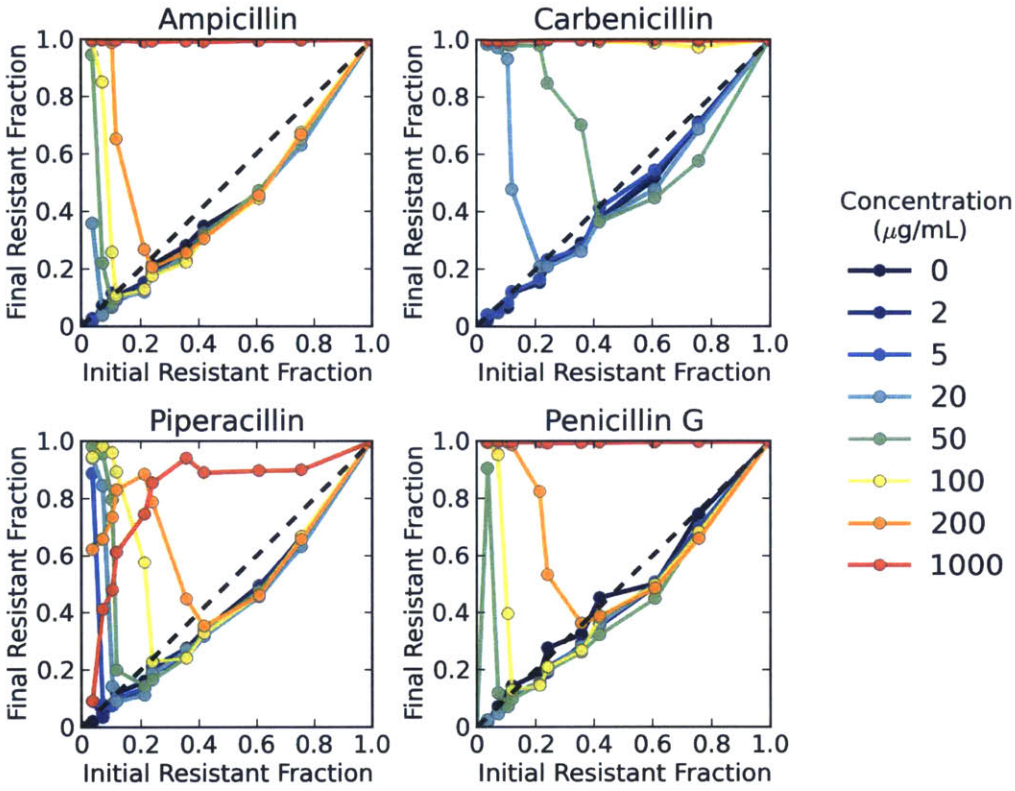
Ampicillin
Carbenicillin
Piperacillin
Penicillin G
Final Resistant Fraction
Initial Resistant Fraction
0
0.2
0.4
0.6
0.8
1.0
Concentration
(μg/mL)
0
2
5
20
50
100
200
1000

Figure B-24: Population dynamics in different β-lactam antibiotics. Examples of difference equation maps collected in the β-lactam antibiotics (A) ampicillin and (B) carbenicillin. (C) Equilibrium fractions extracted from difference equation maps for the β-lactam antibiotics ampicillin, piperacillin, penicillin G and carbenicillin. Consistent with model prediction, the equilibrium fractions are approximately linear in the antibiotic concentration. Deviations from linearity can appear at low concentrations due to the non-zero K_M of Michaelis-Menten hydrolysis of the antibiotic (see main text for explanation). Black dashes lines represent the range over which a line was fit to the data to calculate the slope. (D) The values of the slopes of the equilibrium fraction vs. the antibiotic concentrations acquired at high antibiotic concentrations. The ratio between these slopes should be proportional to the inverse ratio of the hydrolysis rates of these antibiotics. TEM-1 hydrolyzes the antibiotics ampicillin, penicillin G, piperacillin and carbenicillin with approximate kcats of 1200/s, 1100/s, 1000/s and 110/s, respectively [122]. Hence, the model would predict that the slope of carbenicillin as compared to the other antibiotics should be about 10 times larger, which is close to experimental observations. Error bars only capture the error from the linear fit.

We note that the equilibrium fractions for ampicillin are significantly different than those presented in the main text (the equilibrium fractions are off by a factor of $\sim$2-3). The data for this figure (and for supplementary figures 8, 16, 18, and 21) was collected more than a year after the data presented everywhere else in the paper. We do not know what has caused this drift, but we have eliminated differences in the antibiotic stock, in strains or in protocol as possible explanations. The drift could be caused by other parameters that we do not normally control for (e.g., humidity, different filter for de-ionized water, batch-to-batch variations in LB). If anything, the equilibrium fractions here show that the sensitive strains can survive in even larger antibiotic concentrations than indicated in the main text.

Data in subplots (A-D) was acquired at a 100x dilution in an LB medium in the absence of kanamycin.

Appendix C

Supporting Materials for Chapter 3

C.1 Oscillations in models of mutualisms

Mutualistic interactions are generally thought to be stabilizing, with the relative abundances of the two mutualists converging to a fixed ratio over time [92, 98, 123, 124]. Nonetheless, oscillatory dynamics have been observed in a number of theoretical studies of mutualisms [92, 93, 114–116]. The mechanism giving rise to sustained oscillations in many of these studies was mathematical in nature. Specifically, these models incorporated time delays either by using delay differential equations or else by being discrete in time. Such time delays can give rise to exceedingly rich dynamical behavior, including limit cycles and chaos [67, 108, 125]. The use of time delays in ecological models is a practical way of capturing the effects of unknown ecological processes [113, 126]; however, since, at the end of the day, some of the ecological processes remain unknown, the distal cause of any observed oscillations can remain a mystery.

In this section, we show that a few simple mechanistic models of mutualisms can exhibit oscillations in the population abundances of the mutualists when subject to periodic forcing. Importantly, these oscillations occur with a period longer than the period of the driving force. Our failure to observe non-trivial oscillations in a model incorporating only population sizes leads us to suspect that explicitly modelling the interaction between the two mutualists is necessary to recover this dynamical

behavior.

At least anecdotally, we observed more stability in models of cross-feeding interactions than in models of cross-protection interactions when subject to periodic forcing. However, without more rigorous analysis, we advise against interpreting these simulation results too readily since it is not clear how to fairly compare between the models.

C.1.1 Phenomenological model

We begin by exploring a simple phenomenological model of an obligatory mutualism in which the interactions are mediated solely by population densities:

$$\begin{aligned} \frac{dN_1}{dt} &= \gamma_1 N_1 N_2 (1 - \frac{N_1+N_2}{K}) - \delta N_1 \\ \frac{dN_2}{dt} &= \gamma_2 N_2 N_1 (1 - \frac{N_1+N_2}{K}) - \delta N_2 \end{aligned} \tag{C.1}$$

Here, γ_1 and γ_2 are the growth rate of the two mutualists (N_1 and N_2). K is the carrying capacity. δ is the death rate. At low densities, the growth rate of each mutualist increases with the abundance of its partner. The logistic term incorporates competition for a common limiting resource.

We investigated the dynamics of this mutualism under periodic forcing in two ways: (i) by driving the death rate periodically $\delta(t) = \frac{1}{2}(cos(wt) + 1)$, and (ii) by subjecting the population to periodic bottlenecks of constant strength, mirroring our experiments. In the second scheme, the death was entirely due to the periodic bottlenecks, so δ was set to zero. We were unable to produce oscillations with a period longer than that of the periodic forcing using either approach (Fig. C-21, C-22).

C.1.2 Cross-feeding mutualism

To examine the dynamics of a cross-feeding mutualism, we introduced two state variables R_1 and R_2 to keep track of the nutrient concentrations produced by each partner.

$$\begin{aligned}
\frac{dN_1}{dt} &= \gamma_1 f(R_2) N_1 (1 - \frac{N_1+N_2}{K}) \\
\frac{dN_2}{dt} &= \gamma_2 f(R_1) N_2 (1 - \frac{N_1+N_2}{K}) \\
\frac{dR_1}{dt} &= p_1 N_1 - \beta_{21} N_2 f(R_1) \\
\frac{dR_2}{dt} &= p_2 N_2 - \beta_{12} N_1 f(R_2)
\end{aligned} \tag{C.2}$$

Here, N_1 and N_2 are the population sizes of the two mutualists. R_1 and R_2 are the two resources exchanged in the cross-feeding interaction. γ_1 and γ_2 are the growth rates of the two mutualists. f describes how the growth rate depends on the resource abundance. We examined linear (type I, $f(R) = R$) and saturating (type II, $f(R) = \frac{R}{R+h}$) functional responses. K is the carrying capacity. p_1 and p_2 are resource production rates. β_{21} and β_{12} are resource consumption rates. The logistic term incorporates competition for a common limiting resource.

To explore the dynamics of this model in the presence of seasonality, we subjected the population to periodic bottlenecks of constant strength. Specifically, at the end of each cycle, we propagated a fraction of the population into a new environment, mirroring our experimental set up. The simulation results of this cross-feeding model were nuanced with regard to the range of parameters that supported oscillations. Specifically, no oscillations were observed when we propagated the population without carrying over leftover resources. In contrast, carrying over some of the remaining resources when propagating the population produced large oscillations in the relative abundances of the two mutualists. While these oscillations were substantial when using the linear consumption function ($f(R) = R$), the magnitude of oscillations diminished significantly after switching to the more realistic saturating consumption function ($f(R) = \frac{R}{R+h}$). Thus, it seems like it is possible to get oscillations with this model, but under somewhat restrictive conditions.

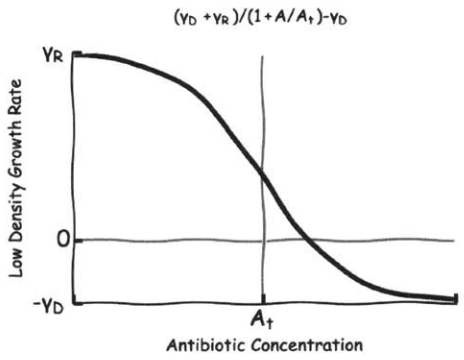

Growth rate in the cross-protection toy model (Eq. C.3)

C.1.3 Cross-protection mutualism

To examine the dynamics of the cross-protection mutualism, we introduced the state variables A_1 and A_2 to keep track of the antibiotic concentrations:

$$\begin{aligned}
\frac{dN_1}{dt} &= (-\gamma_1^D + \frac{\gamma_1^D+\gamma_1^R}{1+A_2/A_2^t})N_1(1-\frac{N_1+N_2}{K}) \\
\frac{dN_2}{dt} &= (-\gamma_2^D + \frac{\gamma_2^D+\gamma_2^R}{1+A_1/A_1^t})N_2(1-\frac{N_1+N_2}{K}) \\
\frac{dA_1}{dt} &= -c_1 A_1 N_1 \\
\frac{dA_2}{dt} &= -c_2 A_2 N_2
\end{aligned} \tag{C.3}$$

Here, γ_1 and γ_2 are the growth rate of the two mutualists (N_1 and N_2). K is the carrying capacity. A_1 and A_2 are the antibiotic concentrations. A_1^T and A_2^T set the scale of antibiotic sensitivity. c_1 and c_2 are antibiotic inactivation rates. The model allows for cell death in both populations (γ_1^D and γ_2^D). The logistic term incorporates competition for a common limiting resource.

To explore the dynamics of this model in the presence of seasonality, we subjected the population to periodic bottlenecks of constant strength. Specifically, at the end of each cycle, we propagated a fraction of the population into a new environment, mirroring our experimental set up. The simulation results of this model were insensitive to whether we carried over leftover antibiotic or not. We found that this model easily gave rise to oscillations with periods longer than the period between subsequent

bottlenecks, especially to period 2 oscillations (Fig. C-6). We also found that the addition of cell death seemed to destabilize the oscillations rather than strengthen them. This destabilization occurred because cell death made the mutualism more likely to collapse (Fig. C-7).

C.1.4 A model incorporating experimental features

To better understand our experimental data, we proceeded to explore the population dynamics using a cross-protection model that incorporated features that are characteristic of the growth of bacteria in the presence of antibiotics:

$$\begin{aligned}
\frac{dN_1}{dt} &= \gamma_1[A_2]N_1(1-\tfrac{N_1+N_2}{K}) \\
\frac{dN_2}{dt} &= \gamma_2[A_1]N_2(1-\tfrac{N_1+N_2}{K}) \\
\frac{dA_1}{dt} &= -V_{max}\tfrac{A_1}{K_m+A_1}N_1(t=0) \\
\frac{dA_2}{dt} &= -c_2A_2N_2
\end{aligned} \tag{C.4}$$

$$\gamma_1[A_2] = \begin{cases} 0 & t < t_{lag} \\ \frac{\gamma_R^1}{1+A_2/IC_{50}} & t \geq t_{lag} \end{cases} \tag{C.5}$$

$$\gamma_2[A_1] = \begin{cases} 0 & t < t_{lag} \\ \gamma_R^2 & t \geq t_{lag} \text{ and } A_1 < MIC_1 \\ -\gamma_D^2 & t \geq t_{lag} \text{ and } A_1 \geq MIC_1 \end{cases} \tag{C.6}$$

In this model, N_1 and N_2 represent the ampicillin and chloramphenicol resistant populations, respectively, while A_1 and A_2 represent the concentrations of the antibiotics ampicillin and chloramphenicol. The dynamics in the presence of the ampicillin were described in detail in a previous study [47]. The dynamics of growth in the presence of chloramphenicol were described in details in [127].

We found that this set of differential equations was adequate to reproduce period-3 like oscillations reminiscent of our experimental data (see Fig. 3-4 for details). However, to reproduce the oscillations at similar ranges of antibiotic concentrations, we had to decrease the death rate of chloramphenicol resistant cells (γ_D^2) as compared to the measured death rate of cells sensitive to ampicillin (Fig. C-4, also see [47]). The simplest interpretation of the need to use a lower death rate is that the actual growth rate of sensitive cells is not a step function in the antibiotic concentration, but rather a smoother function, with a death rate at low antibiotic concentrations that is smaller than the maximal death rate. Overestimating the death of the chloramphenicol resistant population skews the ratio between the two mutualists, leading to a collapse of the mutualism.

Given the highly non-linear form of the differential equations and the large parameter space, the output from these equations is sensitive to variations in parameter values and in functional forms (e.g., a step function vs. a smooth response to the antibiotic). Exhaustively exploring a large parameter space is a challenging task, which means that there may be other combinations of parameter values and functional forms that could reproduce robust period-3 like oscillations. Hence, this model should be viewed with some skepticism.

Despite the aforementioned complications, both this model (Eq. C.4) and its simpler variant (Eq. C.3) make a simple qualitative statement: the oscillations that we observe experimentally are due to the "seasonality" imposed as a result of our daily dilution (Fig. C-6, C-4, C-5). In particular, doing our experiments in a (pseudo)-continuous regime should remove the oscillation in the population abundances (Fig. C-8). This prediction was confirmed experimentally (Fig. 3-2, C-8).

C.2 Mapping the separatrix

To map out the separatrix, we needed to estimate the probability that a mutualism composed of an ampicillin resistant population (N_t^1) and a chloramphenicol resistant population (N_t^2) at time t will reach a "healthy" population size ($N_{t+1}^{total} > 2 \cdot 10^8$ cells/well, Table C.1) at time $t+1$. We assumed that the dynamics were invariant in time. Using this simplification, we divided all the trajectories into 2-step segments and calculated an indicator variable, H, for each segment as follows:

$$H(N_i^1, N_i^2) = \begin{cases} 0 & N_f^{total} < 2 \cdot 10^8 \text{ cells/well} \\ 1 & N_f^{total} \geq 2 \cdot 10^8 \text{ cells/well} \end{cases} \tag{C.7}$$

Here, we replaced the time indexes t and $t+1$ in favor of the i (initial) and f (final) to make the time invariance assumption explicit. To avoid too much writing, we'll let $\vec{x}$ denote an arbitrary position in (N_1, N_2) space, and $\vec{x}_k$ denote the position of the k^{th} data point. To estimate the probability that a population reaches a "healthy" population size ($P(H=1|\vec{x})$), we used Gaussian radial basis functions for interpolation between measured data points. Specifically,

$$n_1(\vec{x}) = \sum_{k}^{\text{data with } H=1} w_k(\vec{x}, \vec{x}_k)$$
$$n_0(\vec{x}) = \sum_{k}^{\text{data with } H=0} w_k(\vec{x}, \vec{x}_k)$$

where w_k is the weight assigned to the k^{th} data point. Basically, we use existing data points to estimate the number of times that the population reaches a healthy population size (n_1) and the number of times it does not (n_0) when starting at a position $\vec{x}$. The weight given to each data point k decays as a Gaussian in the distance between the data point $\vec{x}_k$ and the position of interpolation $\vec{x}$:

$$w_k(\vec{x}, \vec{x}_k) = ce^{-d(\vec{x},\vec{x}_k)^2/(2\sigma^2)}, \tag{C.8}$$

where c and σ are some constants. $d(\vec{x}, \vec{y})$ is the distance between the vector $\vec{x} = (x^A, x^B)$ and the vector $\vec{y} = (y^A, y^B)$ in logarithmic space; i.e., $d(\vec{x}, \vec{y})^2 = (\log_{10}(x^A) - \log_{10}(y^A))^2 + (\log_{10}(x^B) - \log_{10}(y^B))^2$.

Finally, the estimator for the probability of the population to reach a "healthy" population size is simply the fraction of populations that started in "similar" conditions and reached a "healthy" population size:

$$\hat{P}(H = 1) = \frac{n_1}{n_1 + n_0}$$

Plugging in the expressions for n_0 and n_1 from above gives:

$$\boxed{\hat{P}(H = 1|\vec{x}, \sigma) = \frac{\sum_{k}^{\text{data with } H=1} w_k(\vec{x}, \vec{x}_k)}{\sum_{k}^{\text{all data}} w_k(\vec{x}, \vec{x}_k)}} \tag{C.9}$$

This estimator is independent of the value of the constant c that appears in the weights (Eq. C.8) since c cancels out between the numerator and denominator.

C.2.1 Maximum likelihood

We used a maximum likelihood approach to determine the best value of σ to use in conjunction with the estimator of Eq. C.9 (see Fig. C-19 for results). In this analysis, we split the experimental data into two parts: a training data set (D_{train}) and a test data set (D_{test}). Given a particular choice of σ, we trained the model using the training data set and then used this model to evaluate the probability of the test data set.

$$P(D_{test}|\sigma, D_{train}) = \prod_k P(D^k_{test}|\sigma, D_{train})$$

$$\ln P(D_{test}|\sigma, D_{train}) = \sum_k \ln P(D^k_{test}|\sigma, D_{train})$$

$$\ln P(D_{test}|\sigma, D_{train}) = \sum_k \ln P(H = h_k|\sigma, D_{train})$$

Here, D^k_{train} refers to k^{th} test point, and h_k to value of the indicator of the k^{th} test point.

$$\boxed{\hat{\sigma} = \text{argmax}_\sigma \ln P(D_{test}|\sigma, D_{train})} \tag{C.10}$$

Table C.1: An indicator for population health

state at t+1	Healthy (N >2.0e+08)	Unhealthy (2.0e+08 >N >3.4e+06)	Presumed Extinct (3.4e+06 >N)
state at t			
5.1 μg/ml chloramphenicol			
Healthy (N >2.0e+08)	0.97	0.03	0.00
Unhealthy (2.0e+08 >N >3.4e+06)	nan	nan	nan
Presumed Extinct (3.4e+06 >N)	0.00	0.02	0.98
7.6 μg/ml chloramphenicol			
Healthy (N >2.0e+08)	0.83	0.17	0.00
Unhealthy (2.0e+08 >N >3.4e+06)	0.92	0.00	0.08
Presumed Extinct (3.4e+06 >N)	0.00	0.01	0.99
11.4 μg/ml chloramphenicol			
Healthy (N >2.0e+08)	0.80	0.19	0.01
Unhealthy (2.0e+08 >N >3.4e+06)	0.66	0.00	0.34
Presumed Extinct (3.4e+06 >N)	0.00	0.02	0.98
17.1 μg/ml chloramphenicol			
Healthy (N >2.0e+08)	0.76	0.20	0.04
Unhealthy (2.0e+08 >N >3.4e+06)	0.42	0.00	0.58
Presumed Extinct (3.4e+06 >N)	0.00	0.02	0.98
25.6 μg/ml chloramphenicol			
Healthy (N >2.0e+08)	0.76	0.22	0.02
Unhealthy (2.0e+08 >N >3.4e+06)	0.30	0.04	0.66
Presumed Extinct (3.4e+06 >N)	0.00	0.03	0.97
38.4 μg/ml chloramphenicol			
Healthy (N >2.0e+08)	0.46	0.40	0.13
Unhealthy (2.0e+08 >N >3.4e+06)	0.24	0.00	0.76
Presumed Extinct (3.4e+06 >N)	0.00	0.01	0.99

To analyze the collapse of the mutualism, we needed a good indicator of population health. An obvious choice for an indicator of population health is simply the total population size. We defined the population to be "healthy" if the total population size was above $2 \cdot 10^8$ cells/well (about half of the carrying capacity).

This indicator is very convenient in practice because the population size of large populations can be reliably measured using spectrophotometry; however, being based only on the total population size, this indicator ignores other potentially relevant information, such as the relative abundances of various subpopulations, meaning that it may not work. To show that this indicator was useful, we needed to demonstrate that it had at least some predictive power about whether the population was about to collapse. Thus, to evaluate the quality of the indicator, we analyzed the trajectories of many populations across multiple environments. In our analysis, we discretized measurements of population sizes into 3 non-overlapping intervals: (i) "presumed extinct" ($N < 3.4 \cdot 10^6$ cells/well, which is close to the limit of detection), (ii) "unhealthy" ($3.4 \cdot 10^6$ cells/well $< N < 2 \cdot 10^8$ cells/well, and (iii) "healthy" ($N > 2 \cdot 10^8$ cells/well). Then, for each environment, we used all the populations trajectories to estimate the conditional probability of switching from one interval at time t to another interval at time $t + 1$; i.e., estimating $P(Z_{t+1} = z_{t+1} | Z_t = z_t)$, where Z is a discrete random variable, which can assume 1 of 3 possible values corresponding to the 3 intervals. Reassuringly, the "presumed extinct" region remained true to its name: co-cultures which entered this region were unlikely to later attain larger population sizes. Examining the conditional probabilities further showed that this indicator was indeed a good measure of population health. When the population size dropped to less than half of the carrying capacity, it was more likely to go extinct afterwards. Moreover, this indicator was better at harsher environments.

In these experiments, we started 96 co-cultures with different initial subpopulation compositions and measured the total population size of each co-culture over time. The six environments had different chloramphenicol concentrations: 5.1, 7.6, 11.4, 17.1, 25.6, 38.4 μg/ml, but were otherwise the same (100x dilution strength, $\Delta T = 24$ hr, 10 μg/ml ampicillin). It is important to note that the conditional probability is not a proper statistic because there is a hidden variable (the relative abundances of each mutualist), but no obvious way of correctly averaging over it. To make our analysis a bit less dependent on the particular choice of the initial population compositions, we removed the first two days of each trajectory, allowing the dynamics to "equilibrate".

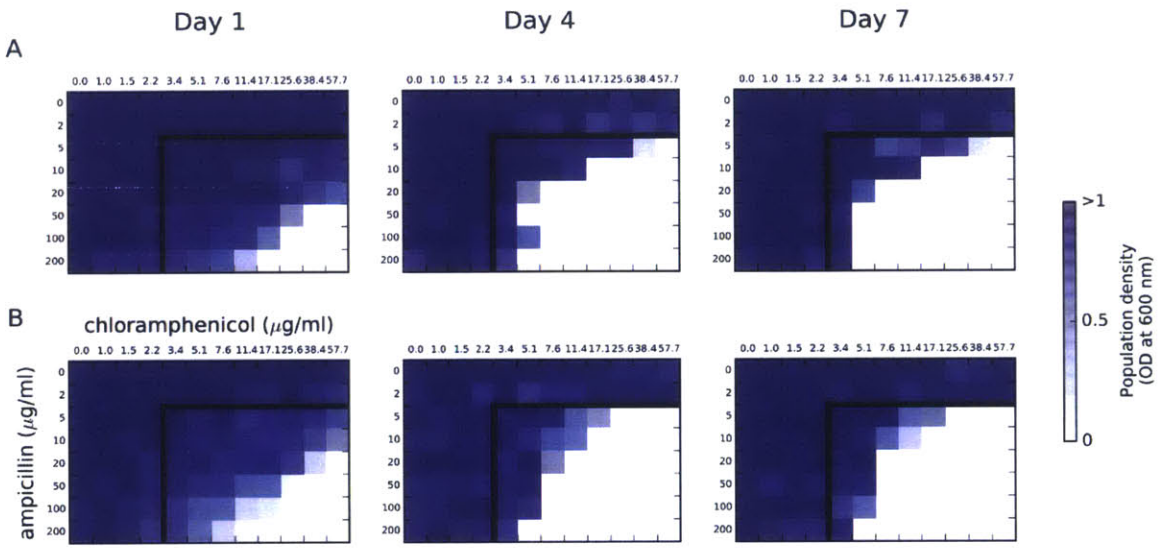

Figure C-1: Comparison between the obligatory region found in two independent experiments at 100x dilution.

Optical density measurements were done at 600 nm. For reference, an optical density of 1 unit corresponds to approximately $4 \cdot 10^8$ cells/well. Cultures were grown in 200 μl of medium.

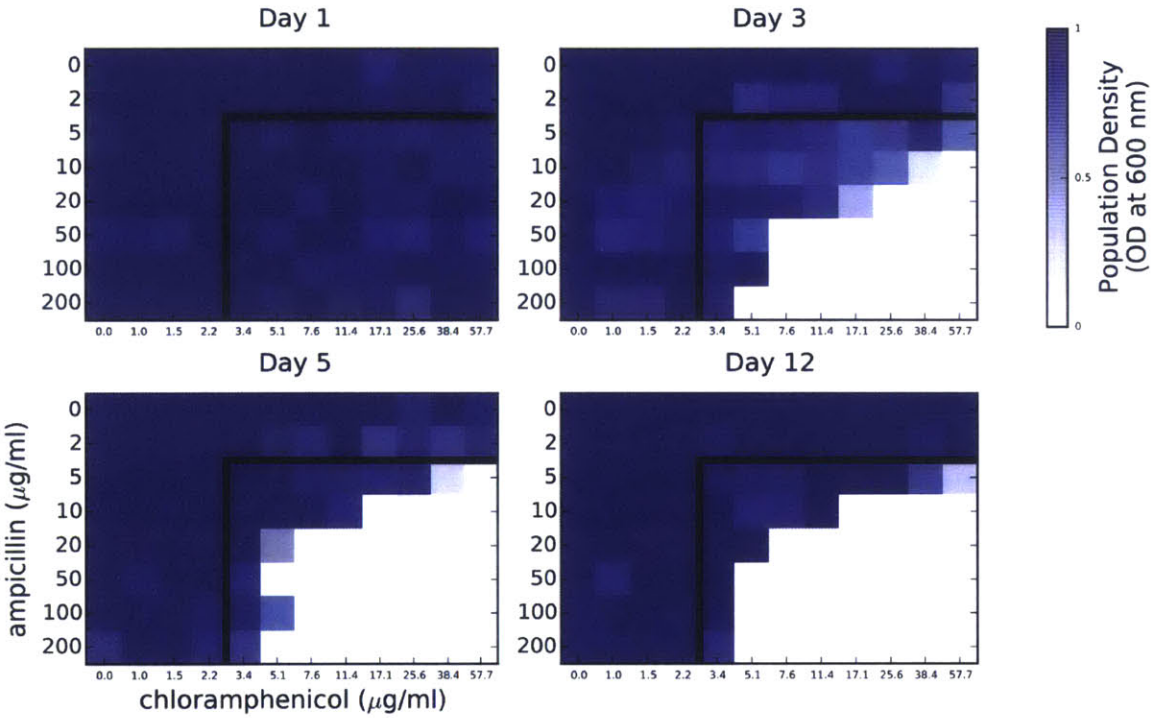

Figure C-2: To systematically examine how the dynamics depend on the antibiotic concentrations, we varied both antibiotic concentrations while fixing the dilution strength at 100x. The co-cultures were started at a high cell density (close to the carrying capacity) on the first cycle to make it easier for the co-culture to survive. The initial ratio between the ampicillin and chloramphenicol resistant subpopulations was 1:4. In the range of antibiotics probed, every single population survived the first growth cycle, but shortly thereafter a significant fraction of these populations went extinct. Nonetheless, after a few cycles, many of the co-cultures stopped collapsing, revealing a substantial range of antibiotic concentrations where the mutualism is successful. A subset of this data is shown in Fig. 3-2. Optical density measurements were done at 600 nm. For reference, an optical density of 1 unit corresponds to approximately $4 \cdot 10^8$ cells/well. Cultures were grown in 200 μl of medium. Black lines denote the range of antibiotic concentrations above which neither mono-culture can grow on its own (Fig. 3-1).

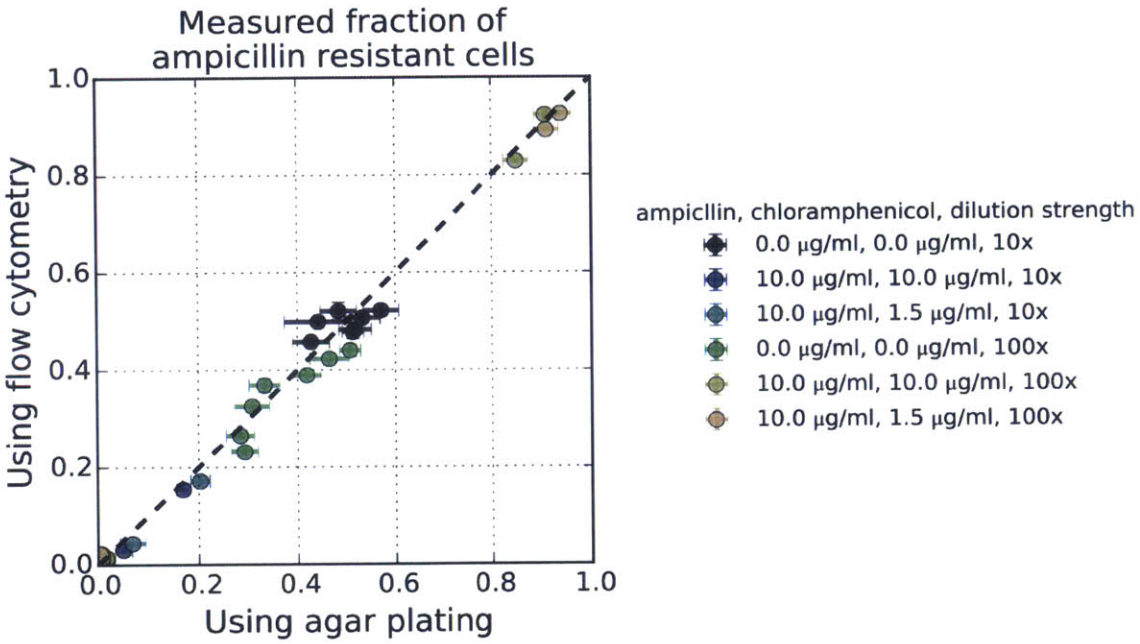

Figure C-3: Flow cytometry and CFU counting measurements are consistent with each other. Shown is the fraction of ampicillin resistant cells out of only *fluorescent* cells that was measured using each method; equality in fraction measurements implies equality in relative abundance measurements. The agreement between flow cytometry and agar plating measurements is excellent. In the presence of antibiotics, there is a small systematic discrepancy ($\Delta f < \sim 0.03$) between the two methods, with flow cytometry usually giving a lower fraction of ampicillin resistant cells than measured using agar plating. A reasonable guess is that in the presence of antibiotics, a small fraction of the ampicillin resistant population is not fluorescent enough to be detected by flow cytometry.

We are careful in pointing out that only *fluorescent* cells were considered because non-fluorescent cells (sensitive cells) were present on agar plates at small quantities (see discussion about emergence of sensitive cells in Fig. C-18). Of course, since the fraction of sensitive cells was so small, doing the analysis without correcting for non-fluorescent cells hardly changes the result. The error bar shown corresponds to the approximate error in the fraction, $f_{err} \approx \sqrt{\frac{f(1-f)}{N}}$. See Fig. C-18 for further details about the data and experiment.

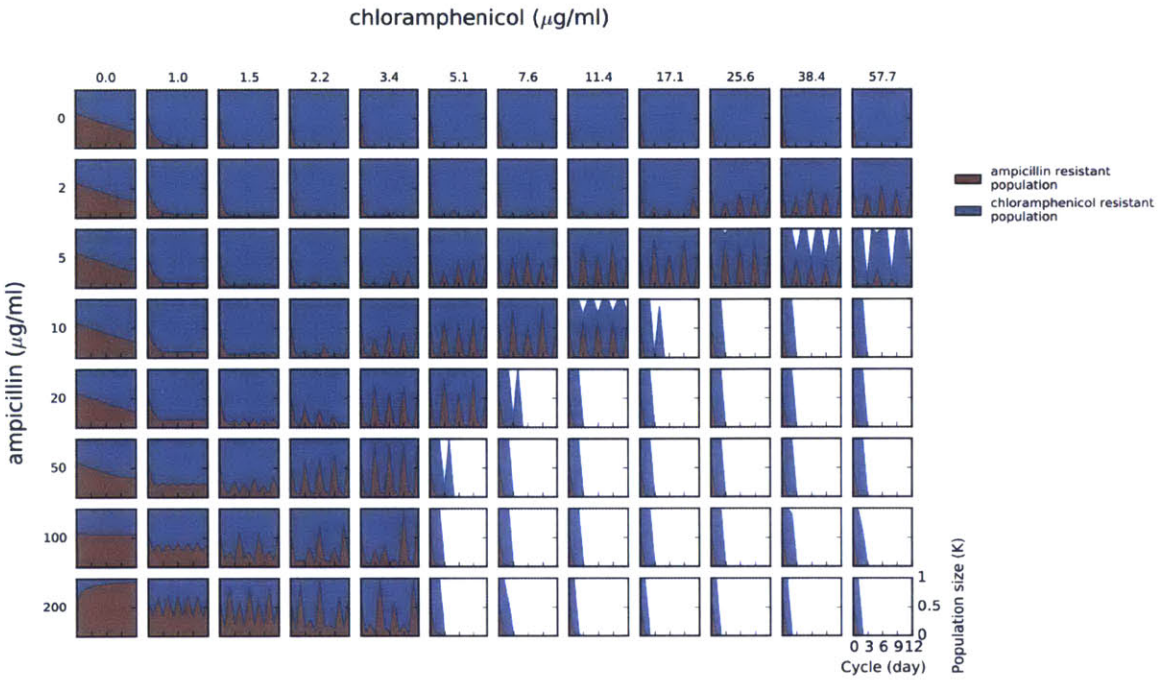
chloramphenicol (μg/ml)
0.0
1.0
1.5
2.2
3.4
5.1
7.6
11.4
17.1
25.6
38.4
57.7
ampicillin (μg/ml)
0
2
5
10
20
50
100
200
ampicillin resistant population
chloramphenicol resistant population
Population size (K)
1
0.5
0
0 3 6 9 12
Cycle (day)

Figure C-4: A model incorporating known experimental features can exhibit robust period 3-like oscillations across a range of antibiotic concentrations (Eq. C.4, C-12). Cells were grown for a period of time (ΔT) in a medium containing both antibiotics. At the end of the growth period, the cell populations (and any left-over antibiotic) were diluted into a fresh medium (which was also supplemented with antibiotics).

At high concentrations of the antibiotic ampicillin, the death rate of sensitive cells was previously measured to be ~ 2.8/hr [47]. However, to get a survival region similar to what we measure experimentally, we had to nearly completely turn off the death rate, reducing it to 0.2/hr. Likely, this discrepancy just reflects that this model does not adequately capture the dynamics of cell death.

In this model, the rate of ampicillin inactivation is proportional to the initial density of ampicillin resistant cells (Eq. C.4, $\frac{dA_1}{dt} \propto -\mathbf{N_1(t=0)}$). We tried altering this rate to be proportional to the concurrent density of ampicillin resistant cells ($\frac{dA_1}{dt} \propto -\mathbf{N_1(t=t)}$), but could not find robust period 3 like oscillations (although oscillations were still present). Exhaustively exploring such a large parameter space is a challenging task, so there may be combinations of parameter values that could produce robust period-3 like oscillations. However, given our present understanding, the interpretation of this result would be that period 3-like oscillations is driven by extra-cellular *beta*-lactamase enzymes carried over from the previous dilution cycle.

The parameter values used in the simulation are provided in the table below. These values should be close to experimentally measured values, with the exception of the death rate.

Model Parameter	Meaning	Value Used
γ_1^R	growth rate of ampicillin resistant cells in absence of chloramphenicol	1.18/hr
γ_2^R	growth rate of chloramphenicol resistant cells in absence of ampicillin	1.21/hr
γ_2^D	death rate of chloramphenicol resistant cells at high ampicillin concentrations	**0.2/hr**
MIC_2	ampicillin concentration above which chloramphenicol resistant cells start to die	2.5 μg/ml
IC_{50}	chloramphenicol concentration at which the growth rate of ampicillin resistant cells drops by half	0.7 μg/ml
K_M	Michaelis-Menten constant for ampicillin inactivation	6.7 μg/ml
K	carrying capacity (density)	$\sim 2.3 \cdot 10^6 cells/\mu l$
V	volume of container in which cells were grown	200 μl
N_{min}	lowest viable population density (finiteness of population size)	~ 1 cell $\equiv 10^{-8} K \cdot V$
C_2	inactivation rate of chloramphenicol	$30/(hr \cdot K)$
V_{max}	hydrolysis rate of ampcillin	22500 $\frac{\mu g}{ml \cdot hr \cdot K}$
t_{lag}	lag time during which no growth occurs (but antibiotic can be inactivated)	1 hr
fold dilution	fold dilution between cycles	100x
ΔT	time between cycles	24 hr

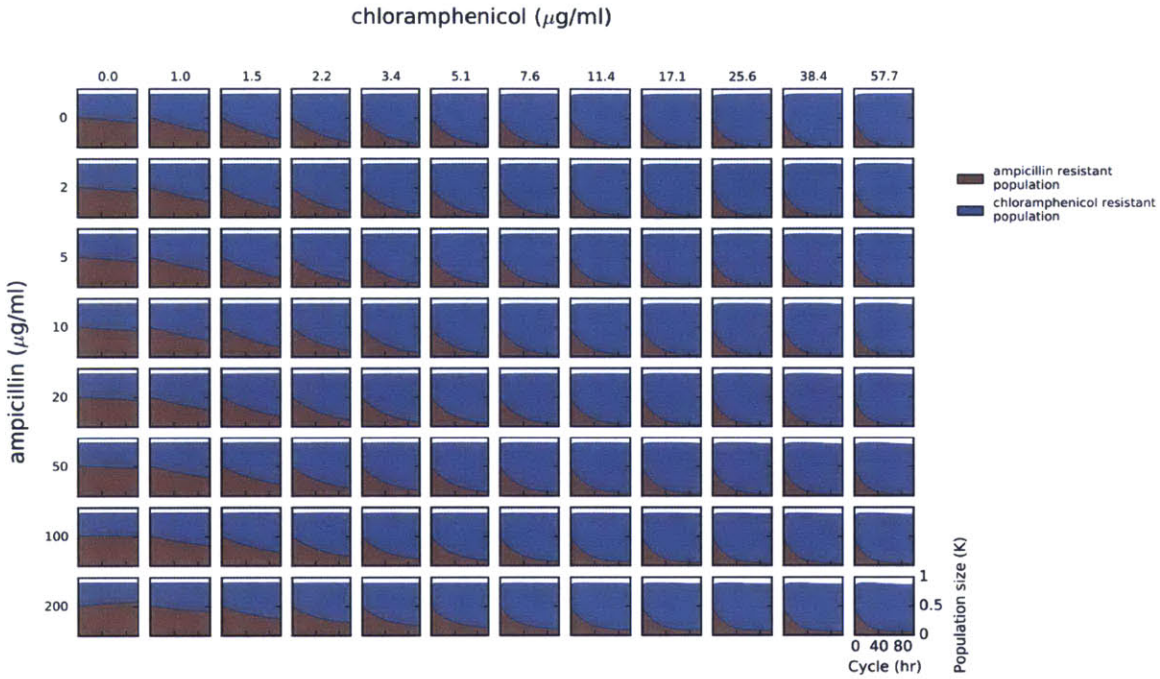

Figure C-5: A model incorporating known experimental features exhibits no oscillations in a (pseudo)-continuous regime (Eq. C.4, compare with Fig. C-4).

The parameter values used in the simulation are provided in the table below. These values should be close to experimentally measured values, with the exception of the death rate.

Model Parameter	Meaning	Value Used
γ_1^R	growth rate of ampicillin resistant cells in absence of chloramphenicol	1.18/hr
γ_2^R	growth rate of chloramphenicol resistant cells in absence of ampicillin	1.21/hr
γ_2^D	death rate of chloramphenicol resistant cells at high ampicillin concentrations	0.2/hr
MIC_2	ampicillin concentration above which chloramphenicol resistant cells start to die	2.5 μg/ml
IC_{50}	chloramphenicol concentration at which the growth rate of ampicillin resistant cells drops by half	0.7 μg/ml
K_M	Michaelis-Menten constant for ampicillin inactivation	6.7 μg/ml
K	carrying capacity (density)	$\sim 2.3 \cdot 10^6 cells/\mu l$
V	volume of container in which cells were grown	200 μl
N_{min}	lowest viable population density (finiteness of population size)	~ 1 **cell** $\equiv 10^{-8} K \cdot V$
C_2	inactivation rate of chloramphenicol	$30/(hr \cdot K)$
V_{max}	hydrolysis rate of ampcillin	22500 $\frac{\mu g}{ml \cdot hr \cdot K}$
t_{lag}	lag time during which no growth occurs (but antibiotic can be inactivated)	**0 hr**
fold dilution	fold dilution between cycles	**1.2x**
ΔT	time between cycles	**1 hr**

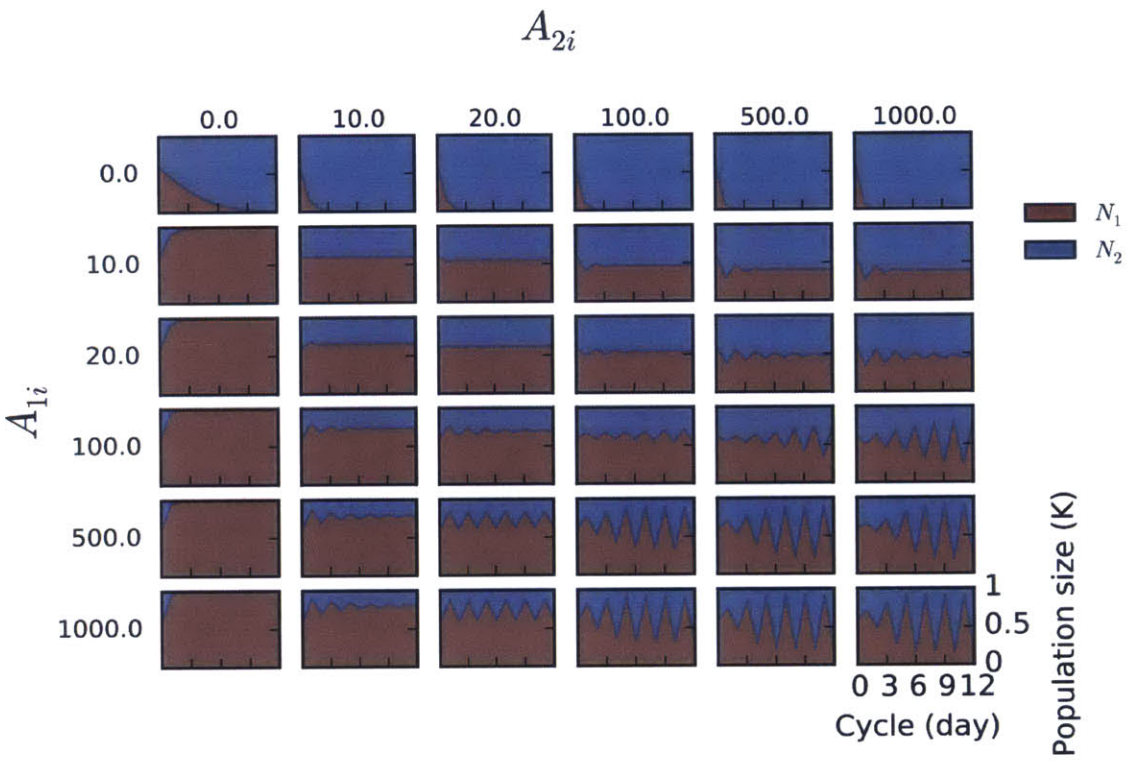

Figure C-6: A "generic" cross-protection mutualism subject to periodic dilution exhibits oscillations of a period longer (period 2) than the driving period. Other periods can be produced by changing the form of the functional response to the antibiotic; for example, using a step function response instead of the smooth function used in Eq. C.3. This simulation was carried out in the absence of cell death. Including cell death in our simulations seemed to significantly reduce the ability of the mutualism to oscillate (Fig. C-7).

Parameters used in simulation: $C_1 = 50.0, C_2 = 100.0, K = 1.0, A_2^t = 1.0, A_1^t = 1.0, \gamma_1^R = 1.0, \gamma_2^R = 1.1, \gamma_1^D = 0, \gamma_2^D = 0$. Population densities at the beginning of the first cycle were $N_{1i} = 0.006, N_{2i} = 0.004$. The differential equations were integrated for $\Delta T = 24$. Parameters are in arbitrary units. At the end of the growth cycle, the population was diluted by a factor 100x. This process was repeated for a number of cycles.

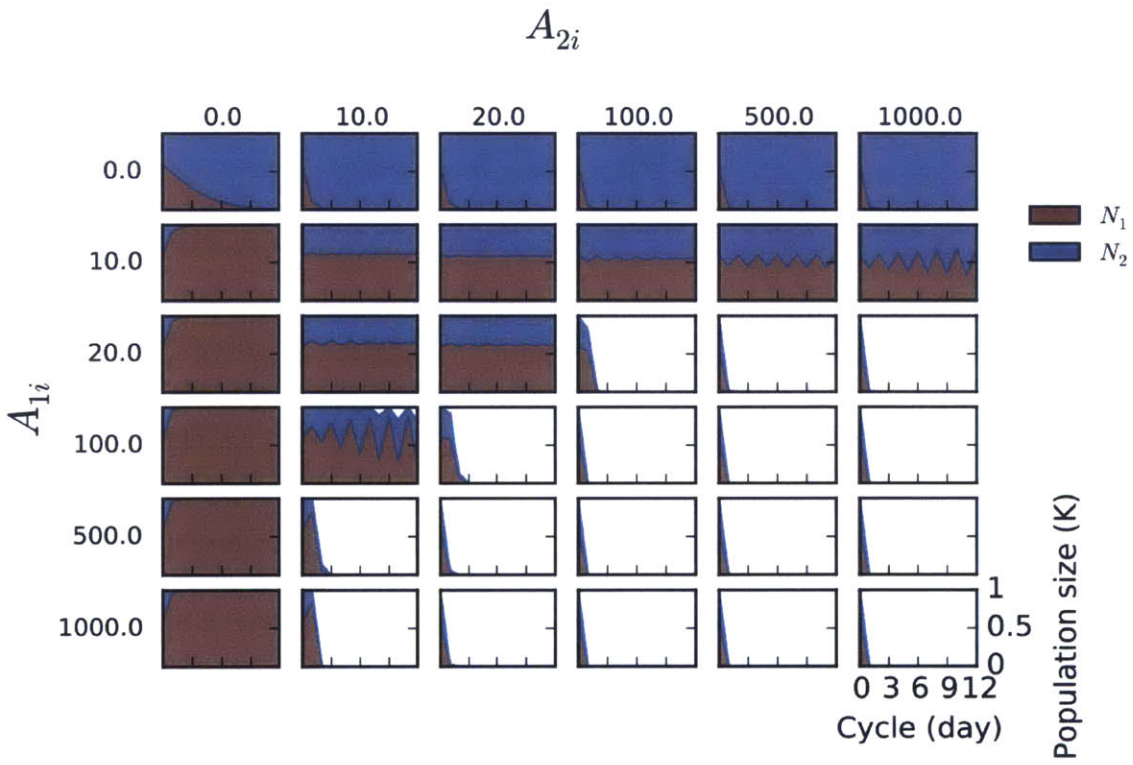

Figure C-7: Including cell death in our simulations seems to cause the mutualism to collapse, which reduces regions where the mutualism can exhibit stable oscillations in the ratio between the two subpopulation sizes. This simulation has the same parameters as the simulation in Fig. C-6, except that the death rates are nonzero ($\gamma_1^D = 0.2, \gamma_2^D = 0.2$).

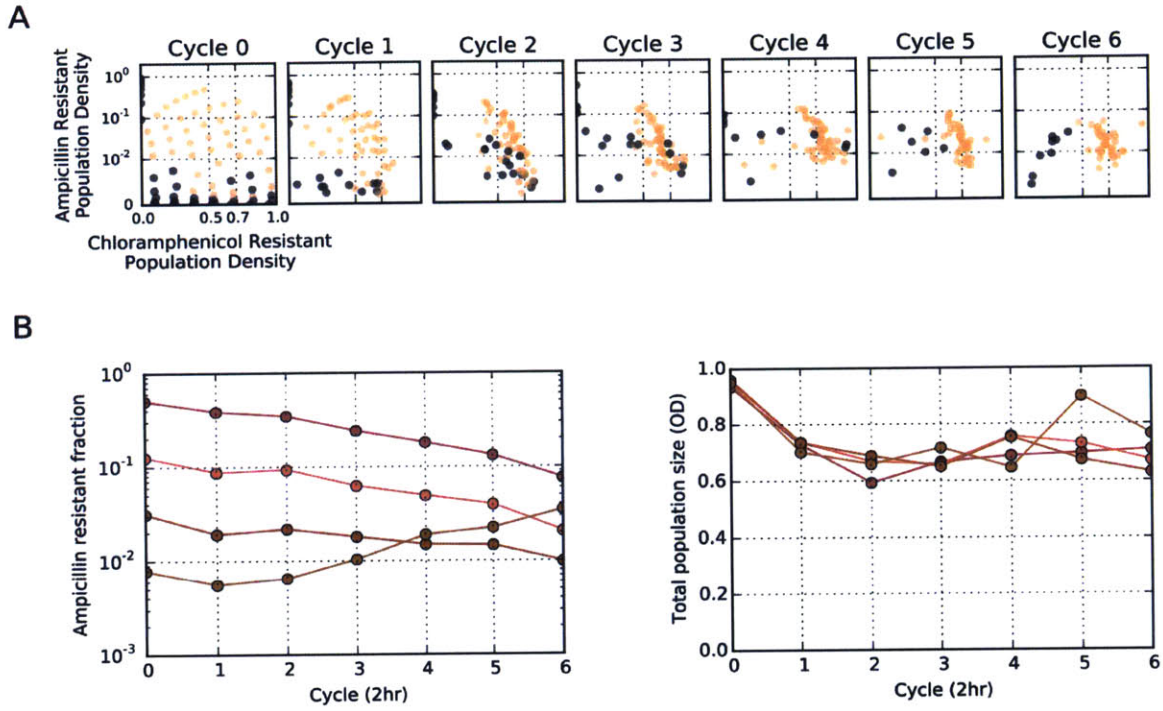

Figure C-8: In a (pseudo)-continuous regime, the co-culture does not exhibit oscillations in the subpopulation abundances. We started co-cultures at a variety of different population compositions. (A) Snapshots of the subpopulation abundances as a function of time. The populations that manage to survive converge toward an equilibrium point with ampicillin and chloramphenicol population densities of 0.02 OD, 0.7 OD, respectively. We color-coded each point along the trajectory according to the overall population density measured on cycle 6. A copper color was assigned if the population density on cycle 6 was larger than 0.5 OD, and a black color otherwise. Hence, for an overview of the trajectories that result in survival, one can simply focus on the set of all copper-colored points. Points corresponding to total population densities lower than $\sim$0.05 OD were removed from the subplots because that density corresponds to the limit of detection. For this reason, the number of black points (i.e., populations with a density smaller than 0.5 OD) decreases with time as some of these populations collapse. We note that the limit of detection is specifically for the total population density, not the relative population abundances. Hence, measurements of populations near the equilibrium point are well-above the limit of detection (since the total population size is $\sim$0.7 OD which is significantly larger than $\sim$0.05 OD). (B) A few selected trajectories over time.

Experiment was done at 10 μg/ml ampicillin and 10 μg/ml chloramphenicol. The time between cycles was 2 hr and the dilution strength was 2x. Optical density measurements were done at 600 nm. For reference, an optical density of 1 unit corresponds to approximately $4 \cdot 10^8$ cells/well. Cultures were grown in 200 μl of medium.

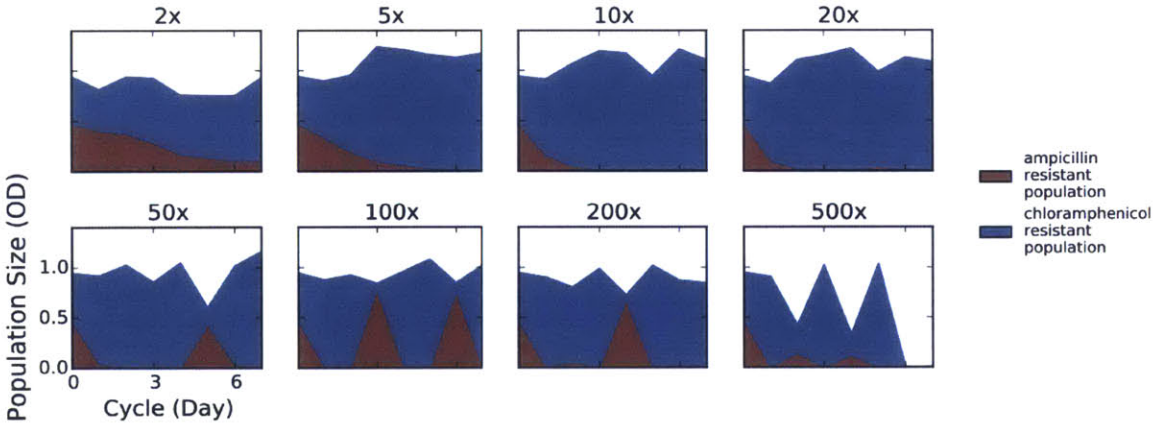

Figure C-9: Population dynamics measured in environments of different dilution strengths. In these experiments, the ampicillin and chloramphenicol concentrations were fixed at 10 μg/ml and 5.1 μg/ml, respectively. When subject to a stronger dilution, the mutualism starts the growth cycle at a smaller population size. Because smaller populations take longer to inactivate the antibiotics, the mutualism may be unable to survive. Consistent with this logic, we found that, at a dilution strength 500x, the mutualism collapsed within a few cycles. At intermediate dilution strengths, the mutualism was able to establish successfully, but with oscillations in the ratio between the population sizes of the mutualists. At still smaller dilutions, the oscillations disappeared as might be expected in light of the stability of the mutualism in the continuous regime (Fig. 3-3B, C-8).

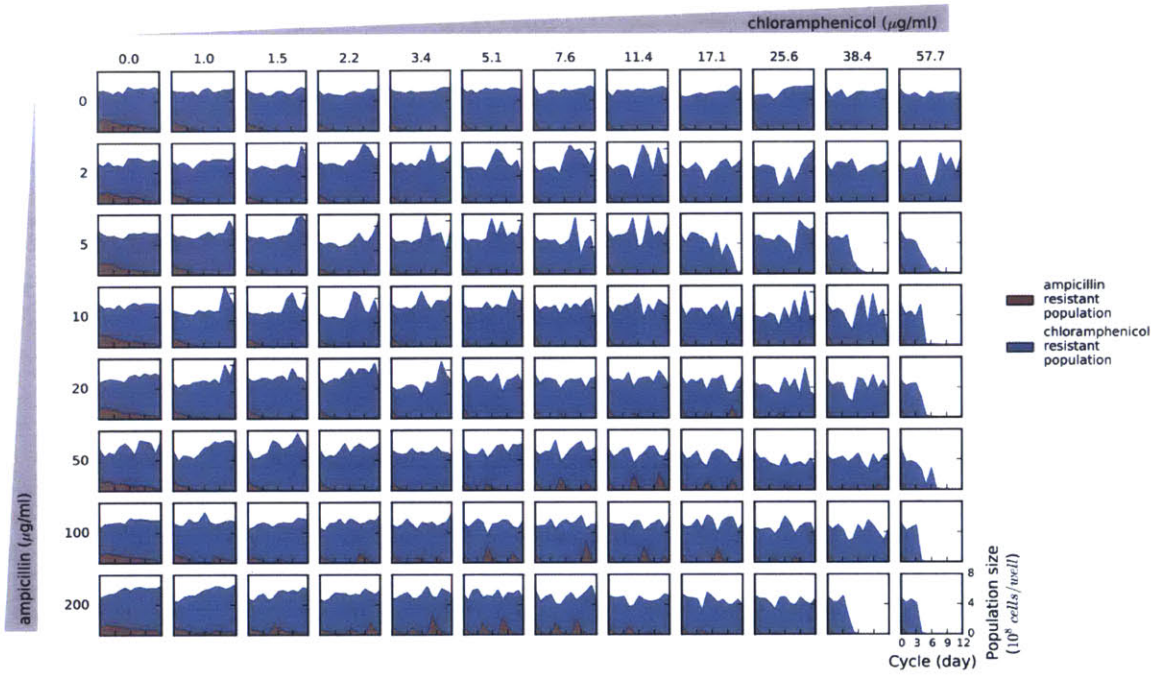

Figure C-10: Population dynamics across different antibiotic concentrations at a dilution strength of 10x. The range of antibiotic concentrations at which the mutualism successfully formed was significantly larger at a dilution strength of 10x as compared to a dilution strength of 100x (Fig. C-12). Similarly, the oscillatory dynamics shifted to higher antibiotic concentrations and exhibited a more variable period.

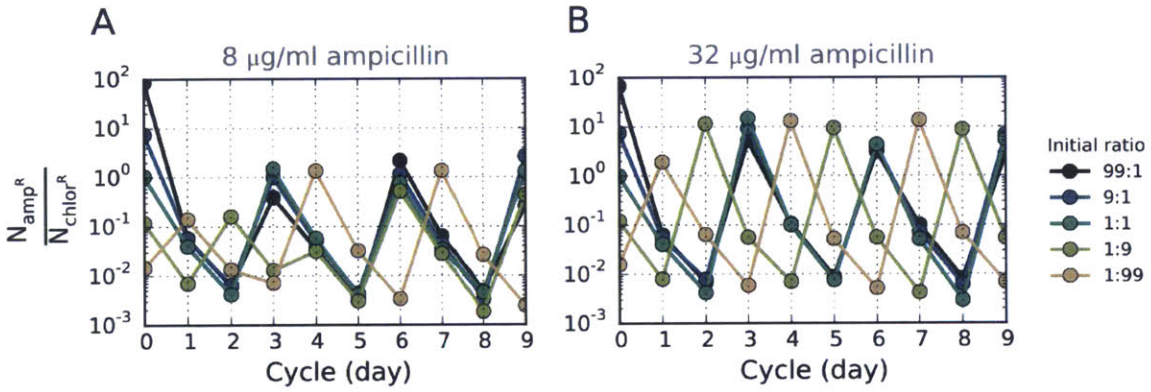

Figure C-11: Oscillations in the ratio between the two mutualist subpopulations appear even at antibiotic concentrations where the mutualism is no longer obligatory. In these experiments, the dilution strength was fixed at 100x, the time between dilutions at 24 hours and the chloramphenicol concentration at 2 μg/ml. In this environment, the ampicillin resistant mono-culture can survive on its own (Fig. 3-1).

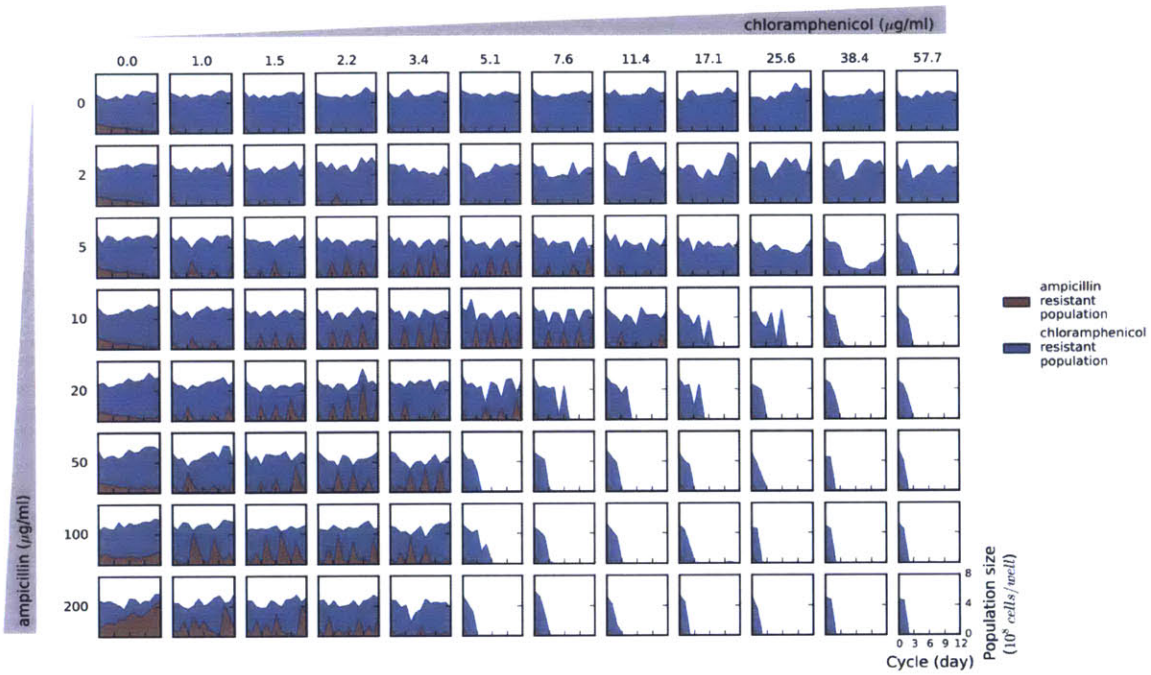

Figure C-12: Population dynamics across different antibiotic concentrations at a dilution strength of 100x. The region of obligatory mutualism corresponds to antibiotic concentrations in which neither of the strains can survive on its own. This region starts at ampicillin concentrations above 2 μg/ml and chloramphenicol concentrations above 2.2 μg/ml (Fig. 3-1). In much of this, successful mutualisms exhibit strong period 3 like oscillations. However, oscillatory dynamics can be seen at lower antibiotic concentrations as well, albeit with additional periods. Although some of the trajectories look aperiodic, it is difficult to know whether these trajectories are truly chaotic, or whether a combination of experimental noise and a slow time to converge produced the observed dynamics. A subset of this data was used to create Fig. 3-2.

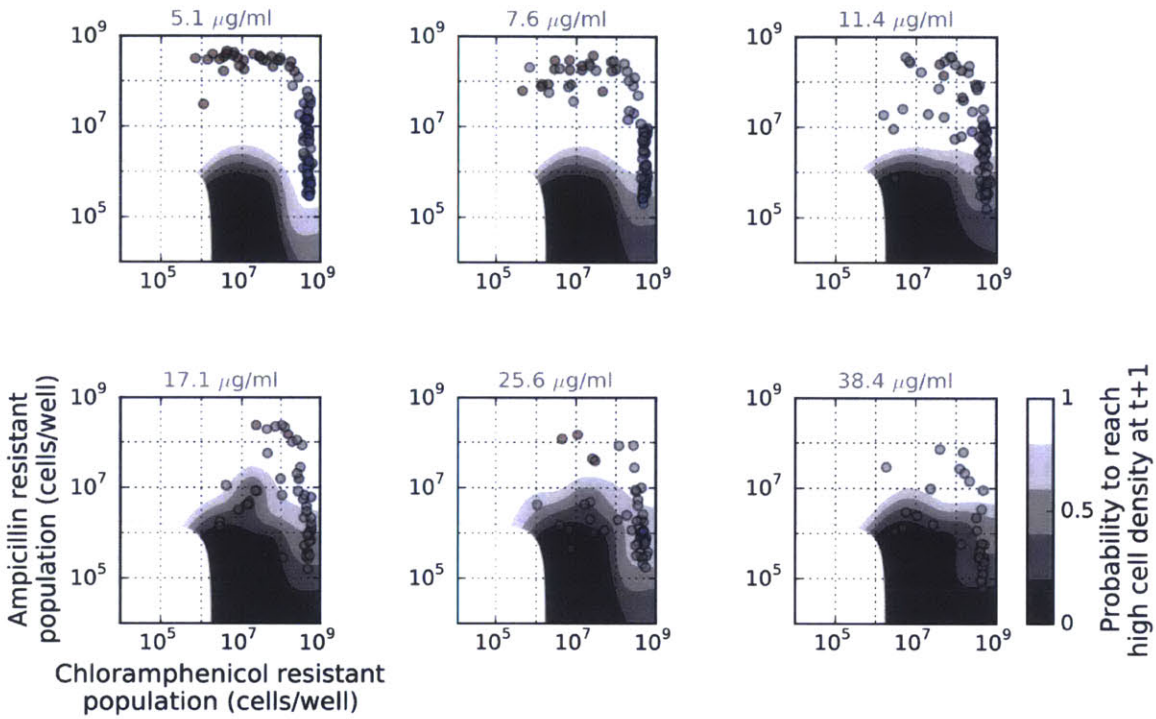

Figure C-13: Trajectories approach the separatrix as the environment deteriorates. For simplicity, we use the same proxy for the "health" of a population ($N_{total} > 2 \cdot 10^8$ cells/well) across all environments. However, in harsher environments it is more difficult to recover from a low population size (Table C.1). This observation means that in harsher environments, the true separatrix could be closer to the trajectories than the shown separatrix.

The data points represent all experimental data from day 2 and on. Color-coding represents the inferred phase of the oscillations (Fig. C-14, C-15).

In estimating the separatrix and the basins, we created 500 different realization of the experimental data by re-sampling the original data (Fig. C-20). We computed the probability surface $P(H = 1|N_1, N_2)$ for each realization and are reporting the probability surface averaged across all realizations. When interpolating the probability surface, we used the same smoothing parameter independent of the environment ($\sigma = 0.34$, Fig. C-19). Please refer to page 103 for more information.

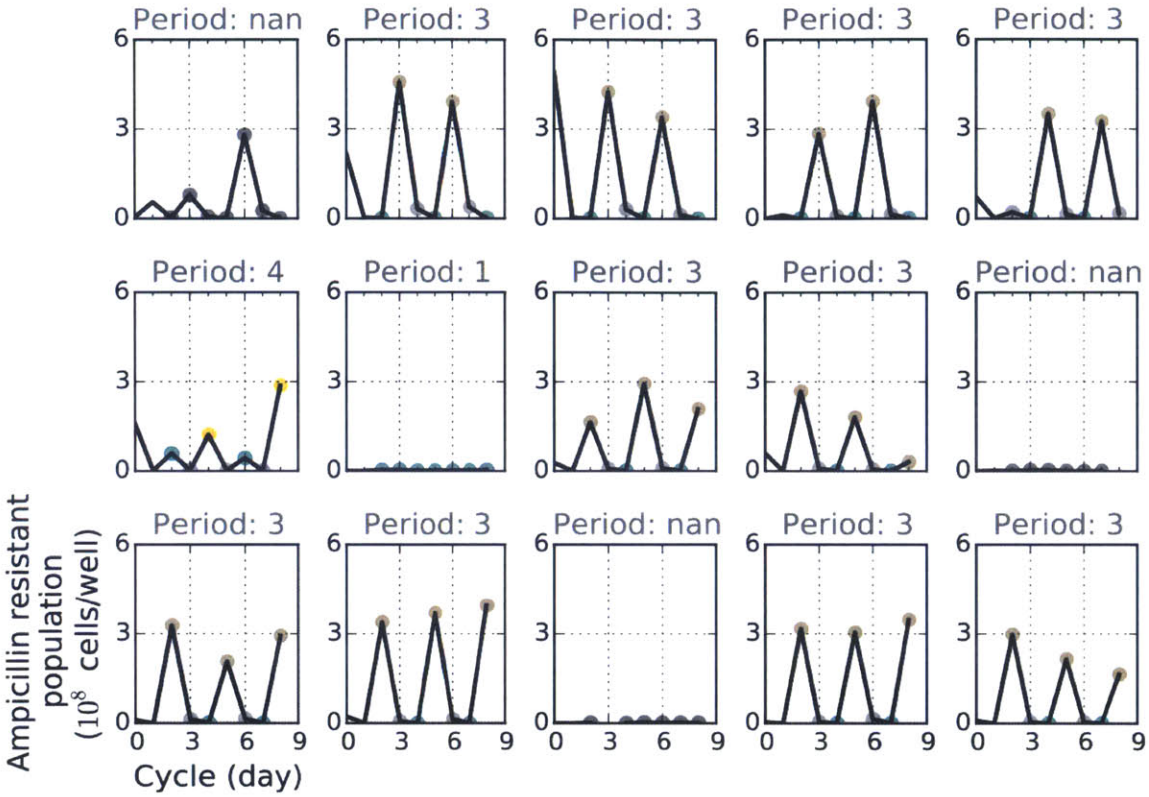

Figure C-14: Most of the mutualisms that survive converge to a period 3 like oscillation within the time frame of the experiment. We tracked multiple co-cultures that were started at different initial subpopulation compositions. The trajectories are color-coded according to the phase of the oscillations. When detecting periods, the first two time points are ignored to allow some extra time for the trajectory to converge to the limit cycle. Experiments were carried at 100x dilution strength, 24 hr dilution cycle, 10 μg/ml ampicillin, 5.1 μg/ml chloramphenicol.

The oscillation period is detected automatically by looking for peaks in the auto-correlation function of the (normalized) ampicillin resistant population size over time. For brevity, let us use $x(t)$ to denote the population size at time t, and $\tilde{x}(t) \equiv \frac{x-E[x]}{\sqrt{Var[x]}}$, where $E[x]$ and $Var[x]$ are the sample average and sample variance of x. We then use $\tilde{x}$ to compute the auto-correlation function $G_{\tilde{x}}[\Delta t] = \Sigma_{t'} \tilde{x}(t' + \Delta t)\tilde{x}(t')$, applying zero-padding as necessary. The assigned period is $\tau \equiv \text{argmax}_{\Delta t > 0} G_{\tilde{x}}[\Delta t]$ as as long as $G_{\tilde{x}}[\tau]$ was above a pre-defined threshold (C), otherwise no period was assigned. We note that we are specifically looking for $\Delta t \neq 0$ since $\Delta t = 0$ is a trivial maximum of the auto-correlation function. Empirically, we found that using $C = 0.2$ was good enough for classifying trajectories (confirmed by visual inspection); however, since this method produces an "all-or-nothing" answer (i.e., the entire trajectory is assigned a period or not), it may miss some trajectories that take a bit longer to converge to the limit cycle.

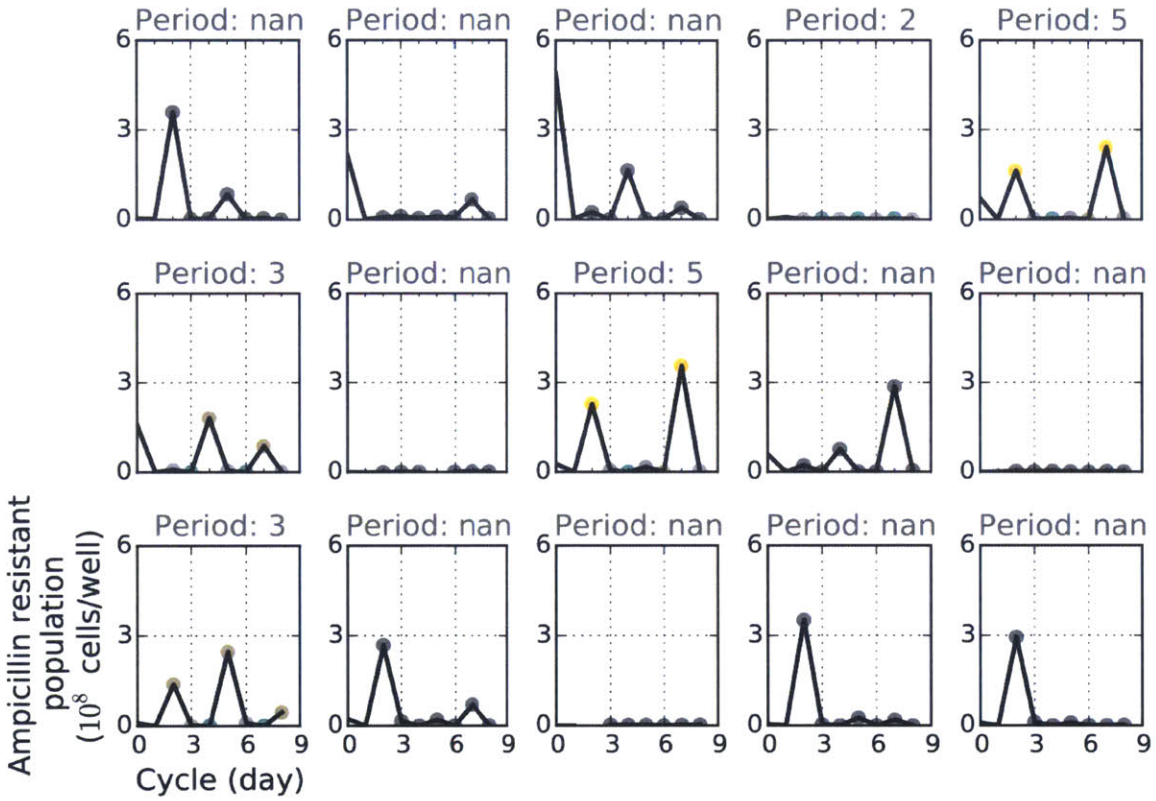

Figure C-15: In harsher environments, where the populations are more likely to collapse, the characteristic period 3 oscillation pattern is lost. We tracked multiple co-cultures that were started at different initial subpopulation compositions. The trajectories are color-coded according to the phase of the oscillations. Experiments were carried at 100x dilution strength, 10 μg/ml ampicillin, 11.4 μg/ml chloramphenicol. Please see Fig. C-14 for details on how periods were computed.

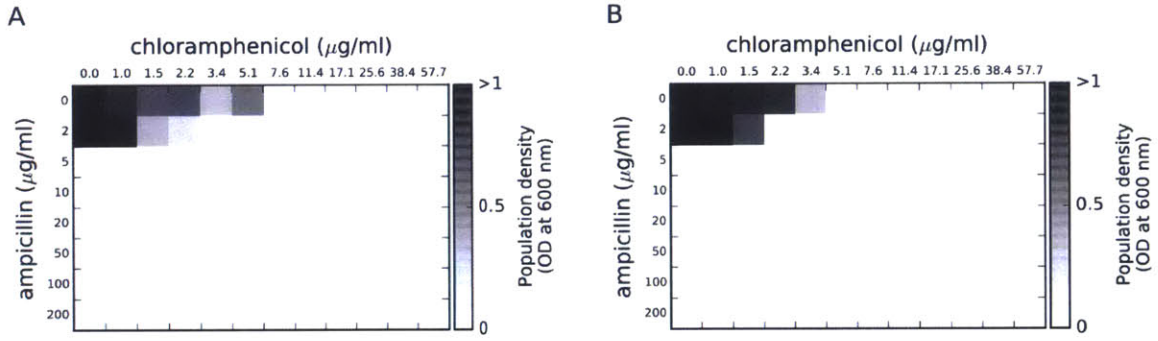

Figure C-16: The sensitive DH5α only survives at low antibiotic concentrations. Plotted is the population density at a dilution factors of 10x (A) and 100x (B).

Optical density measurements were done at 600 nm. For reference, an optical density of 1 unit corresponds to approximately $4 \cdot 10^8$ cells/well. Cultures were grown in 200 μl of medium.

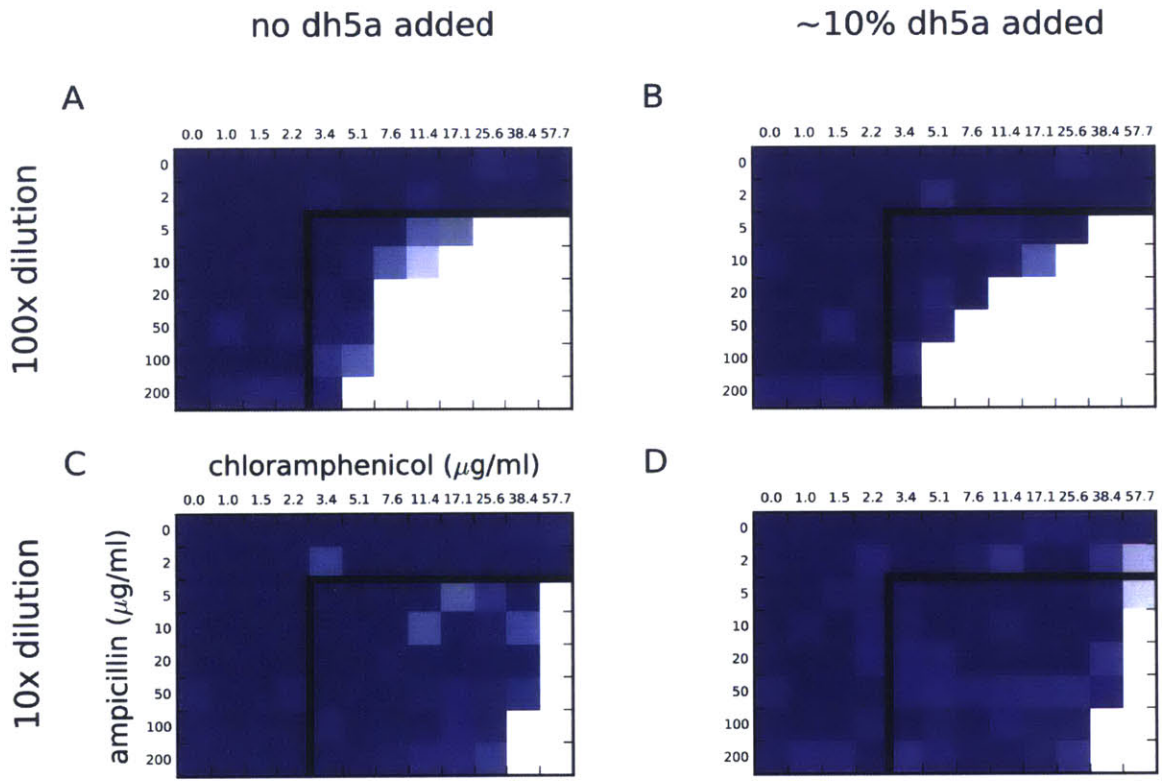

Figure C-17: Addition of a sensitive DH5α strain at a fraction of about 10% of the total population did not significantly affect the region of survival after 7 days of growth. Experiments were carried out at a dilution strength of 100x (subplots A, B) and a dilution strength of 10x (subplots C, D). Optical density measurements were done at 600 nm. For reference, an optical density of 1 unit corresponds to approximately $4 \cdot 10^8$ cells/well. Cultures were grown in 200 μl of medium.

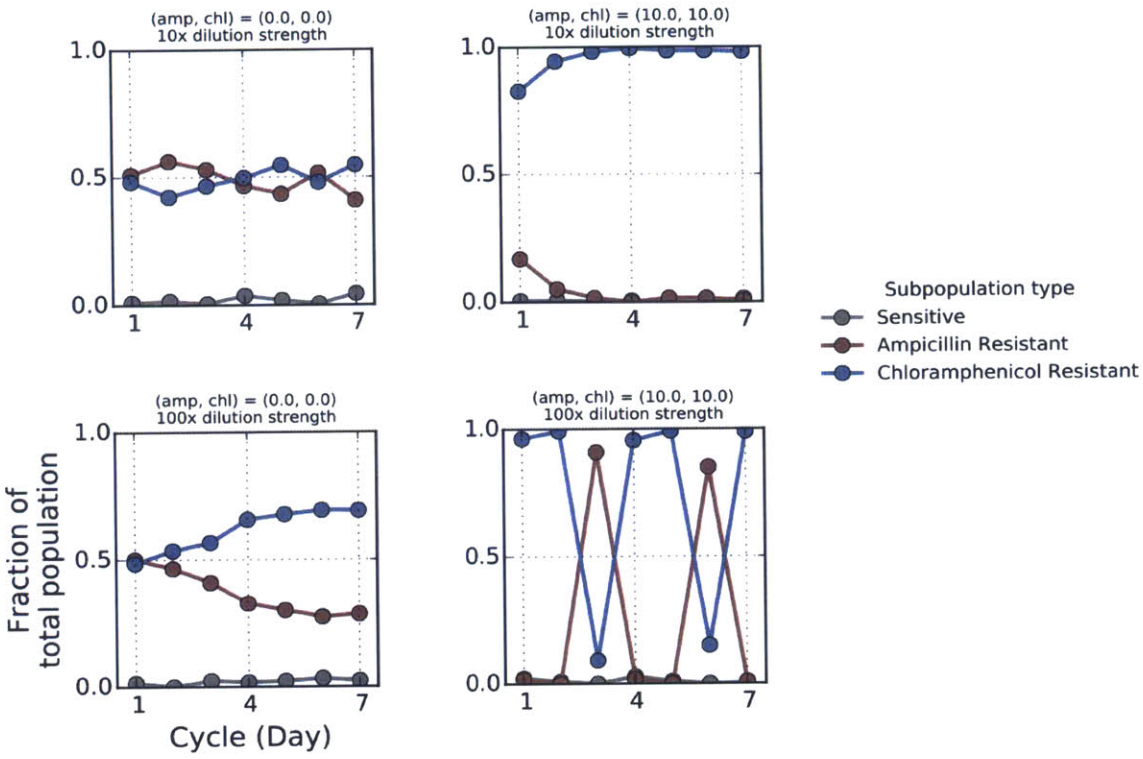
(amp, chl) = (0.0, 0.0)
10x dilution strength
(amp, chl) = (10.0, 10.0)
10x dilution strength
(amp, chl) = (0.0, 0.0)
100x dilution strength
(amp, chl) = (10.0, 10.0)
100x dilution strength
Fraction of total population
Cycle (Day)
1.0
0.5
0.0
1
4
7
Subpopulation type
Sensitive
Ampicillin Resistant
Chloramphenicol Resistant

Figure C-18: A sensitive mutant strain could emerge from within the mutualism via loss of the resistance plasmid. To check whether a sensitive strain could emerge in our experiments, we tracked the relative abundances of different subpopulations in co-cultures which initially contained only ampicillin and chloramphenicol resistant cells at a 1:1 ratio. Because fluorescent markers were carried on the resistance plasmids, sensitive strains, which lost the resistance plasmid, were not fluorescent. The lack of fluorescence meant that we could not detect this strain using flow cytometry; however, fortunately, all 3 strains gave rise to colonies of different color when grown on agar plates (red-fluorescent, yellow-fluorescent or non-fluorescent colonies). Hence, to measure the relative abundances of the different subpopulations, we inoculated a small volume from the co-culture onto Petri dishes containing agar and LB (but no antibiotics), and counted the different colonies. For each data point, at least 50 colonies were counted (in total), with the majority of data points having more than 100 colonies. We confirmed that non-fluorescent colonies were sensitive to both ampicillin and chloramphenicol, as would be expected if these colonies were formed by sensitive cells that lost their resistance plasmid.

The data reveals that although sensitive cells seem to emerge in our co-cultures, these cells are unable to proliferate in the presence of antibiotics, remaining at fractions smaller than $\sim$5% of the bacterial population. Since sensitive cells never reach high abundances, they are unlikely to affect the dynamics observed in our experiments (e.g., Fig. 3-2 3-3 3-4). Consistent with this expectation, the condition corresponding to a dilution strength of 100x, 10 μg/ml ampicillin, and 10 μg/ml chloramphenicol, exhibited period 3 oscillations using counts of colony forming units (Fig. 3-2).

In the subplot titles, ampicillin and chloramphenicol concentrations are reported in μg/ml.

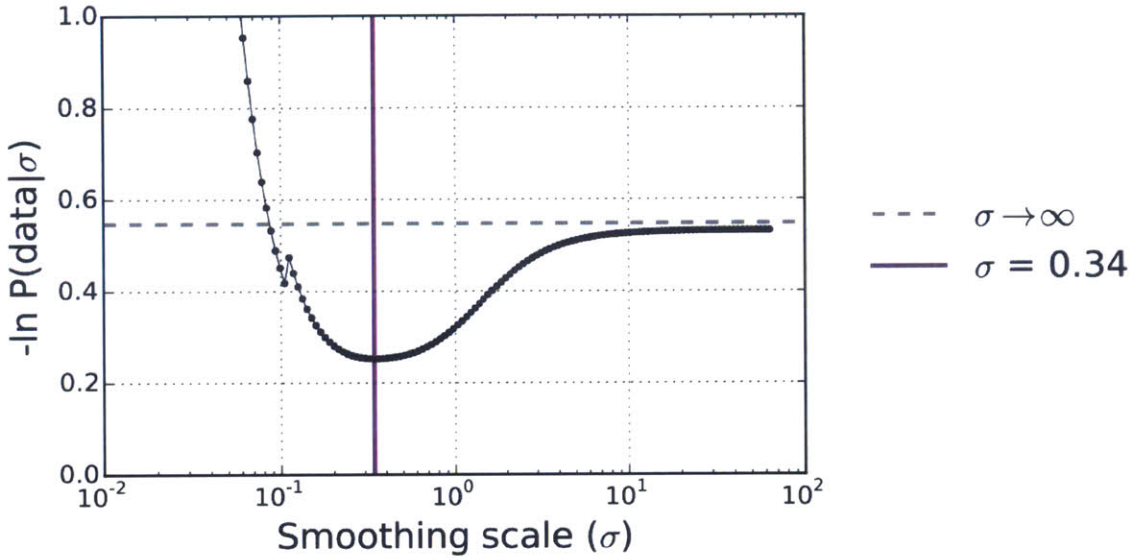

Figure C-19: The smoothing parameter σ was determined to be 0.34 (dimensionless) using maximum likelihood. For each potential value of σ, we trained a model (see page 103) to predict whether a given mutualistic population would attain high cell density in the next cycle. For training we used half of the data available from each environment (Fig. C-20), with training data selected by randomization. Then, we evaluated the likelihood of the seeing the remainder of the data under each model. We note that we trained the model simultaneously in all the different environments, restricting the model to use a single value of σ regardless of the environment. The kink in the likelihood function is a manifestation of the infamous zero-frequency problem where a model assigns zero probability to a particular data point, causing the likelihood to blow up. In this analysis, the easiest way of dealing with this problem was to filter out the misbehaving predictions. In our case, filtering out such data points creates discontinuities (kinks) in the likelihood function, but does not affect the point of maximum-likelihood. As a sanity check, we plotted (in a dashed gray line) what the likelihood should be when $\sigma \to \infty$; i.e., when treating all populations identically regardless of their composition.

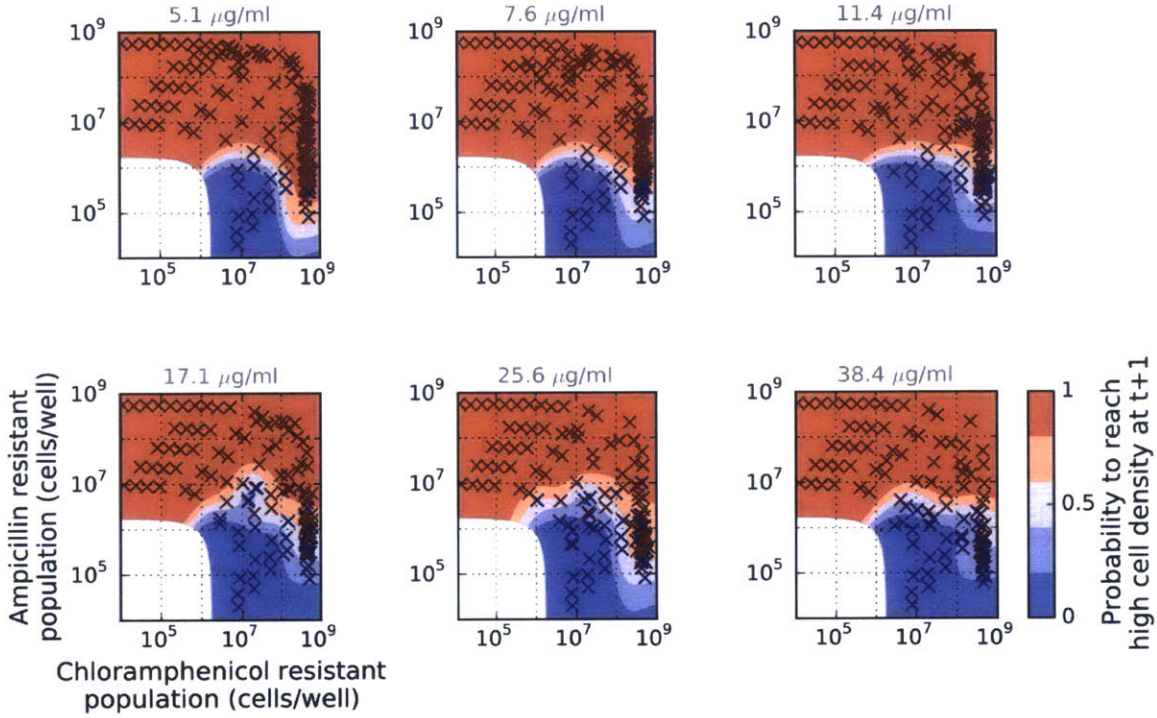

Figure C-20: Experimental data overlaid on top of the interpolated probability surface $P(H = 1|N_1, N_2)$. This surface represents the probability that a mutualistic population composed of an ampicillin resistant population of size N_1 and a chloramphenicol resistant population of size N_2 will reach a high cell density in the next cycle. The same smoothing parameter ($\sigma = 0.34$, Fig. C-19) was used for all environments. Please refer to page 103 for more information.

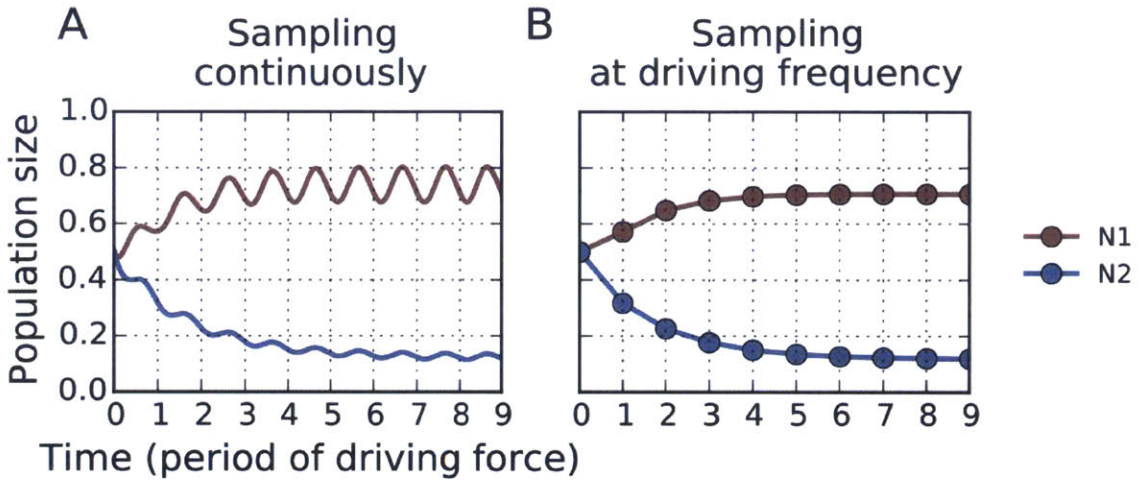

Figure C-21: A driven phenomenological model of obligatory mutualism oscillates at the driving frequency. We did not find parameters for which the model exhibited oscillations of a longer period than the period of the driving force. (A) Shows oscillations in the population size that are locked with the driving frequency. (B) Same as (A), but the population sizes are sampled once per cycle of the driving force (shown to emphasize that the period is locked with the driving force). The model used for this simulation is described in Eq. C.1. Parameters used in the simulations are $\gamma_1 = 3, \gamma_2 = 0.5, K = 1, \delta_0 = 0.1, w = 0.5$. Initial population sizes were $N_1(t = 0) = 0.5, N_2(t = 0) = 0.5$.

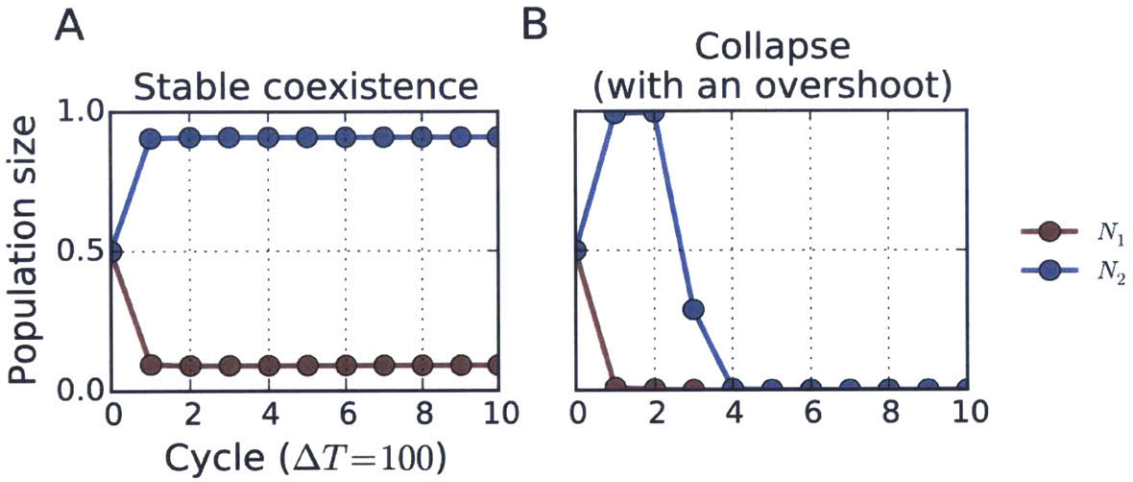

Figure C-22: A simulation in which a phenomenological model of obligatory mutualism was subjected to periodic dilutions did not exhibit oscillations. (A) Shows stable coexistence between the two mutualists. (B) This model can still give rise to some interesting behavior, where the population size of one of the mutualists peaks for a short while before the entire population proceeds to collapse. The model used for this simulation is described in Eq. C.1.

Parameters in (A) $\gamma_1 = 10, \gamma_2 = 100$. Parameters in (B): $\gamma_1 = 1, \gamma_2 = 250$. Common parameters: $K = 1, \delta_0 = 0.0$. Initial population sizes were $N_1(t = 0) = 0.5, N_2(t = 0) = 0.5$. The differential equations were integrated for a duration $\Delta T = 100$. At the end of the growth cycle, the population was diluted by a factor 100x. This process was repeated for a number of cycles.

Bibliography

1. J. Davies, D. Davies, *Microbiology and Molecular Biology Reviews* **74**, 417–433, ISSN: 1092-2172, 1098-5557 (Sept. 2010).
2. G. Taubes, *Science* **321**, 356–361, ISSN: 0036-8075, 1095-9203 (July 2008).
3. H. C. Neu, *Science* **257**, 1064–1073, ISSN: 0036-8075, 1095-9203 (Aug. 1992).
4. T. Frieden, *Centers for Disease Control and Prevention, US Department of Health and Human Services* (2013).
5. S. J. Projan, *Current Opinion in Microbiology* **6**, 427–430, ISSN: 1369-5274 (Oct. 2003).
6. A. H. Delcour, *Biochimica et Biophysica Acta (BBA) - Proteins and Proteomics*, Mechanisms of Drug Efflux and Strategies to Combat Them **1794**, 808–816, ISSN: 1570-9639 (May 2009).
7. H. Nikaido, *Antimicrobial Agents and Chemotherapy* **33**, 1831–1836, ISSN: 0066-4804 (Nov. 1989).
8. B. G. Spratt, *Science* **264**, 388–393, ISSN: 0036-8075, 1095-9203 (Apr. 1994).
9. M. N. Alekshun, S. B. Levy, *Cell* **128**, 1037–1050, ISSN: 0092-8674 (Mar. 2007).
10. A. C. Palmer, R. Kishony, *Nature Communications* **5**, DOI: 10.1038/ncomms5296 (July 2014).
11. V. M. D'Costa *et al.*, *Nature* **477**, 457–461, ISSN: 0028-0836 (Sept. 2011).
12. G. D. Wright, *Nature Reviews Microbiology* **5**, 175–186, ISSN: 1740-1526 (Mar. 2007).
13. J. Davies, *Science* **264**, 375–382, ISSN: 0036-8075, 1095-9203 (Apr. 1994).
14. G. D. Wright, *Advanced Drug Delivery Reviews* **57**, 1451–1470, ISSN: 0169-409X (July 2005).
15. K. Poole, *Journal of Antimicrobial Chemotherapy* **56**, 20–51, ISSN: 0305-7453, 1460-2091 (July 2005).
16. K. Poole, *Annals of Medicine* **39**, 162–176, ISSN: 0785-3890 (Jan. 2007).
17. C. A. Arias, B. E. Murray, *New England Journal of Medicine* **360**, 439–443, ISSN: 0028-4793 (Jan. 2009).
18. R. P. Novick, *Scientific American* **243**, 102–104, 106, 110 passim, ISSN: 0036-8733 (Dec. 1980).

19. C. M. Thomas, K. M. Nielsen, *Nature Reviews Microbiology* **3**, 711–721, ISSN: 1740-1526 (Sept. 2005).

20. V. M. D'Costa, K. M. McGrann, D. W. Hughes, G. D. Wright, *Science* **311**, 374–377, ISSN: 0036-8075, 1095-9203 (Jan. 2006).

21. K. J. Forsberg *et al.*, *Science* **337**, 1107–1111, ISSN: 0036-8075, 1095-9203 (Aug. 2012).

22. V. M. D'Costa, E. Griffiths, G. D. Wright, *Current Opinion in Microbiology*, Antimicrobials/Genomics **10**, 481–489, ISSN: 1369-5274 (Oct. 2007).

23. G. D. Wright, *Current Opinion in Microbiology*, Antimicrobials/Genomics **13**, 589–594, ISSN: 1369-5274 (Oct. 2010).

24. M. B. Elowitz, A. J. Levine, E. D. Siggia, P. S. Swain, *Science* **297**, 1183–1186, ISSN: 0036-8075, 1095-9203 (Aug. 2002).

25. N. Q. Balaban, J. Merrin, R. Chait, L. Kowalik, S. Leibler, *Science* **305**, 1622–1625, ISSN: 0036-8075, 1095-9203 (Sept. 2004).

26. D. M. Weinreich, N. F. Delaney, M. A. DePristo, D. L. Hartl, *Science* **312**, 111–114, ISSN: 0036-8075, 1095-9203 (Apr. 2006).

27. F. J. Poelwijk, D. J. Kiviet, D. M. Weinreich, S. J. Tans, *Nature* **445**, 383–386, ISSN: 0028-0836 (Jan. 2007).

28. L. Tan, S. Serene, H. X. Chao, J. Gore, *Physical Review Letters* **106**, 198102 (May 2011).

29. L. Tan, J. Gore, *Evolution* **66**, 3144–3154, ISSN: 1558-5646 (Oct. 2012).

30. E. Toprak *et al.*, *Nature Genetics* **44**, 101–105, ISSN: 1061-4036 (2012).

31. Q. Zhang *et al.*, *Science* **333**, 1764–1767, ISSN: 0036-8075, 1095-9203 (Sept. 2011).

32. H. A. Lindsey, J. Gallie, S. Taylor, B. Kerr, *Nature* **494**, 463–467, ISSN: 0028-0836 (Feb. 2013).

33. S. Kim, T. D. Lieberman, R. Kishony, *Proceedings of the National Academy of Sciences* **111**, 14494–14499, ISSN: 0027-8424, 1091-6490 (Oct. 2014).

34. H. Goossens, M. Ferech, R. Vander Stichele, M. Elseviers, *The Lancet* **365**, 579–587, ISSN: 0140-6736 (Feb. 2005).

35. N. Fishman, *American Journal of Infection Control* **34**, S55–S63, ISSN: 0196-6553 (June 2006).

36. S. A. West, S. P. Diggle, A. Buckling, A. Gardner, A. S. Griffin, *Annual Review of Ecology, Evolution, and Systematics* **38**, 53–77, ISSN: 1543-592X (Jan. 2007).

37. L. Hall-Stoodley, J. W. Costerton, P. Stoodley, *Nature Reviews Microbiology* **2**, 95–108, ISSN: 1740-1526 (Feb. 2004).

38. P. S. Stewart, J. William Costerton, *The Lancet* **358**, 135–138, ISSN: 0140-6736 (July 2001).

39. N. Høiby, T. Bjarnsholt, M. Givskov, S. Molin, O. Ciofu, *International Journal of Antimicrobial Agents* **35**, 322–332, ISSN: 0924-8579 (Apr. 2010).

40. H. R. Meredith, J. K. Srimani, A. J. Lee, A. J. Lopatkin, L. You, *Nature Chemical Biology* **11**, 182–188, ISSN: 1552-4450 (Mar. 2015).

41. N. M. Vega, J. Gore, *Current Opinion in Microbiology*, Antimicrobials **21**, 28–34, ISSN: 1369-5274 (Oct. 2014).

42. I. Brook, *Review of Infectious Diseases* **11**, 361–368, ISSN: 1058-4838, 1537-6591 (May 1989).

43. B. R. Levin, D. E. Rozen, *Nature Reviews Microbiology* **4**, 556–562, ISSN: 1740-1526 (July 2006).

44. J. M. Smith, E. Szathmáry, *The Origins of Life: From the Birth of Life to the Origin of Language* (Oxford University Press, Oxford, Nov. 2000), ISBN: 9780192862099.

45. M. A. Nowak, *Science* **314**, 1560–1563, ISSN: 0036-8075, 1095-9203 (Dec. 2006).

46. M. H. Perlin *et al.*, *Proceedings of the Royal Society of London B: Biological Sciences*, rspb20090997, ISSN: 0962-8452, 1471-2954 (Aug. 2009).

47. E. A. Yurtsev, H. X. Chao, M. S. Datta, T. Artemova, J. Gore, *Molecular Systems Biology* **9**, 683, ISSN: 1744-4292 (Aug. 2013).

48. D. R. Clark *et al.*, *Frontiers in Bioscience (Landmark Edition)* **14**, 4815–4824, ISSN: 1093-4715 (2009).

49. J. E. Bouma, R. E. Lenski, *Nature* **335**, 351–352, ISSN: 0028-0836 (Sept. 1988).

50. C. Dahlberg, L. Chao, *Genetics* **165**, 1641–1649, ISSN: 0016-6731, 1943-2631 (Dec. 2003).

51. D. I. Andersson, *Current Opinion in Microbiology* **9**, 461–465, ISSN: 1369-5274 (Oct. 2006).

52. I. Brook, *Clinical Microbiology and Infection* **10**, 777–784, ISSN: 1469-0691 (Sept. 2004).

53. L. A. Dugatkin, M. Perlin, R. Atlas, *Journal of Theoretical Biology* **220**, 67–74, ISSN: 0022-5193 (Jan. 2003).

54. L. A. Dugatkin, M. Perlin, J. S. Lucas, R. Atlas, *Proceedings of the Royal Society B: Biological Sciences* **272**, 79–83, ISSN: 0962-8452, 1471-2954 (Jan. 2005).

55. A. S. Hackman, T. D. Wilkins, *Antimicrobial Agents and Chemotherapy* **7**, 698–703, ISSN: 0066-4804, 1098-6596 (May 1975).

56. I. Brook, *Review of Infectious Diseases* **6**, 601–607, ISSN: 1058-4838, 1537-6591 (Sept. 1984).

57. R. A. Bonomo, M. E. Tolmasky, Eds., *Enzyme-Mediated Resistance to Antibiotics: Mechanisms, Dissemination, and Prospects for Inhibition* (ASM Press, Washington, D.C, 1 edition, Apr. 2007), ISBN: 9781555813031.

58. G. Foulds, *Clinical Infectious Diseases* **8**, S503–S511, ISSN: 1058-4838, 1537-6591 (Nov. 1986).

59. D. M. Livermore, *Clinical Microbiology Reviews* **8**, 557–584, ISSN: 0893-8512, 1098-6618 (Oct. 1995).

60. H. Nikaido, S. Normark, *Molecular Microbiology* **1**, 29–36, ISSN: 1365-2958 (1987).

61. J. Gore, H. Youk, A. v. Oudenaarden, *Nature* **459**, 253–256, ISSN: 0028-0836 (Apr. 2009).

62. M. Doebeli, C. Hauert, *Ecology Letters* **8**, 748–766, ISSN: 1461-0248 (2005).

63. M. A. Nowak, K. Sigmund, *Science* **303**, 793–799, ISSN: 0036-8075, 1095-9203 (Feb. 2004).

64. D. M. Livermore, F. Moosdeen, M. A. Lindridge, P. Kho, J. D. Williams, *Journal of Antimicrobial Chemotherapy* **17**, 139–146, ISSN: 0305-7453, 1460-2091 (Feb. 1986).

65. W. Zimmermann, A. Rosselet, *Antimicrobial Agents and Chemotherapy* **12**, 368–372, ISSN: 0066-4804, 1098-6596 (Sept. 1977).

66. A. Dubus, J. M. Wilkin, X. Raquet, S. Normark, J. M. Frère, *Biochemical Journal* **301**, 485–494, ISSN: 0264-6021 (July 1994).

67. R. M. May, *Nature* **261**, 459–467 (June 1976).

68. K. Bush, *Clinical Microbiology Reviews* **1**, 109–123, ISSN: 0893-8512 (Jan. 1988).

69. S. M. Drawz, R. A. Bonomo, *Clinical Microbiology Reviews* **23**, 160–201, ISSN: 0893-8512, 1098-6618 (Jan. 2010).

70. L. Bret *et al.*, *Antimicrobial Agents and Chemotherapy* **41**, 2547–2549, ISSN: 0066-4804, 1098-6596 (Nov. 1997).

71. M. D. Kitzis *et al.*, *Antimicrobial Agents and Chemotherapy* **32**, 9–14, ISSN: 0066-4804, 1098-6596 (Jan. 1988).

72. C. Tan *et al.*, *Molecular Systems Biology* **8**, ISSN: 1744-4292, DOI: 10.1038/msb.2012.49, (visited on 04/10/2015) (Jan. 2012).

73. M. S. Datta, K. S. Korolev, I. Cvijovic, C. Dudley, J. Gore, *Proceedings of the National Academy of Sciences* **110**, 7354–7359, ISSN: 0027-8424, 1091-6490 (Apr. 2013).

74. A. Sanchez, J. Gore, *PLoS Biol* **11**, e1001547 (Apr. 2013).

75. H. Celiker, J. Gore, *Molecular Systems Biology* **8**, DOI: 10.1038/msb.2012.54 (Nov. 2012).

76. R. B. Sykes, M. Matthew, *The Journal of Antimicrobial Chemotherapy* **2**, 115–157, ISSN: 0305-7453 (June 1976).

77. Y. Tanouchi, A. Pai, N. E. Buchler, L. You, *Molecular Systems Biology* **8**, DOI: 10.1038/msb.2012.57 (Nov. 2012).

78. N. Narisawa, S. Haruta, H. Arai, M. Ishii, Y. Igarashi, *Applied and Environmental Microbiology* **74**, 3887–3894, ISSN: 0099-2240, 1098-5336 (June 2008).

79. B. Kerr, M. A. Riley, M. W. Feldman, B. J. M. Bohannan, *Nature* **418**, 171–174, ISSN: 0028-0836 (July 2002).

80. H. A. O'Connell *et al.*, *Applied and Environmental Microbiology* **72**, 5013–5019, ISSN: 0099-2240, 1098-5336 (July 2006).

81. A. C. Palmer, E. Angelino, R. Kishony, *Nature Chemical Biology* **6**, 105–107, ISSN: 1552-4450 (2010).

82. K. Lewis, *Nature Reviews Microbiology* **5**, 48 (Jan. 2007).

83. H. H. Lee, M. N. Molla, C. R. Cantor, J. J. Collins, *Nature* **467**, 82–85, ISSN: 0028-0836 (Sept. 2010).

84. D. Drecktrah *et al.*, *Traffic (Copenhagen, Denmark)* **9**, 2117–2129, ISSN: 1600-0854 (Dec. 2008).

85. H. G. Garcia, R. Phillips, *Proceedings of the National Academy of Sciences* **108**, 12173–12178, ISSN: 0027-8424, 1091-6490 (July 2011).

86. R. Lutz, H. Bujard, *Nucleic Acids Research* **25**, 1203–1210, ISSN: 0305-1048, 1362-4962 (Mar. 1997).

87. J. L. Bronstein, *The Quarterly Review of Biology* **69**, 31–51, ISSN: 0033-5770 (Mar. 1994).

88. J. L. Bronstein, *Trends in Ecology & Evolution* **9**, 214–217, ISSN: 0169-5347 (June 1994).

89. J. L. Bronstein, *Ecology Letters* **4**, 277–287, ISSN: 1461-0248 (May 2001).

90. J. J. Stachowicz, *BioScience* **51**, 235–246, ISSN: 0006-3568, 1525-3244 (Mar. 2001).

91. J. L. Sachs, E. L. Simms, *Trends in Ecology & Evolution* **21**, 585–592, ISSN: 0169-5347 (Oct. 2006).

92. J. N. Holland, D. L. DeAngelis, *Ecology* **91**, 1286–1295, ISSN: 0012-9658 (Apr. 2010).

93. B. McGill, *Ecological Modelling* **187**, 413–425 (2005).

94. D. H. Boucher, S. James, K. H. Keeler, *Annual Review of Ecology and Systematics* **13**, 315–347, ISSN: 0066-4162 (Jan. 1982).

95. J. F. Bruno, J. J. Stachowicz, M. D. Bertness, *Trends in Ecology & Evolution* **18**, 119–125, ISSN: 0169-5347 (Mar. 2003).

96. K. Hosoda *et al.*, *PLoS ONE* **6**, e17105 (Feb. 2011).

97. W. Harcombe, *Evolution* **64**, 2166–2172, ISSN: 1558-5646 (2010).

98. W. Shou, S. Ram, J. M. G. Vilar, *Proceedings of the National Academy of Sciences* **104**, 1877–1882, ISSN: 0027-8424, 1091-6490 (Feb. 2007).

99. S. Pande *et al.*, *The ISME Journal* **8**, 953–962, ISSN: 1751-7362 (May 2014).

100. M. T. Mee, J. J. Collins, G. M. Church, H. H. Wang, *Proceedings of the National Academy of Sciences* **111**, E2149–E2156, ISSN: 0027-8424, 1091-6490 (May 2014).

101. B. Momeni, C.-C. Chen, K. L. Hillesland, A. Waite, W. Shou, *Cellular and Molecular Life Sciences* **68**, 1353–1368, ISSN: 1420-682X, 1420-9071 (Apr. 2011).

102. A. J. Waite, W. Shou, *Proceedings of the National Academy of Sciences* **109**, 19079–19086, ISSN: 0027-8424, 1091-6490 (Nov. 2012).

103. B. E. L. Morris, R. Henneberger, H. Huber, C. Moissl-Eichinger, *FEMS Microbiology Reviews* **37**, 384–406, ISSN: 1574-6976 (May 2013).

104. P. L. Conlin, J. R. Chandler, B. Kerr, *Current Opinion in Microbiology*, Antimicrobials **21**, 35–44, ISSN: 1369-5274 (Oct. 2014).

105. W. V. Shaw, *CRC critical reviews in biochemistry* **14**, 1–46, ISSN: 0045-6411 (1983).

106. M. A. Nowak, *Evolutionary Dynamics: Exploring the Equations of Life* (Belknap Press, Cambridge, Mass, First Edition edition, Sept. 2006), ISBN: 9780674023383.

107. B. Hu, J. Du, R.-y. Zou, Y.-j. Yuan, *PLoS ONE* **5**, e10619 (May 2010).

108. R. M. May, *Science* **186**, 645–647, ISSN: 0036-8075, 1095-9203 (Nov. 1974).

109. B. E. Kendall *et al.*, *Ecology* **80**, 1789–1805, ISSN: 0012-9658 (Sept. 1999).

110. P. Turchin, *Complex population dynamics: a theoretical/empirical synthesis* (Princeton University Press, 2003), vol. 35.

111. K. L. Kausrud *et al.*, *Nature* **456**, 93–97, ISSN: 0028-0836 (Nov. 2008).

112. R. A. Ims, J.-A. Henden, S. T. Killengreen, *Trends in Ecology & Evolution* **23**, 79–86, ISSN: 0169-5347 (Feb. 2008).

113. P. Turchin, A. D. Taylor, *Ecology* **73**, 289–305, ISSN: 0012-9658 (Feb. 1992).

114. X.-P. Yan, W.-T. Li, *Physica D: Nonlinear Phenomena* **227**, 51–69, ISSN: 0167-2789 (Mar. 2007).

115. Y. Li, G. Xu, *Applied Mathematics Letters* **14**, 525–530, ISSN: 0893-9659 (2001).

116. M. E. Gilpin, T. J. Case, E. A. Bender, *The American Naturalist* **119**, 584–588, ISSN: 0003-0147 (Apr. 1982).

117. T. S. Lee *et al.*, *Journal of Biological Engineering* **5**, 1–14, ISSN: 1754-1611 (Sept. 2011).

118. R. P. Shetty, D. Endy, T. F. K. Jr, *Journal of Biological Engineering* **2**, 1–12, ISSN: 1754-1611 (Apr. 2008).

119. J. D. Hunter, *Computing in Science & Engineering* **9**, 90–95, ISSN: 1521-9615 (May 2007).

120. F. Pérez, B. E. Granger, *Computing in Science & Engineering* **9**, 21–29, ISSN: 1521-9615 (May 2007).

121. G. Foulds *et al.*, *Antimicrobial Agents and Chemotherapy* **23**, 692–699, ISSN: 0066-4804, 1098-6596 (May 1983).

122. A. Petit *et al.*, *Biochemical Journal* **305**, 33–40, ISSN: 0264-6021 (Jan. 1995).

123. J. N. Holland, D. L. DeAngelis, J. L. Bronstein, *The American Naturalist* **159**, 231–244, ISSN: 0003-0147 (Mar. 2002).

124. A. M. Dean, *The American Naturalist* **121**, 409–417, ISSN: 0003-0147 (Mar. 1983).

125. S. H. Strogatz, *Nonlinear Dynamics and Chaos: With Applications to Physics, Biology, Chemistry, and Engineering* (Westview Press, Second Edition, Second Edition edition, July 2014), ISBN: 9780813349107.

126. P. Turchin, *Nature* **344**, 660–663 (Apr. 1990).

127. J. B. Deris *et al.*, *Science* **342**, 1237435, ISSN: 0036-8075, 1095-9203 (Nov. 2013).